MOLECULAR PROFILING AND MECHANISMS OF CEREBROVASCULAR FUNCTION IN HEALTH AND NEURODEGENERATION

by

Francisco J. Garcia
B.S. Materials Science and Engineering
B.S. Chemistry
Massachusetts Institute of Technology, 2017

SUBMITTED TO THE DEPARTMENT OF BRAIN AND COGNITIVE SCIENCES IN PARTIAL FULFILLMENT OF THE REQUIREMENTS FOR THE DEGREE OF DOCTOR OF PHILOSOPHY IN BRAIN AND COGNITIVE SCIENCES AT THE MASSACHUSETTS INSTITUTE OF TECHNOLOGY

June 2023

Signature of Author: _____
Department of Brain and Cognitive Sciences

Certified by: _____
Myriam Heiman, Ph.D.
Associate Professor, Picower Institute for Learning and Memory, Department of Brain and Cognitive Sciences, Thesis Supervisor

Accepted by: _____
Mark Harnett, Ph.D.
Graduate Officer
Department of Brain and Cognitive Sciences

Molecular Profiling and Mechanisms of Cerebrovascular Function in Health and Neurodegeneration

by

Francisco J. Garcia

Submitted to the Department of Brain and Cognitive Sciences on May X, 2023 in Partial Fulfillment of the Requirements for the Degree of Doctor of Philosophy in Brain and Cognitive Sciences

ABSTRACT

The unmet medical need for therapies that treat neurological disorders is in part due to our lack of understanding the underlying biological mechanisms and inefficient delivery strategies to target the brain. The cerebrovasculature is essential for proper brain function as it tightly regulates blood flow and supplies the necessary nutrients. Furthermore, the presence of a blood-brain barrier (BBB) provides protection to vulnerable neurons but poses a challenge for drug delivery. In neurodegeneration, BBB breakdown and vascular impairments are hallmarks that precede the onset of disease-specific phenotypes. Efforts to understand the basic biology of cells that comprise the cerebrovasculature as well as the changes that occur in disease have made significant progress with the advent of single-cell technologies. Here we characterize molecular profiles of cell types that comprise the human cerebrovasculature using both *ex vivo* fresh tissue and *post mortem in silico* sorting of human brain tissue samples. Using single-nucleus RNA-sequencing (snRNA-seq), we profile cerebrovascular nuclei across 11 subtypes, including endothelial cells, mural cells, and perivascular fibroblasts. We uncover human-specific expression patterns along the arteriovenous axis and determine previously uncharacterized cell type-specific markers. Next, we use these human-specific signatures to study changes in cerebrovascular cells from patients with Huntington's disease (HD), which reveal activation of innate immune signaling in vascular and glial cell types and a concomitant reduction in the levels of proteins critical for maintenance of blood–brain barrier integrity. Lastly, using a combination of an adeno-associated virus (AAV) approach in combination with a cell type-specific promoter (*CLDN5*) towards brain endothelial cells, we develop an AAV vector for effective gene therapy delivery to the cerebrovasculature. We demonstrate that a single dose of gene therapy targeting the cerebrovasculature to lower levels of huntingtin via a microRNA-mediated mechanism is sufficient to delay the progression of Huntington's disease *in vivo*. Altogether, this work provides both a comprehensive molecular atlas for future studies to study the cerebrovasculature in health and disease contexts as well as tool for development of novel therapeutic strategies towards neurological disorders.

Thesis Supervisor: Myriam Heiman
Title: Associate Professor of Neuroscience

Thesis Committee: Li-Huei Tsai, Alan Jasanoff, Chenghua Gu

Acknowledgements

Almost 10 years ago as a naïve 18-year-old, I started my career at MIT. It is difficult to fathom that that journey is nearing its end. Even more is the realization that a decade ago I had no idea I would be accomplishing the things I am today. Over the course of my undergraduate and graduate careers I have had the privilege of working with some of the greatest minds in the world and I am forever indebted to them for their kindness, generosity, and patience with me as I have grown to become the scientist, researcher, and individual I am today.

First and foremost, I would like to thank my mentor and advisor, Myriam Heiman. I do not exaggerate when I say she is the most intelligent and creative thinker I have ever met. After six years of working in her lab, I am still astounded by the breadth and depth of knowledge that she has. The ideas and types of experiments she comes up with in the blink of an eye are nothing short of pure genius. More importantly though, I admire her humility and kindness. I chose her lab back in 2018 because of her passion for mentorship and desire to cultivate a safe and welcoming environment for every single one of her trainees. I found a home here and for that I cannot express my gratitude enough. Throughout my years in her lab, she has supported me every step of the way and motivated me to succeed even when I encountered personal or scientific struggles. Her dedication to her people is truly exceptional.

I want to thank two outstanding role models that have shaped my thinking and maturity as a researcher and scientist: Polina Anikeeva and Jessica Stolee. I had the pleasure of working in Polina's lab as an undergraduate for over 3 years. It was here that I got my first real exposure to both neuroscience and independent research. Polina took a risk and allowed me to experience true science. Jess was my mentor/boss at Biogen during an unusual time in undergrad when I decided to work both full-time at a biotech and be an MIT student. Nevertheless, she agreed to take me under her wing and show me the ways of industry. But to me, the greatest lesson from Jess was her encouragement to be confident and independent. She pushed me to put my career goals into greater perspective and take steps to accomplish said goals; one of those being to attend graduate school and acquire my PhD.

To my committee – Li-Huei Tsai, Alan Jasanoff, and Chenghua Gu – thank you for your insightful views and comments into my research for these past years. I greatly value your time and support in helping me get through to the end and also for the guidance in choosing my path forward.

A special thanks to all my collaborators and colleagues who contributed to the amazing science we did. In particular, I want to thank Manolis Kellis and Na Sun for being an incredible team to work with and getting our single cell atlas of the brain vasculature out into the community. We worked incredibly hard on this project and it paid off.

To all the members of the Heiman Lab past and present – you're family! Y'all made me laugh, cry, smile, angry, and experience every possible human emotion. Shout out to my fellow magnemite, Preston Ge and Blake Zhou, for sharing that one functional neuron. Our combined intellectual potential is incomparable to anything ever seen in this world. And to our Lab Captain, Vanessa Lau, I give you my sincerest apologies for all the crazy experiments I made

you do with me (and still am even as I finish writing this thesis). Thank you for being so patient with me and being the best lab partner-in-crime. I probably wouldn't have survived graduate school if you weren't here to keep me sane and grounded.

A huge thank you to all the staff members at MIT and BCS who helped in numerous ways throughout my PhD: DCM staff and scientists who helped with my mouse work, Julianne and Sierra for all their hard work in helping graduate students, Jim DiCarlo for helping me in a great time of need at the beginning of my graduate school career, and many others who likely facilitated my experience without me even knowing.

I would like to extend by gratitude to the brain barriers community for creating such a wonderful space for discussion and sharing of science. I have had the pleasure of presenting at these conferences and meetings recently and am amazed by the excellent research being done in this field. Their rigorous work and positive feedback on my contributions have greatly encouraged me to stay in the field. I'm incredibly honored to have been awarded recently two awards: the David S. Miller Junior Scientist Award and the Inaugural Ben Barres Junior Investigator Award. It brings me great pride and joy to represent young, under-represented scientists.

I want to also thank all of my dance friends who helped me stay sane throughout graduate school. Dance has been a powerful emotional outlet for me, but I'd also like to believe it has made me be a better thinker. I have thoroughly enjoyed the creative process of choreographing several contemporary pieces both at MIT and in the greater Boston/Cambridge community. Special shoutout to Michelle Bai, Xochitl Luna, Michaela Purvis, Angie DeWolf, Angela Bragg, Meg Anderson, Jesse Michel, Andrea Garmilla, Maya Redden, Anita Podrug, and so many more of the talented dancers I got to work and train with throughout the years.

To Zygi, thank you so much for entering my life and being a much-needed support. Thank you for constantly reminding me to eat, rest, and overall take care of myself, which I probably still need to do more than I currently do.

Finally – to my beloved family who were saddened when I left home 10 years ago – los amo mucho! I would not be here without y'all and I hope I've made y'all proud.

Thank you everyone!

Table of Contents

List of Figures

Chapter 1: Background

The Cerebrovasculature

The brain is unique in that despite constituting only ~2% of the total body mass, it consumes approximately 20% of the total energy, mostly in the form of oxygen and glucose. This is particularly intriguing given that the brain does not have a reservoir of energy. Therefore, a constant supply of oxygen and nutrients is needed to meet the high energy demands (Iadecola, 2017; Lendahl et al., 2019). To accomplish this, the brain contains a vast network of blood vessels that tightly regulates cerebral blood flow (CBF). The cerebrovasculature is responsible for ensuring proper perfusion of all regions of the brain with an adequate blood supply (cerebral autoregulation) as well as responding to metabolic demands posed by the high energy cost of neuronal activity (functional hyperemia).

The cerebrovasculature is also responsible for protecting the particularly vulnerable neurons of the brain. At the level of capillaries, where most of nutrient exchange occurs across all vascular beds, the cerebrovasculature exhibits highly specialized barrier properties and forms what is known as the blood-brain barrier (BBB). The BBB is particularly important for restricting passive diffusion of small molecules, removal of pathogens and toxins, and active transport of essential nutrients across the cerebrovasculature (Kaplan et al., 2020). As a result, the BBB is highly selective in the types of molecules that can enter the brain, and this has posed a great challenge in drug development for both the design and delivery of drugs that target the central nervous system (CNS). To date, the failure of most clinical trials for pharmaceuticals that target the brain are thought to be due to lack of BBB permeability (Banks, 2016; Pardridge, 2019).

The specialized characteristics of the cerebrovasculature are essential to maintain proper brain function and differentiate it from vascular beds in other organs. However, these properties

are not intrinsic to the vasculature itself, but rather, a consequence of the unique interactions between the vasculature and the surrounding cells. Neurons, glia, and other perivascular cells help shape these specialized properties of the cerebrovasculature, though the precise mechanisms for development and maintenance of the cerebrovasculature as well as how neurons and the cerebrovasculature communicate (neurovascular coupling, NVC) are still mostly unknown (Kaplan et al., 2020).

Development of the cerebrovasculature and blood-brain barrier

The vascular endothelium comprises the inner wall of all blood vessels, which are essential for transporting blood and thereby delivering oxygen and glucose to different organs. While the vasculature is continuous throughout the whole body, each organ has a distinct vascular bed with specialized characteristics to meet the demands of that specific tissue.
At its core, all vasculatures are comprised of a single layer of endothelial cells lining the wall of blood vessels and exhibit a phenotypic "zonated" organization ranging from arteries/arterioles to capillaries to venules/veins, referred to as the arteriovenous axis. The respective zones of the arteriovenous axis display distinct functional characteristics: 1) Blood flow is regulated at the level of arteries/arterioles and carry oxygenated blood away from the heart, 2) transport and exchange mechanisms are regulated at the level of capillaries, and 3) immune surveillance and waste clearance are regulated at the level of venules/veins and carry deoxygenated blood towards the heart (Aird, 2007a, 2007b).

At the molecular level, vascular zones display distinct gene expression programs that specify endothelial cell identity (dela Paz & D'Amore, 2009; Wälchli et al., 2023). Endothelial specification of arterial versus venous fate occurs during embryonic development as angioblasts

originating from the mesoderm migrate to form the dorsal aorta. The notochord and floor plate of the neural tube initiate the differentiation cascade by secreting sonic hedgehog which then acts on somites adjacent to migrating angioblasts to release vascular endothelial growth factor (VEGF) and then bind to the VEGF receptor 2 (VEGFR2) expressed on the surface of angioblasts. VEGF signaling leads to activation of the Notch signaling pathway and subsequently leads to arterial specification, including expression of arterial-specific genes like *Efnb2, Bmx,* and *Hey1*. In a subset of angioblasts expressing the transcription factor *Nr2f2,* VEGF and Notch signaling pathways are blocked, and this promotes the specification of venous identity, leading to expression of venous-specific markers like *Ephb4*.

In the development of the cerebrovasculature, these processes are conserved, but brain endothelial cells begin to acquire their specialized properties as they vascularize the neuroectoderm through the processes of angiogenesis and barriergenesis (Wälchli et al., 2023). After angioblasts have begun to migrate and differentiate, they form a primitive perineural vascular plexus around the neural tube and then radially invade to form new blood vessels through the process of angiogenesis. Branching and proliferation of vascular sprouts eventually anastomose to form the capillary bed (Engelhardt, 2003). As the vasculature of the brain is forming, neural progenitor cells secrete important factors to induce the specialized barrier properties. Most notably, canonical Wnt signaling has been shown to be essential for angiogenesis of the CNS vasculature (Daneman et al., 2009). Wnt7a/b ligands are secreted by neural progenitor cells and bind onto Frizzled receptors expressed by endothelial cells. In conjunction with co-receptors such as Lrp5/6, Gpr124, and Reck, Wnt signaling stabilizes β-catenin (*Ctnnb1*) that then translocates into the nucleus to activate transcription of essential barrier components, including the glucose transporter GLUT1 (*Slc2a1*) and the tight junction

protein CLDN5 (*Cldn5*). The BBB localizes to capillaries and begins restriction of paracellular transport through expression of additional junctional and scaffolding proteins such as occludin (*Ocln*) and tight junction protein 1 (*Tjp1*), thereby preventing most molecules that would normally diffuse into the tissue from entering the brain. Instead of relying on traditional diffusion mechanisms, the BBB acquires a rich and extensive gene expression pattern of transporters that regulate the import (e.g. *Slc2a1* and *Slc7a5*) and export (e.g. *Abcb1a* and *Abcg2*) of specific molecules (Langen et al., 2019). Recent work has also shown that the docosahexaenoic acid transporter (DHA), MFSD2A, is essential for proper development of the BBB by inhibiting transcytosis via suppression of caveolae vesicular trafficking. Importantly, *Mfsd2a* is specifically expressed by brain endothelial cells in capillaries and deletion of *Mfsd2a* in mice has shown to cause microcephaly as well as BBB leakage via increased transcytosis (Andreone et al., 2017; Ben-Zvi et al., 2014; Wood et al., 2021). Homozygous inactivating mutations of *MFSD2A* in humans cause autosomal recessive primary microcephaly, a neurodevelopmental disorder with severe intellectual disability (Guemez-Gamboa et al., 2015; Khuller et al., 2021), likely due to inefficient transport of DHA into the brain and improper development of the BBB. The active suppression of transcytosis along with the restriction of paracellular transport and specialized expression of transporters on brain endothelial cells collectively highlight the unique barrier properties of the cerebrovasculature which are acquired during development.

Gene expression patterns of brain endothelial cells

Though the functional specialization of brain endothelial cells has been appreciated for several decades, the underlying molecular constituents that define these cells at a genome-wide level both in development and adulthood had not been fully explored until recently (Hupe et al.,

2017; Vanlandewijck et al., 2018). Using translating ribosome affinity purification (TRAP) (Heiman et al., 2014, 2008) to genetically tag polysomes of all endothelial cells, Hupe et al. identified unique molecular signatures of brain endothelial cells compared to other organs across multiple stages of mouse embryonic development. While this work demonstrated several brain endothelial cell-specific transcription factors to be associated with BBB formation and maturation, it lacked the resolution to resolve known heterogeneity of the vasculature. By combining a transgenic reporter line for brain endothelial cells with single cell RNA-sequencing (scRNA-seq), Vanlandewijck et al. reported for the first time a molecular atlas of the adult mouse brain vasculature that captured the functional heterogeneity of endothelial cells as described by the arteriovenous hierarchy. Known "zonated" genes such as *Bmx, Efnb2, Sema3g* in arterioles, *Mfsd2a* in capillaries, and *Nr2f2* and *Vcam1* in venules were confirmed by scRNA-seq, but additional highly specific markers were identified not only as specific to zones but also specific to brain endothelial cells. Importantly though, this study demonstrated that much like the architectural organization of the cerebrovasculature, the transcriptional programs of brain endothelial cells exhibit a gradual, continuous shift along the arteriovenous axis.

The mouse cerebrovasculature atlas provided a much-needed molecular landscape to further our understanding of brain vascular biology. However, species-specific differences even across mammals are to be expected and could perhaps account for some of the observed differences in drug transport between animal models and humans (Deo et al., 2013; Syvänen et al., 2009). Most recently, our work and others have generated molecular atlases of the human cerebrovasculature and identified key differences in gene expression patterns between mice and humans, as described extensively in subsequent chapters (Garcia et al., 2022; Winkler et al.,

2022; Yang et al., 2022). These studies provide important insights into what uniquely defines human brain vasculature cell types and the relevance to human disease.

Role of mural cells in development and function of the cerebrovasculature

Sitting on the basement membrane of endothelial cells are a class of cells known as mural cells, which includes both vascular smooth muscle cells (VSMCs) and pericytes. VSMCs are located on larger caliber vessels whereas pericytes are located on capillaries. Particularly in arteries and arterioles, the abluminal surface of blood vessels is almost completely enwrapped by VSMCs; in contrast, venule, vein, and capillary mural cells display distinct morphologies with less surface coverage (Lendahl et al., 2019). Functionally, both VSMCs and pericytes display contractile properties (Fernández-Klett et al., 2010), though whether pericytes actually regulate capillary cerebral blood flow (CBF) remains a controversy. This question is of particular importance given that ~85% of the cerebrovasculature is comprised of capillaries (Sweeney, Kisler, et al., 2018) and correspondingly, pericytes account for the majority of mural cells in the brain. *In vivo* optical imaging techniques have demonstrated evidence to support both hypotheses. On one hand, pericytes, defined by lack of smooth muscle actin, *Acta2*, expression, were shown to not affect microvessel diameter or CBF after optogenetic or whisker stimulation at various parts of the capillary bed (Hill et al., 2015). In contrast, similar optogenetic experiments as well as ablation experiments of individual pericytes have shown that capillary pericytes do regulate CBF though with slower kinetics compared to upstream mural cells (Hartmann et al., 2021). It has been suggested that the confounding evidence for the contractile properties of pericytes and influence on CBF may be in part due to the subtype of pericyte interrogated in the respective experiments (Attwell et al., 2016). Several works have

demonstrated that pericytes are morphologically heterogenous along the capillary bed, with pericytes proximal to large vessels displaying distinct structures compared to those more distal, deep within the capillary network. “Mesh” pericytes display extensive number of processes that engulf blood vessels and are localized closer to pre-capillary arterioles and on lower branch order capillaries; whereas, “thin-stranded” pericytes have fewer processes, typically along the long axis of the blood vessel, and localize on higher branch order capillaries.

Nevertheless, pericytes are essential for normal cerebrovascular function as they interact closely with the endothelium and play important roles in development to establish the BBB. Endothelial cells secrete platelet-derived growth factor (PDGF-B) to recruit PDGF receptor-β (PDGFR-β)-expressing pericytes onto the basement membrane. While *Pdgfb* and *Pdgfrb* null mice are perinatally lethal, experiments performed on adult viable, pericyte-deficient mice has shown that loss of pericyte coverage leads to increased BBB permeability to many low- and high-molecular weight tracers and alters the gene expression profiles of brain endothelial cells (Armulik et al., 2010; Hellström et al., 1999). Additional work in neural crest-derived pericytes has shown that the transcription factor *Foxf2* is required for proper pericyte differentiation and development of the BBB via PDGFR-β and transforming growth factor (TGFβ) signaling (Reyahi et al., 2015).

At a molecular level, while anatomically distinguishable, VSMCs and pericytes share similar gene expression programs and thus, remain poorly defined. *ACTA2* is well-accepted to be a marker of VSMCs; however, traditional markers for pericytes like *PDGFRβ* or *CSPG4* are not specific enough and are also expressed by VSMCs and oligodendrocyte precursor cells (OPCs), respectively. Additional markers described for VSMCs and pericytes include CD13 (*ANPEP*) and CD146 (*MCAM*) though their precise role in mural cell subtypes has not been extensively

explored (Smyth et al., 2018). Work using scRNA-seq has demonstrated that VSMC gene expression shows little heterogeneity across different organs in contrast to pericytes, which display a greater degree of organotypicity (Muhl et al., 2020). Furthermore, unlike endothelial cells, mural cells do not display gradual phenotypic zonation at the gene expression level along the arteriovenous axis. In the brain, VSMCs and pericytes exhibit distinct gene expression patterns despite having some overlap in functional properties (Garcia et al., 2022; Vanlandewijck et al., 2018). This could in part be due to the developmental origin of mural cells since VSMCs are derived from the mesoderm whereas, brain pericytes are mostly derived from the neural crest (Armulik et al., 2011).

Astrocytes in blood-brain barrier maintenance and neurovascular coupling

While endothelial cells and mural cells form the core cellular components of all blood vessels, it is clear that the specialized properties of the cerebrovasculature originate in part due to the interaction with brain cell types, as previously described. The majority of cells in the brain are glia, which includes astrocytes, oligodendrocytes, OPCs, and microglia. Astrocytes are particularly important in the context of cerebrovascular biology given that they directly interact both with the vasculature through extension of their end-feet and with neurons at the level of the synapse ("tri-partite synapse") (Abbott et al., 2006).

In the context of the BBB, astrocytes mature and tile the cerebrovasculature postnatally with their end-feet. Therefore, they are not necessary for induction of BBB properties, but numerous studies have shown that they are essential for maintenance in the adult. BBB damage from astrocyte ablation causes downregulation of tight junction proteins and leads to leakage of small molecules and large plasma proteins, like fibrinogen (Heithoff et al., 2021). In addition,

astrocytes serve as the major regulator of water homeostasis through their contact with the vasculature and the polarized expression of aquaporin-4 (AQP4), the predominant water channel in the brain, at end-feet (Vandebroek & Yasui, 2020). This role has drawn considerable attention after the discovery of the "glymphatic" system which describes the clearance of brain interstitial fluid along paravascular routes formed by astrocytic end-feet and mediated in part through the action of AQP4 channels (Iliff et al., 2012).

Most notably, though, astrocytes have been studied as mediators of NVC. During brain activity, neurons release neurotransmitters and K^+ into the extracellular space in close proximity to astrocyte processes which induces an intracellular astrocytic Ca^{+2} signal partially mediated by activation of astrocyte metabotropic glutamate receptors. The Ca^{+2} signal propagates down end-feet on arterioles and activates Ca^{+2}-sensitive large conductance K^+ channels, including KCNMA1, to locally release K^+ in the vicinity of VSMCs and consequently, modulate vascular tone (Filosa et al., 2006; Girouard et al., 2010). The degree and polarity of these astrocytic Ca^{+2} signals have been shown to modulate the levels of perivascular K^+ release, and thus modulate the vasoactive response of VSMCs, both dilatory and constrictive. Importantly, astrocytes can also release ATP that acts on purinergic receptors, P2Y1, expressed on mural and endothelial cells to exert vasoactive effects via activation of endothelial nitric oxide synthetase (eNOS) (Toth et al., 2015). Interestingly, NVC in the barrel cortex has also been shown to be partially mediated by arteriolar caveolae and is independent of eNOS signaling. In particular, ectopic expression of MFSD2A in arteriolar endothelial cells partially attenuates NVC by inhibiting formation of caveolae (Chow et al., 2020). At a gene expression level, a recent study utilized chemogenetics and RNA-sequencing to demonstrate that glutamatergic neuronal activity modulates BBB efflux transporter, including p-glcyoprotein (*Abcb1a*), Mrp4 (*Abcc4*), *Abca3,* and *Abcd4,* and circadian

clock, including *Dbp, Tef,* and *Hlf,* gene expression and function (Pulido et al., 2020). The observation of circadian gene regulation is of particular interest given the diurnal rhythms in waste clearance and the role of astrocytes in the aforementioned glymphatic system.

Central nervous system fibroblasts are distinct brain cell types along the cerebrovasculature

Single-cell technologies have enabled unbiased profiling of CNS cell types to uncover cell type-specific transcriptional programs and define specialized populations of cells (Saunders et al., 2018; Zeisel et al., 2018). These studies along with others have demonstrated the presence of distinct fibroblast populations both in the meninges and perivascular spaces within the brain parenchyma, but only until recently have studies emerged to begin understanding the physiological role of these cell types in the brain (DeSisto et al., 2020; Vanlandewijck et al., 2018). The small amount of work on CNS fibroblasts have implicated them in fibrotic scarring during injury (Dorrier et al., 2021; Månberg et al., 2021) and also as playing important roles in the production of essential extracellular matrix (ECM) proteins (Farbehi et al., 2019).

The meninges is comprised of three protective membranes that surround the brain: the dura, arachnoid, and pia maters. Distinct populations of meningeal fibroblasts with specific gene markers have been identified in each of the layers during development. For example, pial fibroblasts differ from arachnoid and dural fibroblasts by their expression of markers like *S100a6* and *Ngfr* (DeSisto et al., 2020; Dorrier et al., 2022). These fibroblasts in particular are localized on non-fenestrated blood vessels within the pia and continue to be present even as pial arteries invade into the brain parenchymal space. Using two-photon live imaging with *Col1a1*-GFP mice to label fibroblasts *in vivo*, studies have shown that meningeal and perivascular fibroblasts have similar morphology even as the pial vessels enter the brain parenchyma, though whether the

function and gene expression profiles of meningeal versus perivascular fibroblasts are distinct, remains unknown. It has been proposed that CNS fibroblasts can also play a role in glymphatic clearance, though further work is needed to elucidate precise functions of these recently described cell populations (Mastorakos & McGavern, 2019; Rasmussen et al., 2022).

Emerging studies on cerebrovascular interactions with glial cell types

Advances in sequencing and imaging technologies have enabled the dissection of cellular and molecular mechanisms at higher resolution. Furthermore, the increased recognition of cerebrovascular interactions in normal health and disease and the importance of understanding the contributions of distinct cell populations has prompted many avenues of research to understand cerebrovascular biology at a cell type-specific level. This has extended beyond the traditional scope of cell types involved in BBB formation and maintenance (mural cells and astrocytes) and neurovascular coupling (astrocytes and neurons) into lesser studied cell types in the context of the cerebrovasculature, including microglia, oligodendrocytes, and OPCs.

Microglia are the resident immune cell type of the brain, originating from the embryonic yolk sac, which then migrate into the neuroepithelium by crossing the pial surface during development and populate the brain. As an immune cell, much of what is known about microglia has been studied in the context of diseased states rather than normal physiological function (Li & Barres, 2018; Salter & Stevens, 2017). Less is known about the homeostatic roles of microglia, though recent works has shown microglia play essential roles in synaptic pruning during development (Stevens & Schafer, 2018). In the context of the cerebrovasculature, only a handful of studies have directly addressed the direct interactions between microglia and the cerebrovasculature (Knopp et al., 2022). Juxtavascular microglia, defined as having 30% or more

of their soma associated with blood vessels, were found to be closely associated with the cerebrovasculature in the first week of mouse postnatal development. This work demonstrated that microglia migrate along blood vessels during development and occupy spaces devoid of astrocytic end-feet. Interestingly, the decrease in migratory behavior of microglia coincided with the maturation of astrocytic end-feet, suggesting perhaps that microglia may play a yet to be identified role in the development of the BBB (Mondo et al., 2020). The precise signaling mechanisms by which microglia interact with the vasculature are still mostly unknown; however, another recent study demonstrated that P2RY12+ microglia communicate with brain endothelial cells in part via pannexin 1, PANX1, channels. Importantly, elimination of microglia lead to capillary dilation and CBF increase, which was recapitulated in both $P2RY12^{-/-}$ and $PANX1^{-/-}$ mice, demonstrating the functional role of cerebrovasculature-associated microglia (Bisht et al., 2021). The observation that microglia modulate CBF during NVC has also been observed in the context of microglia depletion and pharmacological interventions (Császár et al., 2022).

Much like microglia, oligodendrocyte lineage cells, which include oligodendrocytes and OPCs, have been extensively studied outside the context of the cerebrovasculature, though more recent studies have begun to highlight these interactions. OPCs serve as the major reservoir for oligodendrocytes, which are the main source of myelination in the CNS. In the developing mouse brain, OPCs populate the brain in three consecutive waves from separate origins: 1) the medial ganglionic eminence (MGE) and anterior entopenduncular area (AEP), 2) the lateral and caudal ganglionic eminence (LGE and CGE), and 3) the postnatal cortex (Kessaris et al., 2006). Recent works have shown that the cerebrovasculature plays an essential role in the population of OPCs and consequently, the differentiation into mature oligodendrocytes. In particular, OPCs, which only emerge after the establishment of the perineural vascular plexus, have been shown to

utilize the cerebrovasculature as a scaffold for migration during development, in part mediated by Wnt-Cxcr4 signaling (Tsai et al., 2016). Furthermore, the regulation of OPC migration termination and thereby initiation of OPC differentiation into oligodendrocytes, has been shown to occur via the displacement of OPCs by astrocyte end-feet. Astrocyte-derived semaphorins 3a and 6a act as repellent cues for OPCs to detach from the vasculature and begin differentiation (Su et al., 2023).

In this context, oligodendrocyte lineage cell interactions with the cerebrovasculature are essential for proper development; however, the role of these interactions in the adult brain has been less explored. While the majority of energy consumption occurs at synapses in the grey matter, electrical signals must propagate along myelinated axons in the white matter and require a modulated amount of oxygen and glucose (Weber, 2002). Oligodendrocyte myelination demarcates the regions of white matter in the brain, and as such, could potentially mediate communication between the cerebrovasculature and axons. An "axo-vascular" coupling mechanism has been suggested, whereby oligodendrocytes act as sensors of neuronal activity and initiate a signaling cascade in white matter regions to induce vessel dilation via astrocytes (Restrepo et al., 2022).

Cerebrovascular dysfunction in disease

As previously described, cerebrovascular structure and function depend on processes that rely on the close interactions between numerous cell types. The importance of the cerebrovasculature extends across lifespan and as such, is greatly involved in numerous neuro-developmental, -psychiatric, and -degenerative diseases (Guey et al., 2021; Pollak et al., 2018; Sweeney, Kisler, et al., 2018; Sweeney et al., 2019). Furthermore, cerebrovascular diseases,

including strokes, aneurysms, small vessel diseases (SVDs), and vascular malformations (AVMs), are a great burden worldwide being the second leading cause of death, with strokes accounting for a large percentage in both men and women (Tong et al., 2019).

Strokes, including both ischemic (reduction of blood flow) and hemorrhagic (bleeding), are associated with a number of factors including SVDs. Approximately 1.5% of SVDs are hereditary, caused by single-gene mutations (Guey et al., 2021). The most common of the hereditary SVDs is CADASIL (cerebral autosomal dominant arteriopathy with subcortical infarcts and leukoencephalopathy), caused by mutations in the *NOTCH3* gene (Joutel et al., 1996). NOTCH3 mutations lead to protein aggregation along the vasculature (granular osmiophilic materials) and consequently, ischemic white matter lesions, lacunar infarcts, cognitive decline, and dementia. Interestingly, NOTCH3 is predominantly expressed in VSMCs and pericytes, highlighting the primary origin of the disease in the cerebrovasculature. Several mouse transgenic lines have been generated based on the most common mutations, though none of them recapitulate the full spectrum of phenotypes observed in humans (Ayata, 2010). Furthermore, works in induced pluripotent stem cell (iPSC) – derived models have shown a failure in mural cells carrying the *NOTCH3* mutation to stabilize capillary structure (Kelleher et al., 2019). In contrast to CADASIL, CARASIL, the recessive form of the disease, is caused by biallelic missense mutations in the *HTRA1* gene (Hara et al., 2009; Zhang et al., 2022). *HTRA1* is predominantly expressed in astrocytes, so perhaps the mechanisms underlying CARASIL depend on differential roles of astrocytes in relation to the cerebrovasculature (e.g. inflammatory response or glymphatic clearance) as opposed to mural cell dysfunction (J. Chen et al., 2018). Cerebral amyloid angiopathy (CAA) is another form of SVD and closely linked with Alzheimer's disease (AD) (Biffi & Greenberg, 2011; Lendahl et al., 2019), discussed in further

detail below. CAA is characterized by amyloid-β (Aβ) deposits along vessel walls, though not in all cases does Aβ induce pathology. Hereditary forms of CAA have been found in Dutch, Iowa, Arctic, Flemish, and Italian families carrying either duplication or missense autosomal dominant mutation in the *APP* gene (Cabrejo et al., 2006; Sellal et al., 2017). Clinical manifestations include recurrent lobar intracerebral hemorrhaging, seizures secondary to cortical lesions, and premature cognitive impairments (Guey et al., 2021).

Little is known about the role of the cerebrovasculature and BBB in neuropsychiatric disorders. The evidence for BBB impairment has mostly come from cerebrospinal fluid (CSF)/blood measurements or post-mortem human studies in schizophrenic individuals. The leading hypothesis for the interaction between BBB function and schizophrenia implicates immune dysfunction. Genome-wide association studies (GWAS) of schizophrenia have identified several immune-related genetic loci (Schizophrenia Working Group of the Psychiatric Genomics Consortium, 2014) that support the role of microglia and neuroinflammation in the pathophysiology of the disease. Furthermore, elevated levels of reactive oxygen species and cytokines, including interleukins-1α, -1β, -6, and tumor necrosis factor α, have been found in blood samples of individuals with schizophrenia. Coupled with the increased CSF:blood ratio of albumin, these studies collectively implicate BBB permeability as a potential contributor to the progression of the disease. In addition, more than 1000 single nucleotide polymorphisms (SNPs) have been identified that could potentially alter the substrate specificity of p-glycoprotein, the predominant efflux transporter expressed on the cerebrovasculature. Given that many antipsychotics, including risperidone, aripiprazole, and paliperidone, are potent substrates of p-glycoprotein whereas clozapine and quetiapine act as inhibitors, the role of the cerebrovasculature in schizophrenia and other psychiatric disorders may be of great importance

for the development of suitable therapies. However, much is still unclear about the exact roles the cerebrovasculature plays. For example, unlike cerebrovascular and neurodegenerative diseases, it is unclear whether BBB dysfunction precedes psychosis or if the degree of BBB dysfunction affects the disease progression (Pollak et al., 2018). However, given the growing evidence for the important roles the cerebrovasculature plays in other neurological diseases, it is likely that more attention will be given into studying these interactions in the context of neuropsychiatric disorders.

The next section provides a thorough review on the role of the cerebrovasculature in neurodegenerative diseases, which has provided a framework for rethinking approaches for not only studying these diseases but also approaches for developing interventions.

The Cerebrovasculature in Neurodegeneration

An interesting phenomenon across the neurodegenerative diseases is that specific populations of neurons in particular brain regions are preferentially affected, often referred to as enhanced or selective vulnerability (Fu et al., 2018). For example, in Alzheimer's disease (AD), pyramidal neurons of the entorhinal cortex and hippocampus are more vulnerable, whereas, in Parkinson's disease (PD) and Huntington's disease (HD) it is the dopaminergic neurons of the substantia nigra and medium spiny neurons (MSNs) of the striatum, respectively. Accumulation of a pathological protein (Aβ and tau in AD, α-synuclein in PD, and mutant huntingtin in HD) in these vulnerable neurons is often a hallmark of the disease that leads to cytotoxicity, cell death, and progression of degeneration. Interestingly, the expression of these toxic proteins is not restricted to the vulnerable neuronal populations and in fact, is present across many different

neuronal and non-neuronal cell types. The exact mechanisms of how these toxic proteins lead to selective degeneration of specific neurons are still being understood.

Despite the selective vulnerability of neurons, a common feature across the neurodegenerative diseases is cerebrovascular dysfunction. CBF alterations, impaired cerebrovascular reactivity, and impaired neurovascular coupling have been shown in AD but recent research has begun to show that this is also present in PD, HD, amyotrophic lateral sclerosis (ALS), and multiple sclerosis (MS) (Sweeney, Kisler, et al., 2018; Sweeney et al., 2019). Interestingly, these changes to the cerebrovasculature occur at early stages in disease progression and often precede the onset of disease-specific phenotypes. Whether these changes contribute significantly or is causal to the disease progression, however, remains an open question.

At the cellular and molecular level, BBB breakdown is a shared characteristic and follows similar trends across the neurodegenerative diseases. This includes dysregulation of essential genes for BBB integrity like tight junction proteins and transporters, including CLDN5, p-glycoprotein, and GLUT1, which consequently leads to corresponding functional consequences including, impaired barrier function, reduced waste clearance, and decreased transport function of essential nutrients. Importantly, the impaired barrier function allows for extravasation of inflammatory signals, such as cytokines and chemokines, to promote further breakdown and degeneration. Most recently, research in AD and normal aging has shown that BBB breakdown involves not only the paracellular route, which includes tight junction proteins, but also the transcellular route. In particular, increased rates of transcytosis and a decrease in the caveolae-inhibiting transporter, *MFSD2A*, have been shown to occur during normal aging (Yang et al., 2020). Overall, with the increasing number of profiling studies both in humans and in

animal models of neurodegeneration, the precise mechanisms of cerebrovascular and BBB dysfunction are being better understood and will provide key insights into new approaches for development of therapeutic interventions (Garcia et al., 2022; Yang et al., 2022).

Cerebrovascular dysfunction in vascular dementia, Alzheimer's disease, and normal aging

There is a longstanding recognition that vascular dementia and AD share a lot of the hallmark pathologies, and refinement of the terminology that delineates the two has considerably evolved over the past several years (Bir et al., 2021; Iadecola, 2013; O'Brien & Thomas, 2015). Though vascular dementia is considered the second leading cause of dementia after AD, the terminology itself is controversial given that vascular pathologies are heterogenous in nature and cover a broad spectrum of insults that can cause cognitive impairments to different degrees. In fact, DSM-V modifications have now removed the necessity of memory impairment as a criterion for dementia, and correspondingly, the nomenclature "vascular cognitive impairment" (VCI) has been proposed as a more unifying term to encompass the different contributors of the disease.

As previously discussed, in the context of hereditary cerebrovascular diseases (i.e. CADASIL, CARASIL, and familial CAA), the contributions of the cerebrovasculature to vascular dementia are more clear (Ayata, 2010; Cabrejo et al., 2006; Hara et al., 2009). In addition, infarctions to large vessels are more indicative of a primary vascular pathology and thus, a clear diagnosis of VCI. However, the contribution of small vessel insults to cognitive impairment are more heterogenous and the presence in both VCI and AD has made differential diagnoses more challenging. This is particularly true in early stages of disease where dysfunction of the cerebrovasculature presents itself as subtle leaks that can be detected through the usage of

dynamic contrast-enhanced (DCE) magnetic resonance imaging (MRI) with gadolinium tracers (Barisano et al., 2022; Montagne et al., 2015; Nation et al., 2019). Genetic studies have provided key insights into the risk factors associated with both VCI and AD. For example, the *APOE ε4* allele is well-established as an increased susceptibility gene for AD but not for sporadic VCI (Verghese et al., 2011). Nevertheless, many of the top GWAS hits for AD have been shown to exhibit high levels of expression in the cerebrovasculature, highlighting the potential contributions of the cerebrovasculature in driving disease (Yang et al., 2022).

At the cellular and molecular level, many lines of evidence highlight the early changes of the cerebrovasculature, particularly in AD. Neuroimaging studies have revealed that both diminished glucose transport (as shown by fluorodeoxyglucose-PET) and p-glycoprotein function (as shown by verapamil-PET) in the hippocampus are observed in early and mild forms of AD, respectively. The decrease in glucose transport could be in part due to the observed reduction in GLUT1 levels using human *post mortem* tissue analyses. This methodology has also shown reduced levels of tight junction proteins and alterations to the capillary basement membrane as well as loss of pericyte coverage and numbers in the cortex and hippocampus (Sweeney, Sagare, et al., 2018). Most recently, a human atlas of the cerebrovasculature in AD has implicated ECM-maintaining pericytes as selectively vulnerable and suggests an evolutionary transfer of AD risk genes from microglia to cerebrovascular cell types (Yang et al., 2022). Furthermore, iPSC-derived models of the BBB have dissected potential mechanisms of dysfunction in *APOE ε4* carriers. In particular, inhibition of calcineurin-NFAT signaling was shown to reduce the CAA pathology recapitulated *in vitro*. In addition, *in vivo* administration of cyclosporine A, an inhibitor of calcineurin/NFAT signaling, into *APOE ε4* mice demonstrated reduced *APOE* expression and vascular amyloid. Given that both APOE and NFAT are highly

expressed in pericytes, collectively these studies implicate pericytes as both potential drivers of disease pathology and therapeutic targets.

Cerebrovascular dysfunction in Parkinson's disease, ALS, and multiple sclerosis

PD is the second most common neurodegenerative disease after AD, and as mentioned previously, preferentially affects the dopaminergic (DA) neurons of the substantia nigra pars compacta (SNpc) in the midbrain. In particular, DA neurons projecting to the basal ganglia and involved in locomotion display a high degree of vulnerability and degenerate preferentially. Familial forms of the disease have been linked to autosomal dominant mutations in *SNCA, LRRK2, ATXN2, ATXN3, MAPT, GCH1, DCTN1* and *VPS35* (Houlden & Singleton, 2012). In the context of the cerebrovasculature, several neuroimaging and post-mortem studies have demonstrated alterations in the affected brain regions of PD. For example, diminished p-glycoprotein function detected by verapamil-PET imaging has been observed in the mid-brain of PD individuals as well as increased leakage of gadolinium tracer by DCE-MRI in the basal ganglia. Furthermore, increased endothelial cell number in the SNpc and increased endothelial integrin αvβ3 expression in the SNpc, locus coeruleus, and putamen have been observed in *post mortem* human tissue (Sweeney, Sagare, et al., 2018).

Similarly, cerebrovascular dysfunction has been observed in the affected regions of ALS and multiple sclerosis (MS). ALS, which preferentially affects motor neurons of the spinal cord and motor cortex, exhibits reduced pericyte coverage in the cervical spinal cord as well as enlarged perivascular spaces in the medulla, cervical and lumbar spinal cord (Sweeney, Sagare, et al., 2018). Most recently, the enlargement in perivascular spaces has been linked with dysfunction of perivascular fibroblasts in pre-symptomatic stages of both humans with sporadic

ALS and mouse models. In particular, marker proteins of perivascular fibroblasts, SPP1 and COL6A1, were found to accumulate in perivascular spaces and associated changes to vascular gene expression preceded even the early microglial response (Månberg et al., 2021). In contrast, MS, which is an autoimmune demyelinating disease and thus, affects predominantly white matter regions, also displays enlarged perivascular spaces, but these changes may be due more to observed increases in leukocyte infiltration and degradation of tight junction proteins in these regions. Indeed, immune cells have been found in these enlarged perivascular spaces within MS patients (Lendahl et al., 2019; Sweeney, Sagare, et al., 2018).

Cerebrovascular dysfunction in Huntington's disease

Across the neurodegenerative diseases, vascular changes are often confounded with other disease-related characteristics. For example, AD has a heterogeneous etiology and is often confounded with VCI and CAA; additionally, MS has a known autoimmune component that is known to affect the vasculature. Unlike these diseases which have multiple disease associated genetic risk factors, HD is caused by a mutation in the huntingtin (*HTT*) gene and follows an autosomal dominant inheritance pattern (Macdonald, 1993). The mutation arises as an expanded CAG tract in exon 1 of the gene which leads to translation of a toxic mutated huntingtin (mHTT) protein. The trinucleotide repeat sequence has been well established to be inversely correlated with age-of-onset (Andrew et al., 1993). In humans, the normal CAG repeat length ranges from 10-35 repeats, whereas in HD patients, repeat length can range from 36-121 or more repeats. Individuals in the 27-35 range are not considered at risk to developing symptoms. However, due to the somatic instability in the repeat sequence, individuals in this range are at risk of having children with an expanded sequence within the disease-causing range. Furthermore, individuals

in the 36-39 range are considered to have reduced penetrance of the disease and may or may not develop symptoms (Kay et al., 2017). Somatic instability in HD has been shown in both humans and mouse models to be associated with the mismatch repair pathway, including *MSH3* and *MSH2* which are highly expressed in neurons and correlates well with evidence demonstrating that the instability is greater in neurons compared to glia (Gonitel et al., 2008; Shelbourne et al., 2007). The link between somatic instability and selective vulnerability of striatal neurons is of particular interest given recent human genetic and transcriptomic studies which identified age-of-onset modifiers in loci close to mismatch repair genes, including *MSH3*, *MSH2*, and *FAN1* (Genetic Modifiers of Huntington's Disease (GeM-HD) Consortium, 2019), and demonstrated that the DNA mismatch repair pathway is upregulated in both direct- and indirect-pathway spiny projection neurons (dSPNs and iSPNs) (H. Lee et al., 2020).

As previously mentioned, HTT is ubiquitiously expressed but preferentially affects the MSNs (also referred to as SPNs) that reside in the basal ganglia, primarily the neostriatum. Both the caudate nucleus and putamen are considerably affected at early stages, though cortical atrophy is also observed at late stages of the disease. Neuropathological severity is classified on a grading scale ranging from 0-4 with grade 1 and 4 exhibiting 50% and 95% loss of striatal neurons, respectively. Furthermore, astrogliosis is another neuropathological characteristic that arises later in the disease progression (Vonsattel et al., 1985). The precise mechanisms by which mHTT leads to degeneration are not well understood, though studies have demonstrated both gain-of-function toxicity and loss-of-function effects and that iSPNs display a higher vulnerability compared to dSPNs (Reiner et al., 1988). Most recently, a genome-wide *in vivo* synthetic lethality screen identified modifiers of mHTT toxicity and validated *Nme1* as a suppressor that can ameliorate HD phenotypes *in vivo* when overexpressed (Wertz et al., 2020).

Furthermore, human and mouse model transcriptional studies utilizing TRAP and snRNA-seq have revealed that early gene expression changes in the vulnerable SPNs implicate mitochondrial dysfunction in the activation of innate immune signaling (H. Lee et al., 2020).

In the cerebrovasculature, basal ganglia perfusion deficits and other neurovascular abnormalities have been documented in both pre-symptomatic and symptomatic patients with HD since the 1980s and 1990s (Garnett et al., 1984; Harris et al., 1999; Lin et al., 2013; Vis et al., 1998). Similar findings have also been shown in both human and mouse models of HD with more recent advanced imaging approaches (Cepeda-Prado et al., 2012; J. J. Chen et al., 2012; Franciosi et al., 2012; Hua et al., 2014; Wolf et al., 2011). However, only until recently has attention been given into understanding the underlying cellular and molecular mechanisms of cerebrovascular dysfunction in HD and its contributions to both the pathogenesis and progression of the disease. Studies have shown that BBB breakdown in the striatum is marked by a decrease in tight junction proteins, similar to other neurodegenerative disorders, as well as an increase in small vessel density and reduced vessel diameter (Di Pardo et al., 2017; Drouin-Ouellet et al., 2015; Liu et al., 2021). In addition, increased pericyte number and activation marked by expression of RGS5 and NG2 were found to occur in early stages of disease progression within the R6/2 mouse model of HD (Padel et al., 2018). Importantly, these vascular changes in animal models preceded the onset of both behavioral abnormalities and neuronal dysfunction. Most recently and discussed in further detail in Chapter 3, our own single-cell study in human HD patients has characterized gene expression changes in endothelial, mural, and fibroblast cell populations associated with innate immune activation and BBB dysfunction (Garcia et al., 2022).

Advances in Next-Generation Sequencing Technologies and Cell Type-Specific Tools

Differential roles of distinct cell populations in normal brain function as well as the previously described selective vulnerability in disease has made the disentanglement of cell type-specific mechanisms an important consideration in studying the brain. The advancement of next-generation sequencing (NGS) platforms, in particular single-cell technologies (Macosko et al., 2015), and novel genetic tools (Chan et al., 2017; Ravindra Kumar et al., 2020) for labeling specific populations has allowed for the dissection of these mechanisms at higher resolutions than previously done. Furthermore, the extension of these approaches across animal models and into humans is facilitating the identification of species-specific differences (Hodge et al., 2019) as well as the development of novel therapeutic approaches for numerous brain diseases and disorders.

Bulk RNA sequencing and translating ribosome affinity purification

Methods for DNA/RNA sequencing have rapidly evolved in the past decade, with increasing number of methodologies being developed for specific purposes. The founding method, Sanger sequencing, developed in 1977 is still employed in modern research, though to a limited extent given the low throughput compared to current NGS technologies. The bulk of modern sequencing strategies rely on Illumina platforms, first developed by Solexa and Lynx Therapeutics. These platforms support many types of protocols including whole genome sequencing, chromatin immunoprecipitation (CHIP) sequencing, RNA sequencing, and others (Slatko et al., 2018).

RNA sequencing has become an indispensable tool for studying differential gene expression patterns and has recently evolved to study various aspects of biology, including cell

type-specific translatome profiling, single cell gene expression, spatial transcriptomics, etc. The advent of more sophisticated technologies in RNA sequencing has been particularly important in studying the brain given the complex cellular composition (Stark et al., 2019). Bulk RNA sequencing approaches *in vivo* or with *post mortem* tissue are difficult to interpret due to the lack of cell type-specific resolution. Discerning the origin of important molecular signatures becomes incredibly difficult and oftentimes the key differential changes can be masked by irrelevant contributions from unaffected cell types. Furthermore, given the lack of high throughput proteomic approaches, transcriptional profiling is often used as a proxy for predicting protein composition, though in reality, RNA and protein levels do not necessarily have a one-to-one correspondence and a large fraction of total RNA includes non-coding transcripts. Recent approaches to address these two issues *in vivo* have employed the usage of mouse transgenic reporter lines to fluorescently tag actively translating ribosomes for immunoprecipitation in specific cell populations. This translating ribosome affinity purification (TRAP) methodology developed by Heiman et al., 2014, 2008, was developed to study the translatome of specific CNS cell types. Since then, many further studies have employed the TRAP methodology to study gene expression patterns in other brain cell types and in the context of disease (Doyle et al., 2009; H. Lee et al., 2020).

Single cell RNA-sequencing and spatial transcriptomics

TRAP-seq and other similar approaches (Sanz et al., 2009) for cell type-specific translatome profiling allow for high resolution interrogation of gene expression programs. However, the necessity of transgenic lines to interrogate specific cell populations is time-intensive and low throughput. Furthermore, only one cell type can be interrogated at a time, and

thus, information about other cells that are likely to have impact on the gene expression profiles is lost. The advent of single cell (Macosko et al., 2015) and single nucleus RNA-sequencing (Habib et al., 2017) approaches allowed for a high throughput approach to interrogate the transcriptional programs of thousands of cells from an individual sample. In particular, snRNA-seq has been heavily employed in the context of human studies due to the compatibility with frozen human *post mortem* tissue, allowing for not only the generation of high resolution molecular atlases, but also the dissection of cell type-specific mechanisms across multiple neurodegenerative diseases (Al-Dalahmah et al., 2020; Garcia et al., 2022; Kamath et al., 2022; H. Lee et al., 2020; Mathys et al., 2019; Yang et al., 2022).

The utility of single-cell transcriptomics has expanded beyond neuroscience and has now become a workhorse in all subfields of molecular and cellular biology. The commercialization of these approaches into companies, most notably 10x Genomics, has allowed for standardization of protocols and accessibility of reagents for labs all over the world. Even so, in complex tissue organs, understanding the organization of cells can provide important insights into cell-cell interactions and the layout of molecules *in situ,* which is lost with traditional RNA- and scRNA-seq approaches. Inspired by lower throughput spatial localization of transcripts using *in situ* hybridization (ISH), many recent spatial transcriptomic technologies have recently been developed to scale up the coverage of the genome that can be interrogated on fixed tissue that preserves the anatomical structure. Notably, seqFISH, MERFISH, and 10x Genomics' Visium technology all provide approaches for visualizing the spatial distribution of transcripts in various types of tissue samples (K. H. Chen et al., 2015; Lubeck et al., 2014; Ståhl et al., 2016).

Non-invasive viral tools for cell type-specific CNS transduction

Recent advances in single-cell and transcriptome profiling technologies has greatly enriched the types of data that can be collected from biological experiments, particularly in the brain and in disease contexts. These protocols have yielded an abundance of molecular resources for further understanding biological mechanisms. Correspondingly, improvements in the development of genetic tools for targeting the CNS has allowed for the testing of promising hypotheses. In particular, directed evolution of adeno-associated viruses (AAVs) that have improved transduction efficiency in the CNS and can be administered non-invasively has enabled for effective forms of *in vivo* gene transfer and gene therapies. Novel viral serotypes derived from the AAV9 capsid, named PHP.eB and PHP.S, have shown to exhibit increased transduction efficiency of neurons in both the brain and spinal cord, respectively (Chan et al., 2017). These AAVs can bypass the BBB and thus, are non-invasive, as they can be administered intravenously at a sufficient dose in a single injection. Furthermore, compared to traditional AAVs which often require high titers, these derivatives are able to achieve high transduction efficiencies at significantly lower doses. When coupled with cell type-specific promoters and enhancers, these tools provide a fast, targeted approach for selectively perturbing distinct cell populations in the CNS of both transgenic and non-transgenic animals. Importantly, recent work using the same directed evolution approach has now resulted in the development of an additional class of AAVs that can effectively transduce neuronal populations in non-human primates (NHPs) (X. Chen et al., 2022), demonstrating the translatability of these tools across species and the promise it holds for future gene therapy approaches to treat neurological disorders.

Summary and Thesis Aims

In this thesis I aim to bridge knowledge gaps in cerebrovasculature structure and function by creating a transcriptomic profile of the human cerebrovasculature in health and neurodegeneration. Using single-nucleus RNA-sequencing (snRNA-seq) and a developed blood vessel enrichment (BVE) protocol, I profile cell types of the human cerebrovasculature from freshly-resected *ex vivo* tissue and *in silico* sorting from frozen *post mortem* tissue samples. Furthermore, I use the same methodology to profile the human cerebrovasculature of patients with Huntington's Disease (HD) using *post mortem* tissue. Finally, I aim to understand cell type-specific mechanisms of cerebrovasculature dysfunction in HD using non-invasive genetic perturbation experiments in HD mouse models.

In the second chapter, I develop a protocol for enriching blood vessels from human and mouse brain tissue and subsequently isolate nuclei to profile cerebrovasculature cell types using snRNA-seq. Freshly-resected *ex vivo* tissue is obtained from epileptic patients undergoing surgical resection through a collaboration with Dr. Mustafa Sahin's laboratory at Boston Children's Hospital (BCH). Similarly, previously sequenced *post mortem* samples from the Religious Order Study and Memory and Aging Project (ROSMAP) in collaboration with Professor David Bennett at Rush University and Professor Li-Huei Tsai at MIT are used as an independent, complementary dataset to the *ex vivo* samples. Datasets are analyzed in collaboration with Professor Manolis Kellis' laboratory at MIT's Computer Science and Artificial Intelligence Laboratory (CSAIL). Finally, validation of key marker genes is performed via immunofluorescence on frozen brain tissue sections followed by pathway analysis to interrogate functional roles of profiled cell types.

In the third chapter, I utilize the same experimental and analysis paradigms to profile cerebrovasculature cell-types from *post mortem* tissue of HD patients (Grades 1-4) and age-matched controls acquired from the NIH NeuroBioBank and University of Alabama at Birmingham. I perform snRNA-seq and differential gene expression analysis to determine transcriptionally dysregulated genes and pathways in HD, focusing on cell types comprising the cerebrovasculature, namely endothelial cells, mural cells, and fibroblasts.

Finally, in the fourth chapter, I develop and characterize a viral construct capable of brain-wide transduction of endothelial cells *in vivo* after a single intravenous injection. I use this adeno-associated virus (AAV) to test casual mechanisms underlying cerebrovasculature dysfunction in HD. Specifically, I utilize this AAV approach to specifically lower levels of *HTT* in brain endothelial cells via a microRNA-mediated mechanism. Following AAV administration into two distinct mouse models of HD (zQ175 and R6/2), I conduct behavioral testing to assess motor phenotypes followed by molecular studies to assess overall therapeutic benefit of this intervention. I demonstrate that a gene therapy strategy targeting the cerebrovasculature and administered at pre-symptomatic stages of the disease is sufficient to delay the disease progression *in vivo*.

In the fifth chapter, I present preliminary data on several on-going projects as future directions. Namely, I discuss the translatability of brain vasculature-targeting AAVs in different disease contexts as well as to uncover basic molecular mechanisms of cerebrovascular-coupling. In particular, I demonstrate the presence of subpopulations of vasculature-coupled cell types in the mouse and human brain and propose strategies for interrogating their distinct transcriptional, structural, and functional programs. Lastly, I demonstrate the feasibility of studying region-specific properties of the brain vasculature through the redesign of the developed viral construct

to target specific brain endothelial organelles, including the mitochondria for proteomics and the ribosome for translatome profiling.

Chapter 2: Molecular Profiling of the Human Cerebrovasculature in Health

The following text and figures have been adapted from previously published work by Francisco J. Garcia and co-authors. For original article, see [Garcia, Francisco J., et al. "Single-cell dissection of the human brain vasculature." Nature 603.7903 (2022): 893-899.]

The cerebrovasculature exhibits specialized barrier properties that regulate the transport of biomolecules and maintain brain homeostasis. Structural imaging and molecular studies have yielded important insights into the mouse cerebrovasculature (Sabbagh et al., 2018; Saunders et al., 2018; Vanlandewijck et al., 2018). However, human brains exhibit increased complexity and energetic needs, likely accompanied by human-specific adaptations, which remain uncharacterized. Moreover, cerebrovascular dysfunction and blood-brain barrier (BBB) breakdown are hypothesized to play important roles not only in aging (Montagne et al., 2015) but also in neurodegenerative diseases (Sweeney, Kisler, et al., 2018; Sweeney et al., 2019). Thus, understanding the human cerebrovasculature, both in physiologic and pathological conditions, is a pressing need for scientific and clinical reasons.

Here, we address this challenge by reporting the first comprehensive single-cell molecular atlas of human cerebrovasculature cells, across ~17,000 nuclei from *ex vivo* freshly-resected surgical human brain tissue using a cerebrovascular cell enrichment protocol, and an *in silico* cell sorting method from *post mortem* human brain tissue. We computationally integrate these datasets to characterize 11 subtypes of cells, including endothelial, mural, and perivascular fibroblast cell subtypes. Our studies reveal unique human-specific transcriptomic signatures along the arteriovenous axis and elucidate transcriptional changes in cerebrovasculature cell types in Huntington's disease (HD). Our study highlights the unique cell type-specific and species-specific characteristics in humans and provides a framework for mechanistic dissection of pathological state dysfunctions.

Ex vivo and *in silico* vasculature enrichment

Owing to low abundance in the brain and poor capture efficiency with droplet-based sequencing methodologies, cerebrovasculature cells have been challenging to characterize at

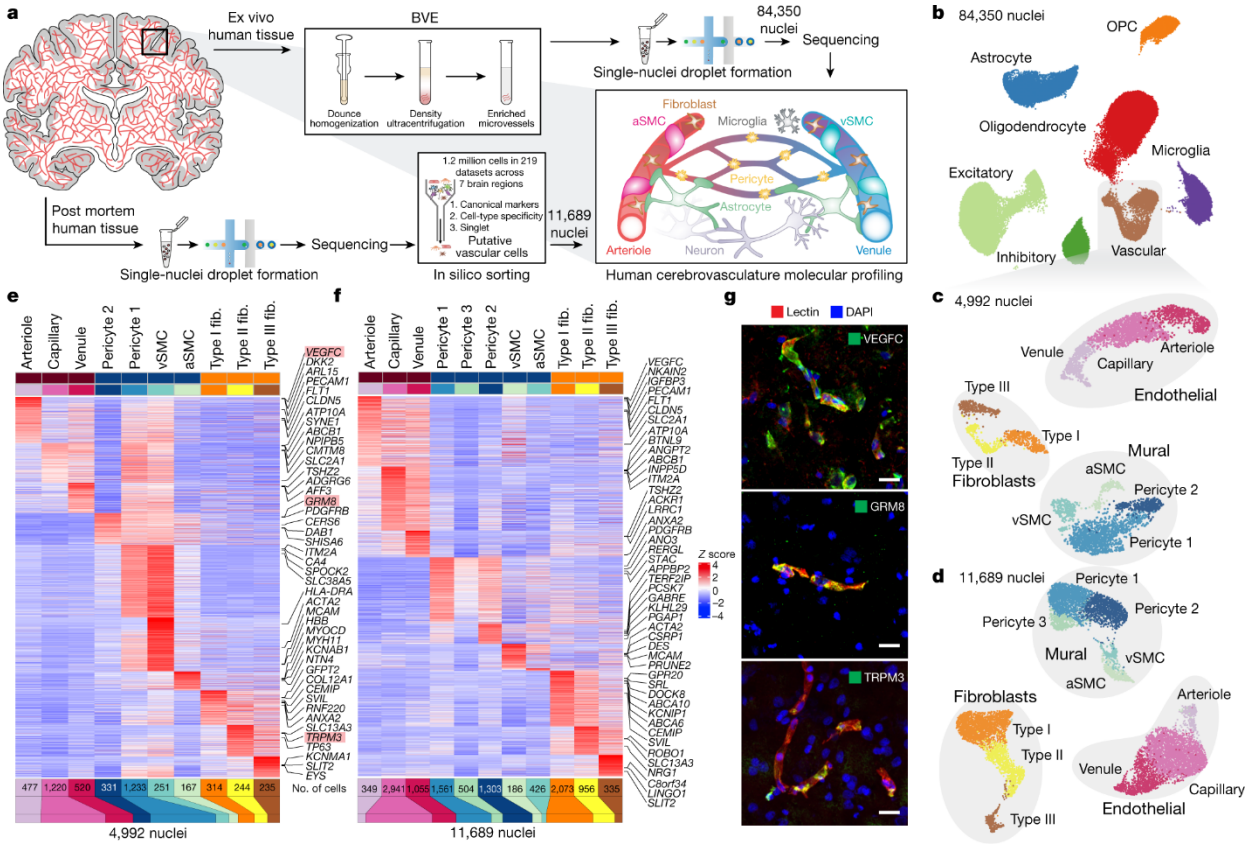

Fig. 1 snRNA-seq profiling of the human cerebrovasculature. a. Experimental schematic. **b**, Global uniform manifold approximation and projection (UMAP) of 84,350 profiled nuclei from *ex vivo* human temporal cortex. OPC, oligodendrocyte precursor cell. **c**, UMAP of 4,992 profiled vascular nuclei from the cluster highlighted in **b**. **d**, UMAP of 11,689 *in silico*-sorted vascular nuclei from *post mortem* human brains. **e**, **f**, Genes expressed at high levels in the subclusters in **c** and **d**, respectively. Fib., fibroblast. **g**, Validation of expression of the markers VEGFC, GRM8 and TRPM3 (highlighted in pink in **e**) by indirect immunofluorescence staining (each in green pseudocolour). Representative images shown from $n = 3$ independent biological replicates for each marker. Brightness and contrast enhanced for visualization. DAPI, 4′,6-diamidino-2-phenylindole. Scale bars, 20 μm.

single-cell resolution. Previous studies in mice have used transgenic reporter lines and fluorescence-activated cell sorting to enrich for cerebrovasculature cells, but these methods are

incompatible with human studies (Vanlandewijck et al., 2018). To address this challenge, we developed a blood vessel enrichment (BVE) protocol (**Fig. 1a**, top) to enrich for human vascular cell types from fresh and frozen brain tissue for single-cell applications by dextran-based density ultracentrifugation (Y.-K. Lee et al., 2019), and used the resulting microvessel-enriched pellet as input for single-nucleus RNA-seq (snRNA-seq) profiling (Mathys et al., 2019). We validated our protocol using mouse cortical samples, showing enrichment for markers of endothelial and mural cells (**Extended Data Fig. 1a**), and no enrichment for other cell types. However, we found that our purification captured astrocytic endfeet (Y.-K. Lee et al., 2019), as they remain attached to the vasculature post-enrichment (**Extended Data Fig. 1b**).

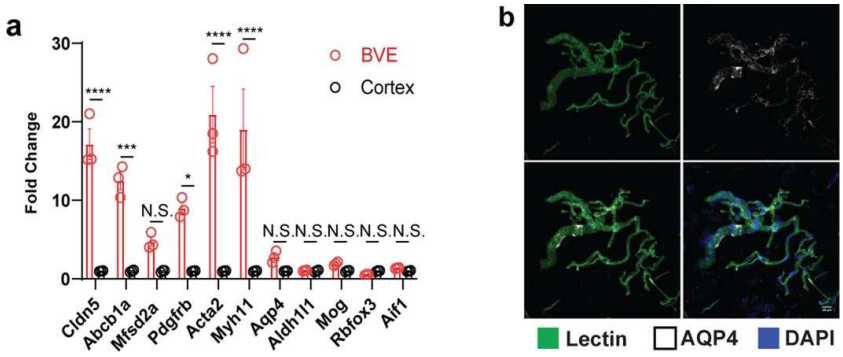

Extended Data Fig. 1. Validation of Blood Vessel Enrichment (BVE) protocol. a. qPCR of canonical cell type markers for endothelial *Cldn5* ($p < 0.0001$), *Abcb1a* ($p = 0.0002$), *Mfsd2a* ($p = 0.9556$), mural *Pdgfrb* ($p = 0.0388$), *Acta2* ($p < 0.0001$), *Myh11* ($p < 0.0001$), astrocytes *Aqp4* ($p > 0.9999$), *Aldh1l1* ($p > 0.9999$), oligodendrocytes *Mog* ($p > 0.9999$), neurons *Rbfox3* ($p > 0.9999$), and microglia *Aif1* ($p > 0.9999$) from mouse cortex, ordinary one-way ANOVA, $*p < 0.05$, $**p < 0.01$, $***p < 0.001$,$****p < 0.0001$, n.s. = not significant. Error bars denote standard deviation of the mean from $n = 3$ independent biological replicates. **b**. Representative immunofluorescence of blood vessels enriched from mouse cortex using the BVE protocol. $n = 3$ independent biological replicates for immunostaining. Brightness and contrast enhanced for visualization. Scale bar, 20 μm.

We applied our BVE protocol to *ex vivo* fresh-frozen tissue from 17 temporal lobe surgical resections of patients with intractable epilepsy, selecting only healthy tissue distal to epileptic foci (**Supplementary Table 1**), thus providing samples free from hypoxia and death-

induced effects, and avoiding the decreased RNA quality associated with long *post mortem* intervals. For seven samples, we used standard snRNA-seq (H. Lee et al., 2020) to confirm the absence of BVE-induced biases (**Extended Data Fig. 2a, b**). We next complemented our BVE-captured dataset with *in silico* sorting of data from *post mortem* samples across seven different brain regions from control individuals without neurological pathology as part of the Religious Orders Study and Rush Memory and Aging Project (ROSMAP) cohort and reported here (Bennett et al., 2018). We used a combination of canonical vasculature markers and whole-transcriptome cellular signatures, separately from our BVE protocol, to ensure independence (**Fig. 1a**, bottom, Methods).

After quality control, from the *ex vivo* samples, we obtained 84,350 single nuclei (**Fig. 1b** and **Extended Data Fig. 2c–e**), including 16 subtypes of excitatory neurons, 6 subtypes of inhibitory neurons, oligodendrocytes, oligodendrocyte precursor cells, astrocytes and microglia. From the *ex vivo* samples, we also profiled 4,992 vascular cells, a 13.7-fold enrichment from previous studies (Mathys et al., 2019) (5.48% versus ≈0.4%), and complemented this with 11,689 cells sorted *in silico*. We distinguished 11 subtypes of vascular cells (**Fig. 1c, d**), including (*ex vivo/in silico*): 3 subtypes of endothelial cells (n = 2,217/4,345); 5 subtypes of mural cells (n = 1,982/3,980), including 1,564/3,358 pericytes and 418/622 smooth muscle cells (SMCs); and 3 subtypes of perivascular fibroblasts (n = 793/3,364). Most cerebrovascular subtypes in the *ex vivo* BVE dataset were also found in our *post mortem in silico*-sorted dataset, validating the consistency of cell types across experimental platforms and sample cohorts. Pericytes exhibited greater heterogeneity in the *in silico*-sorted dataset (3 versus 2 subtypes), although this may be due to a larger number of profiled cells compared to the *ex vivo* dataset.

Genes and pathways defining cell types

We next created an atlas of human cerebrovascular cells and revealed their defining molecular characteristics by combining our experimental and computational enrichment strategies. We found robust expression of 17,212 genes (each in 50+ cells), including 3,164 differentially expressed genes among cell types (ctDEGs) in *ex vivo* and 3,470 ctDEGs in *post mortem* datasets, which expanded the previously known set of canonical markers for each cell type and enabled us to infer candidate functional roles for each cell type. We confirmed robust differential expression for known marker genes in endothelial (*CLDN5*), mural (*TAGLN*), fibroblast (*CEMIP*), astroglial (*GFAP*), neuronal (*CAMK2A*), oligodendrocyte (*PLP1*) and microglial (*CSF1R*) cell types (**Fig. 1e, f** and **Supplementary Table 2**). In addition, we identified markers for subtypes of these cells, separating endothelial cells into arteriole (*VEGFC* and *ARL15*), capillary (*MFSD2A* and *SLC7A5*) and venule (*TSHZ2* and *ADGRG6*), mural cells into arteriolar SMC (aSMC) (*ACTA2* and *MYH11*), venular SMC (vSMC) (*MYOCD* and *CD74*) and pericytes (*GRM8* and *PDGFRB*), and fibroblasts into type I (*ABCA10* and *FBLN1*), type II (*TRPM3* and *MYRIP*) and type III (*KCNMA1* and *SLC4A4*).

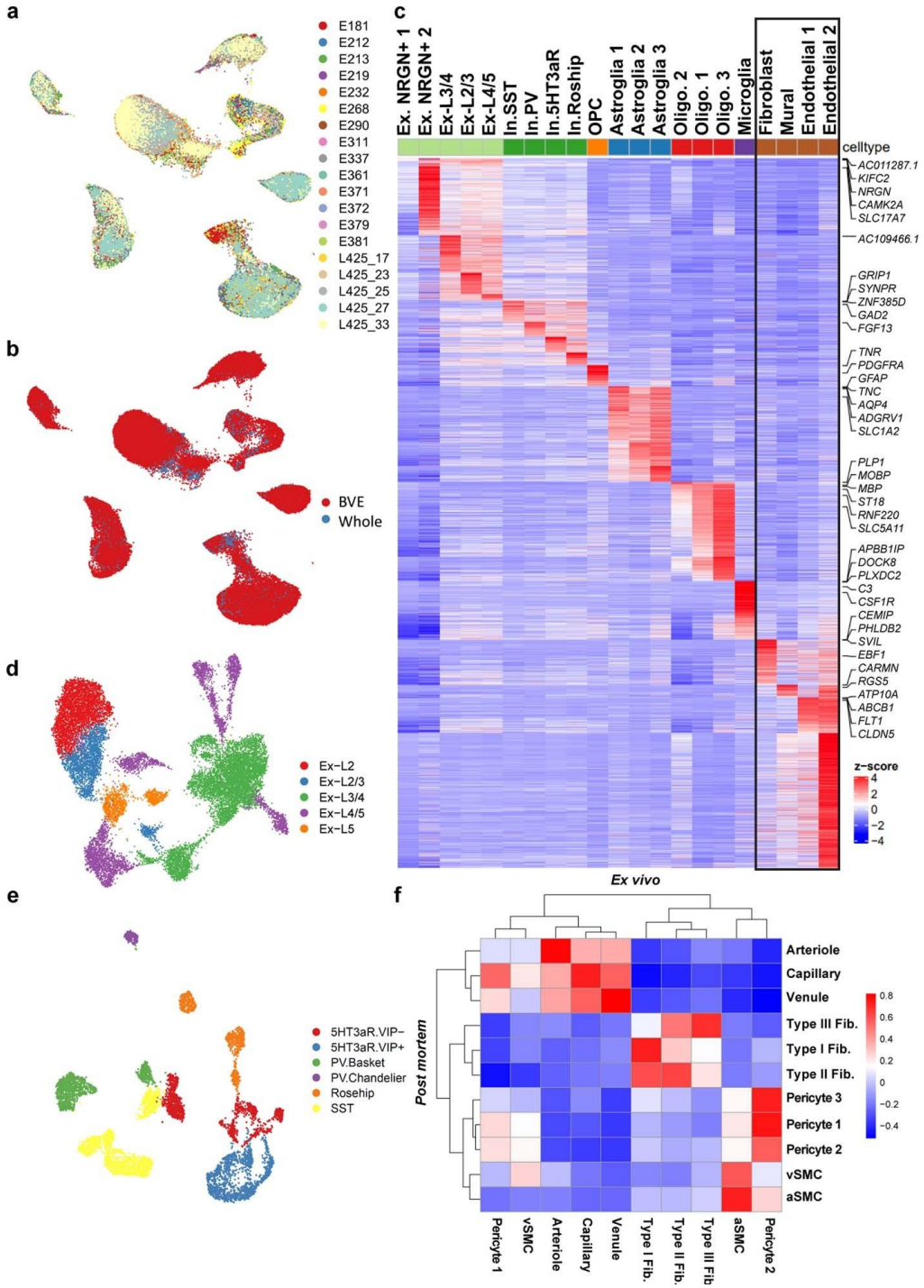

Extended Data Fig. 2. Characterization of human snRNA-seq data from human temporal cortex. a. UMAP of *ex vivo* dataset by patient ID. **b**. UMAP of *ex vivo* dataset by experimental protocol. **c**. Heatmap of top cell-type differentially-expressed genes (ctDEGs) in major cell types from *ex vivo* human tissue. **d**. UMAP sub-clustering of excitatory neurons. **e**. UMAP sub-clustering of inhibitory neurons. **f**. Correlation heatmap between *ex vivo* and *post mortem* vascular cell types.

Several of these marker genes, including *ARL15*, *TSHZ2*, *GRM8* and *TRPM3*, have not previously been identified for cerebrovascular cell types. We confirmed that these ctDEGs and corresponding cell types were consistent between our *ex vivo* and *post mortem* samples (**Extended Data Fig. 2f**), indicating that they hold across sample types and methodologies. Indeed, the marker genes *VEGFC*, *GRM8* and *TRPM3* exhibited corresponding protein expression in human cerebrovascular cell types by immunofluorescence (**Fig. 1g**).

Integration of human and mouse snRNA-seq

To evaluate whether cerebrovasculature expression profiles are conserved across species and platforms, we used canonical correlation analysis to integrate 4,992 *ex vivo* and 11,689 *post mortem* human cells with 3,406 C57BL/6 mouse cells (Vanlandewijck et al., 2018). To match cell types and correct for species and experimental differences, we projected each cell on a common two-dimensional embedding that corrects for covariates (age, sex, regions, sequencing platforms and post-mortem interval) (**Extended Data Fig. 3a, b**), and found broad cell-type conservation across species and platforms (**Fig. 2a, b** and **Extended Data Fig. 3c, d**).

Despite sharing cell-type identities, we found extensive expression differences between species, with 7.3% of genes showing on average twofold changes (n = 1,261) for each cell type, and 15.6% of these human–mouse DEGs (hmDEGs) being uniquely expressed in one species (**Extended Data Fig. 3e** and **Supplementary Table 3**). Whereas endothelial cells and SMCs showed no significant differences in cell-type proportions, pericytes and type II fibroblasts showed differential proportions (**Extended Data Fig. 3f**). These observed differences in expression did not stem from proportion changes, as they were not enriched for cell-type marker genes (**Extended Data Fig. 3g**). hmDEGs were highly consistent between *ex vivo* and *post*

mortem samples (80% agreement, $P < 2.2 \times 10^{-16}$). In each cell type, hmDEGs were strongly enriched for ctDEGs (12× endothelial cells, 14× fibroblasts, 15× pericytes, 9× SMCs), indicating that cell-type identity markers vary highly between species.

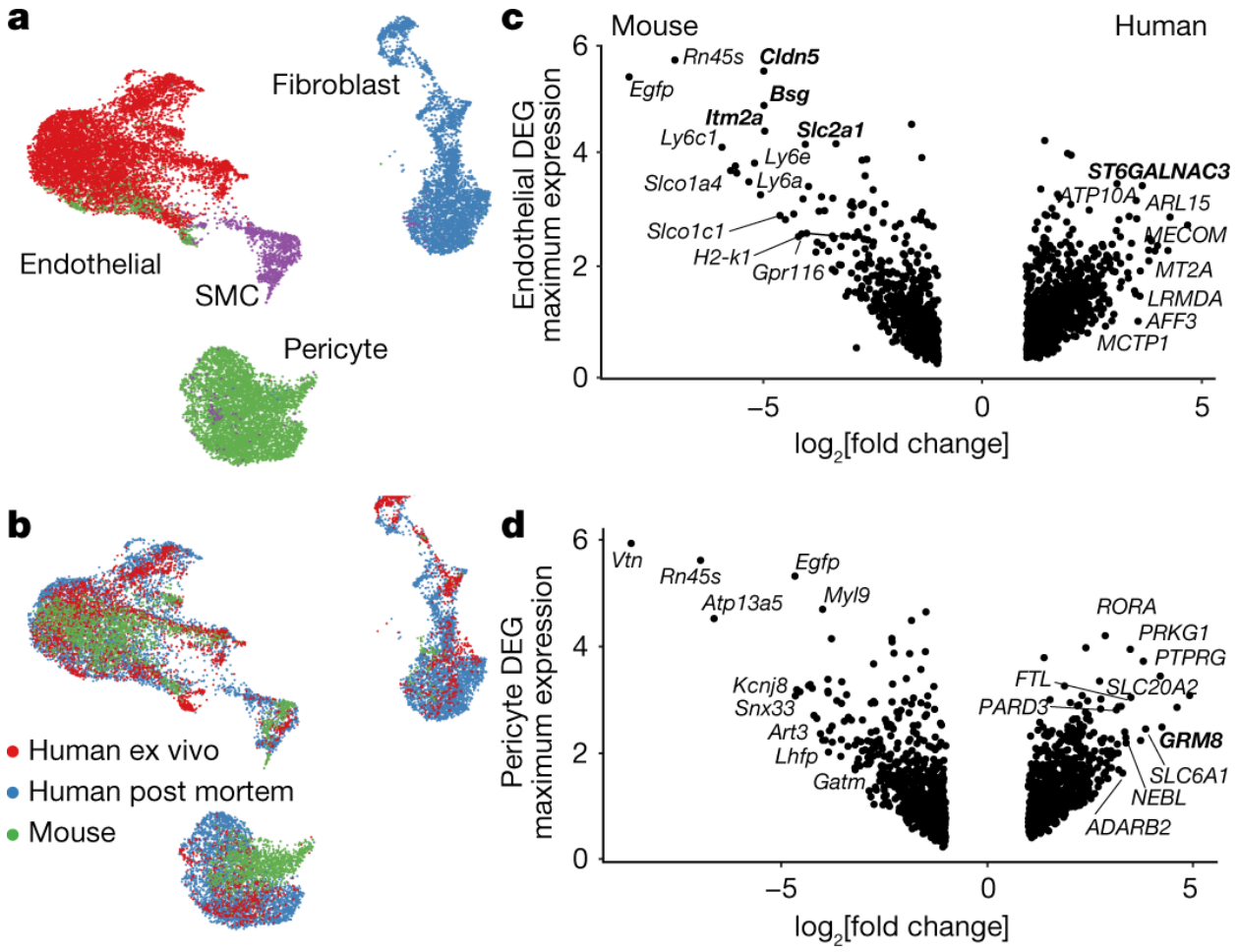

Fig. 2 Integrative analysis of human *ex vivo*, *post mortem* and mouse cerebrovascular cell types. a, **b**, UMAP visualization of integrated cells from human *ex vivo*, human *post mortem* and mouse, coloured by cell types (**a**) and data source (**b**). **c**, **d**, hmDEGs in endothelial cells (**c**) and pericytes (**d**). The *x* axis represents the log-transformed fold change and the *y* axis represents the maximal expression level. The top genes are highlighted for mouse (left) and human (right). Genes that were also cell-type markers are shown in bold.

hmDEGs showed cell-type-specific gene ontology enrichments that provide insight into species-specific functional specialization. For example, endothelial cells showed 742 human-increased genes, with enrichments in regulation of axonogenesis (**Fig. 2c** and **Extended Data**

Fig. 3h), whereas pericytes showed 650 human-increased genes enriched in regulation of endothelial cell migration (**Fig. 2d and Extended Data Fig. 3i**). Similarly, SMCs showed 469 human-increased and 641 mouse-increased genes (**Extended Data Fig. 3j**), respectively,

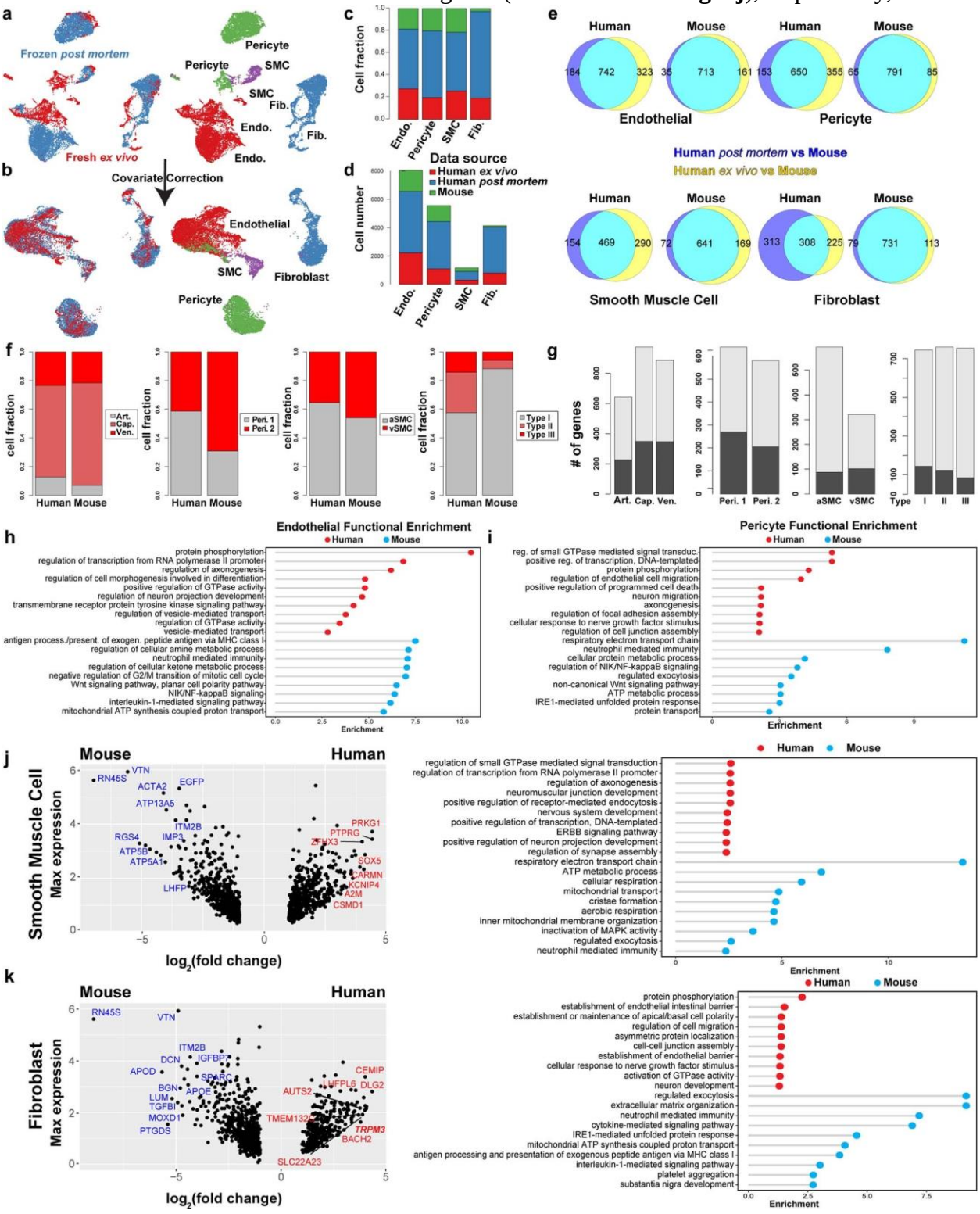

Extended Data Fig. 3. Integrative analysis of *ex vivo, post mortem,* and mouse datasets. **a**. UMAP plot of integrated human snRNA-seq datasets without covariate correction shown by platform and cell type and **b**. with covariate correction by platform and cell type **c**. Cell fraction distribution of single nuclei across all datasets by cerebrovasculature cell type. **d**. Cell number distribution of single nuclei across all datasets by cerebrovasculature cell type. **e**. Venn diagram overlap of genes between human *post mortem* vs. mouse and human *ex vivo* vs. mouse. **f**. Cell fraction and **g**. gene comparison of vascular cell types between mouse and human datasets. **h–i**. Representative functional enriched terms of human- and mouse-specific/highly expressed genes in endothelial (**h**) and pericytes (**i**). Human-mouse differentially expressed genes (hmDEGs) smooth muscle cells (**j, left**), and fibroblast (**k, left**). X-axis represents the log-transformed fold change and y-axis represents the maximal expression level. The top genes are highlighted in blue for mouse and red for human. Genes that were also cell type markers are bolded. **j–k. (right panels)**, the representative functional enriched terms of human- and mouse-specific/highly expressed genes.

whereas fibroblasts showed 308 human-increased and 731 mouse-increased genes (**Extended Data Fig. 3k**), respectively. In SMCs, the human-increased genes included PICALM, which is associated with Alzheimer's disease and involved in amyloid-β clearance through the brain vasculature (Zhao et al., 2015), and the muscle-differentiation-associated long noncoding RNA CARMN (Y.-H. Lim et al., 2018).

Comparison of post mortem versus *ex vivo* samples revealed 232 tissue-source DEGs (tsDEGs) (1.34%) at the same threshold (8× fewer than mouse), and revealed many functional changes associated with ageing, as expected given the age difference between our samples (*ex vivo* average: 15.8 years; *post mortem* average: 86.8 years). Gene ontology analysis of tsDEGs included: decreased BBB maintenance and increased vascular endothelial growth factor (VEGF) signalling in pericytes and decreased cell–cell adhesion and membrane assembly in fibroblasts (**Supplementary Table 3**). Although these changes are consistent with known dysfunctions of the cerebrovasculature due to aging (Montagne et al., 2015), they could reflect differences in *post mortem* and *ex vivo* tissue quality.

Human-specific endothelium zonation

Brain endothelial cells show phenotypic zonation along the arteriovenous axis (Vanlandewijck et al., 2018). Although poorly understood, zonated characteristics arise in disease, including pathologies of small calibre arteries in cerebral arteriopathies, and capillaries

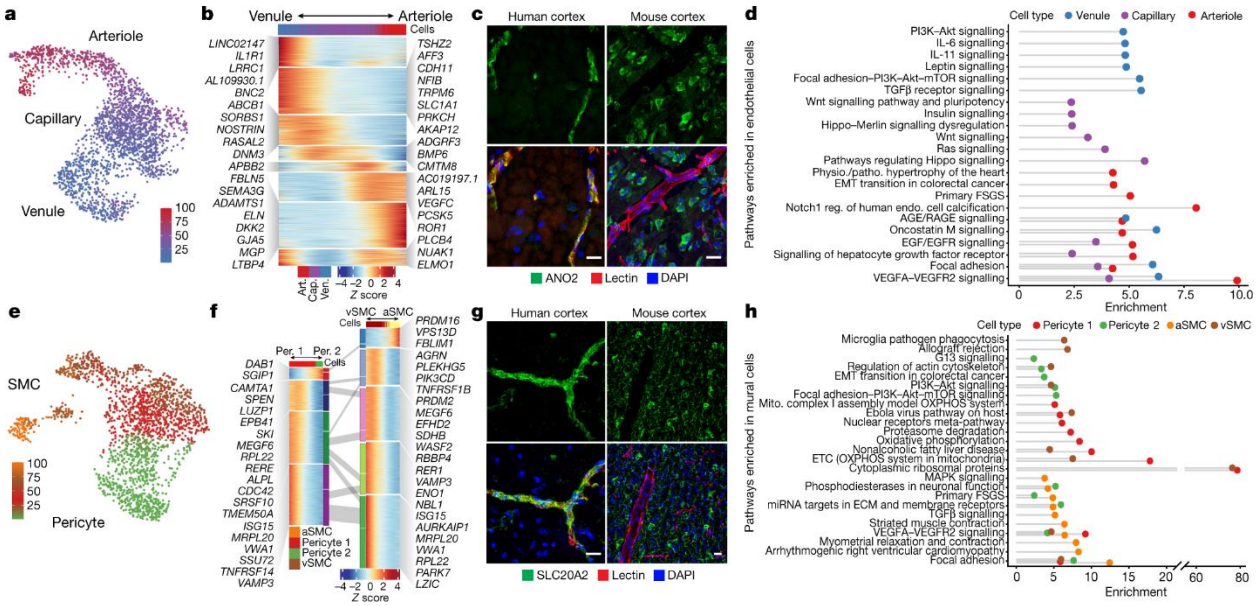

Fig. 3. Molecular zonation of human brain endothelial and mural cells. a, Zonal gradient of endothelial cell transcriptomes (normalized pseudotime predicted from Monocle3 (range 1–100)). **b**, Genes expressed at higher levels along the endothelial gradient. Art., arteriole; cap., capillary; ven., venule. **c**, Indirect immunofluorescence of expression of the human endothelial marker ANO2, and its mouse homologue, in brain cortex. **d**, Pathway analysis along endothelial zones. Physio., physiological; patho., pathological; EMT, epithelial-to-mesenchymal transition; FSGS, focal segmental glomerulosclerosis; reg., regulation; endo., endothelial; AGE, advanced glycation endproduct; RAGE, receptor for AGE. **e**, Zonal gradient of mural cell transcriptomes (normalized pseudotime predicted from Monocle3 (range 1–100)). **f**, Genes expressed at higher levels along the mural gradients. Grey lines depict shared genes across gradients. Per., pericyte. **g**, Indirect immunofluorescence of the expression of the human mural marker SLC20A2, and its mouse homologue, in brain cortex. **h**, Pathway analysis along mural zones. Mito. mitochondrial; OXPHOS, oxidative phosphorylation; ETC, electron transport chain. Representative images in **c** and **g** shown from $n = 3$ independent biological replicates for each marker. Brightness and contrast enhanced for visualization. Scale bars, 20 μm.

in neurodegenerative disorders (Joutel et al., 1996; Sweeney, Kisler, et al., 2018). To profile human endothelial molecular zonation signatures, we developed a continuous quantitative measure of spatial cell positioning using a linear regression model, focusing specifically on *ex vivo* nuclei. We found 1,802 genes that exhibited a gradient of expression along the arteriovenous axis, including 147 transcription factors and 76 transporters (**Extended Data Fig. 4a, b**), indicating a gradual transcriptional continuum (**Fig. 3a, b**). We found that human zonation (**Fig. 3b**) was conserved in a previous mouse dataset (Vanlandewijck et al., 2018) (**Extended Data Fig. 5a**); however, the set of zonated genes highly diverged, with only a small subset of zonated genes conserved between species (≈10%) (**Extended Data Fig. 5b**). We found conservation between markers of human and mouse arterioles (*VEGFC*, *BMX* and *EFNB2*) and capillaries (*MFSD2A* and *TFRC*), but venule markers differed. For example, *SLC38A5* was expressed in both capillaries and venules in human, but only in venules in mouse. *TSHZ2* and *LRRC1* were both venule zonated in human, but showed no expression in mouse endothelium. We found that several transcription factors known to promote endothelial or arterial fate, including *HEY1* and *GATA2* (Park et al., 2013), are arteriole zonated, and also reveal several new venule-zonated transcription factors, including *TSHZ2*, *BNC2* and *ETV6*.

We experimentally validated the zonated expression of several genes using freshly resected cortical tissue, confirming human-specific capillary/venule zonation of ANO2 (**Fig. 3c**), which lacks endothelial cell expression in mouse (Saunders et al., 2018), human-specific venule zonation of TSHZ2 (**Extended Data Fig. 5c**) and human–mouse-conserved arteriole zonation of VEGFC (Vanlandewijck et al., 2018). We also found human-specific expression of the metallothioneins MT1E and MT2A (**Extended Data Fig. 5d, e**) that show astrocytic but not vascular expression in mouse.

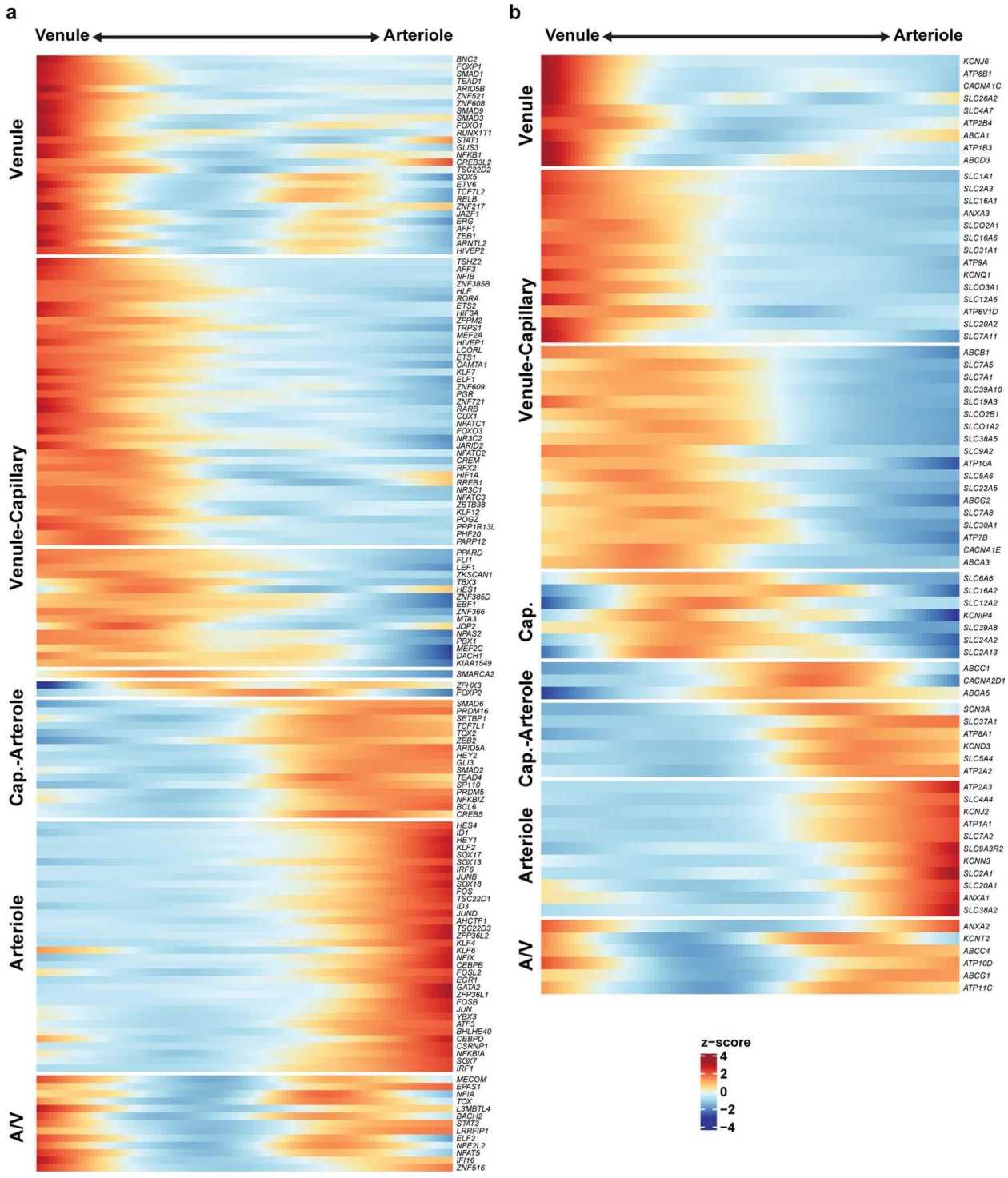

Extended Data Fig. 4. Zonation gene expression analysis of human endothelial cells. a. Heatmap of 147 zonated transcription factors along the endothelial gradient. **b**. Heatmap of 76 zonated transporters along the endothelial gradient.

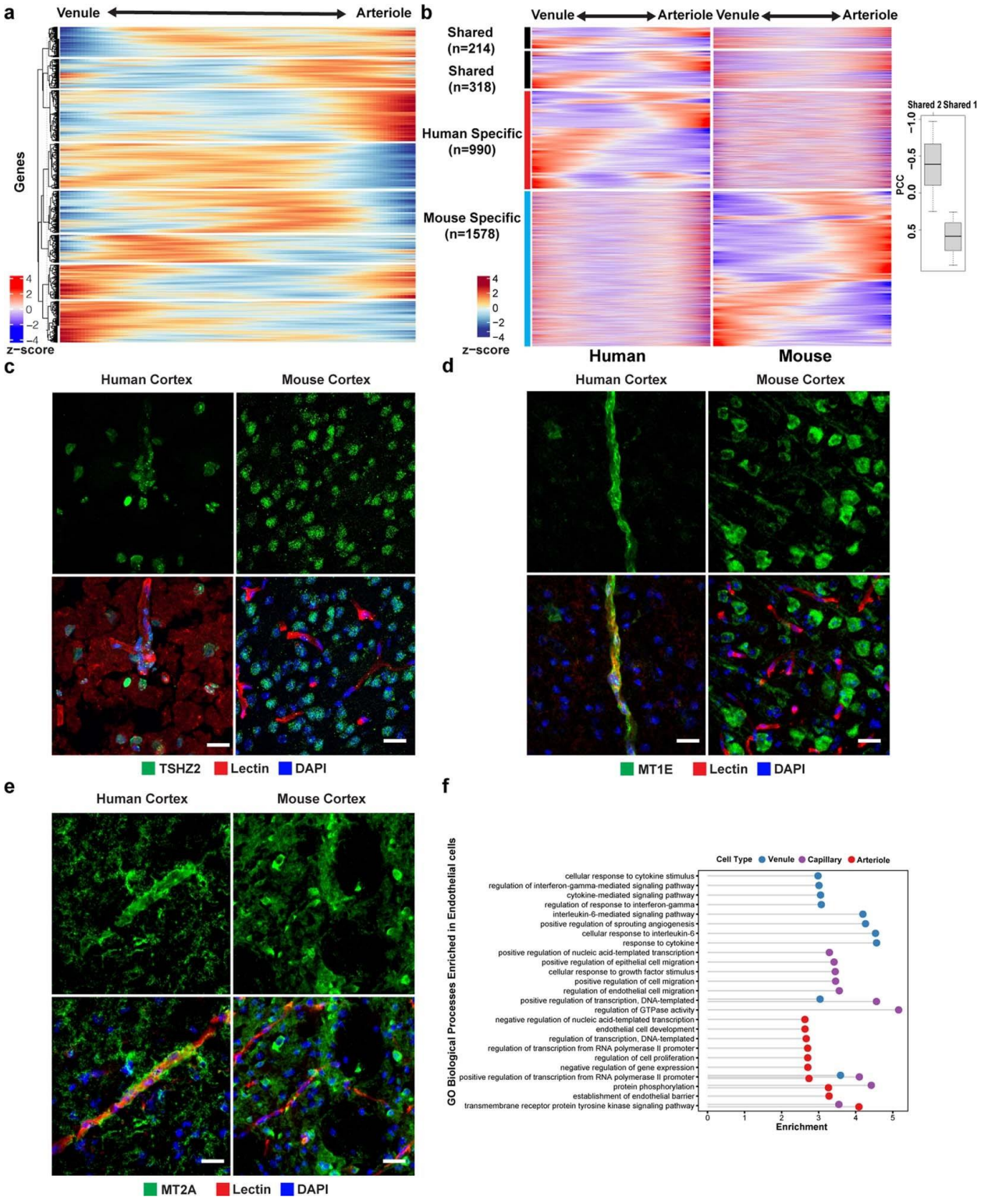
a
Venule
Arteriole
Genes
z-score
b
Venule
Arteriole
Venule
Arteriole
Shared (n=214)
Shared (n=318)
Human Specific (n=990)
Mouse Specific (n=1578)
z-score
Human
Mouse
Shared 2 Shared 1
PCC
c
Human Cortex
Mouse Cortex
TSHZ2
Lectin
DAPI
d
Human Cortex
Mouse Cortex
MT1E
Lectin
DAPI
e
Human Cortex
Mouse Cortex
MT2A
Lectin
DAPI
f
Cell Type
Venule
Capillary
Arteriole
GO Biological Processes Enriched in Endothelial cells
cellular response to cytokine stimulus
regulation of interferon-gamma-mediated signaling pathway
cytokine-mediated signaling pathway
regulation of response to interferon-gamma
interleukin-6-mediated signaling pathway
positive regulation of sprouting angiogenesis
cellular response to interleukin-6
response to cytokine
positive regulation of nucleic acid-templated transcription
positive regulation of epithelial cell migration
cellular response to growth factor stimulus
positive regulation of cell migration
regulation of endothelial cell migration
positive regulation of transcription, DNA-templated
regulation of GTPase activity
negative regulation of nucleic acid-templated transcription
endothelial cell development
regulation of transcription, DNA-templated
regulation of transcription from RNA polymerase II promoter
regulation of cell proliferation
negative regulation of gene expression
positive regulation of transcription from RNA polymerase II promoter
protein phosphorylation
establishment of endothelial barrier
transmembrane receptor protein tyrosine kinase signaling pathway
Enrichment

Extended Data Fig. 5. Zonation in human brain endothelial cells. a. Gene zonation analysis of mouse brain endothelial cells from Vanlandewjick et al. **b**. Integrated zonation analysis of human and mouse brain endothelial cell profiles. Pearson correlation coefficient of shared genes shown on right. **c**. Indirect immunofluorescence of TSHZ2 expression in human and mouse brain cortex. **d**. Indirect immunofluorescence of MT1E/MT1 expression in human and mouse brain cortex. **e**. Indirect immunofluorescence of MT2A/MT2 expression in human and mouse brain cortex. **f**. Enriched Gene Ontology terms in endothelial zones. Representative images in **c., d**., and **e**. from $n = 3$ independent biological replicates for each marker. Brightness and contrast enhanced for visualization. Scale bar, 20 μm.

Differentially zonated genes were enriched in distinct gene ontologies and pathways (**Fig. 3d** and **Extended Data Fig. 5f**). For example, venule-zonated genes were enriched in interleukin signaling pathways, consistent with the central role of venules in leukocyte adhesion and cytokine release (Ley et al., 2007). Arterial-zonated genes were enriched in Notch signalling, consistent with the role of Notch alterations in arteriopathies. These results show that although zonated functional organization is a conserved characteristic across species, the human cerebrovasculature exhibits a species-specific gene expression pattern.

Human mural cell molecular zonation

Studies of mural cells have elucidated distinct morphologies along the vasculature, but they remain poorly defined at the molecular level (Attwell et al., 2016). We found that unlike endothelial cells, mural cells exhibit two distinct and separate transcriptional gradients for pericytes and SMCs, regardless of their position along the arteriovenous axis (**Fig. 3e**) and not previously observed in mice (Vanlandewijck et al., 2018). In total, we identified 1,820 zonated genes in pericytes (**Extended Data Fig. 6a, b**) and 2,756 in SMCs (**Extended Data Fig. 7a, b**) that exhibit distinguishable expression patterns (**Fig. 3f**). We found that the zonated genes in SMCs

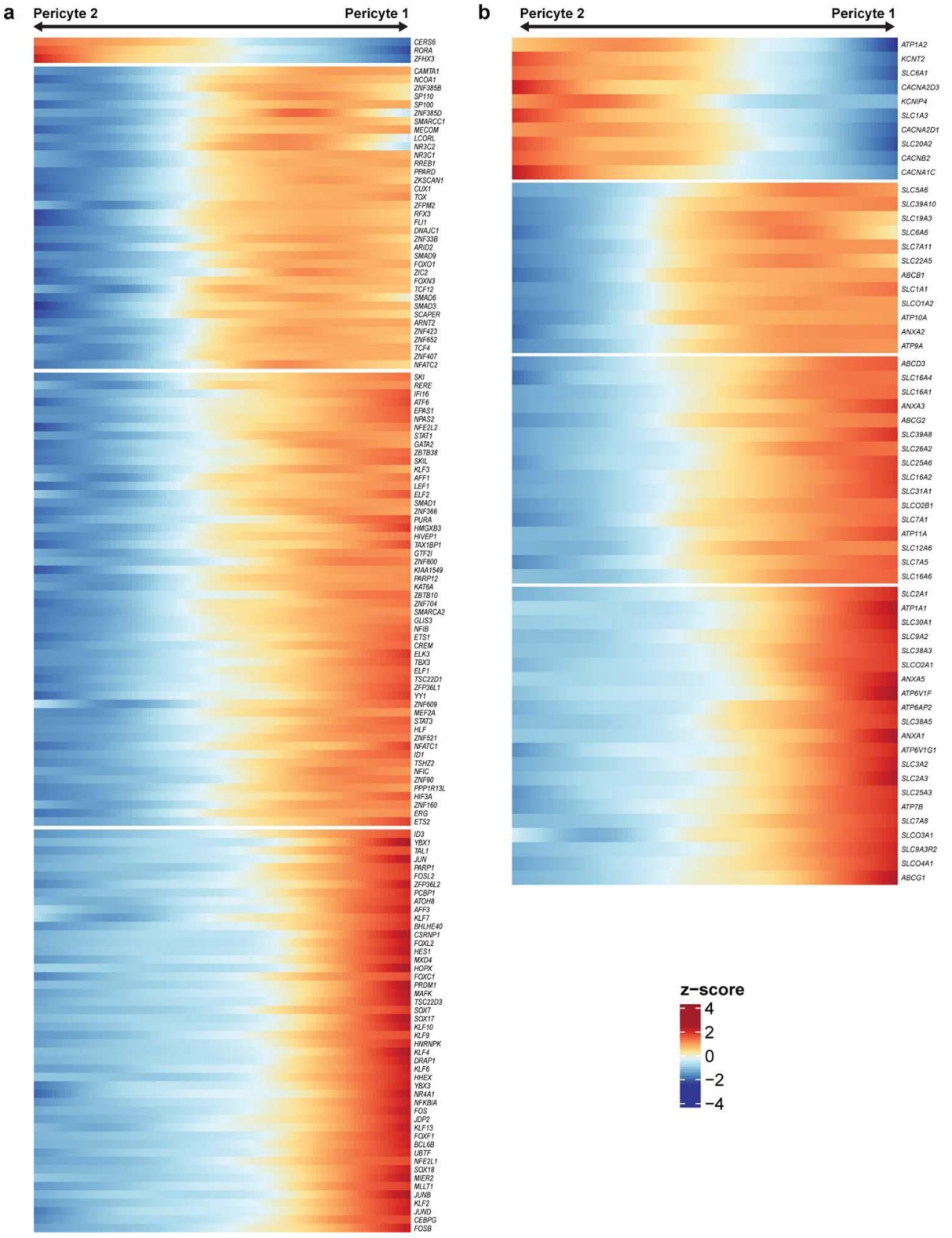

Extended Data Fig. 6. Zonation gene expression analysis of human pericytes. a. Heatmap of zonated transcription factors along the pericyte gradient. **b**. Heatmap of zonated transporters along the pericyte gradient.

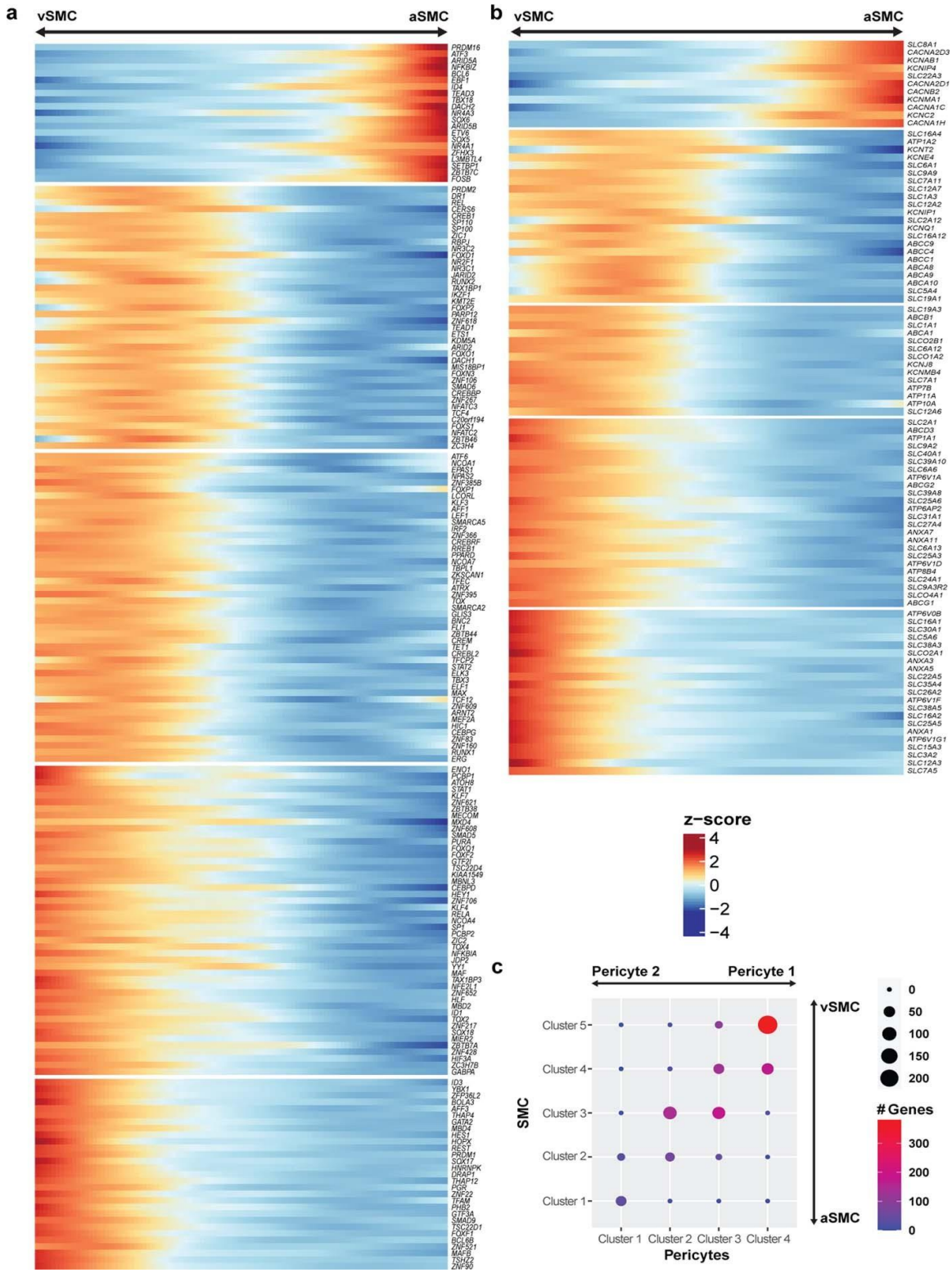

Extended Data Fig. 7. Zonation gene expression analysis of human SMCs. a. Heatmap of zonated transcription factors along the SMC gradient. **b**. Heatmap of zonated transporters along the SMC gradient. **c**. Overlap matrix across the zonated pericyte and SMC clusters.

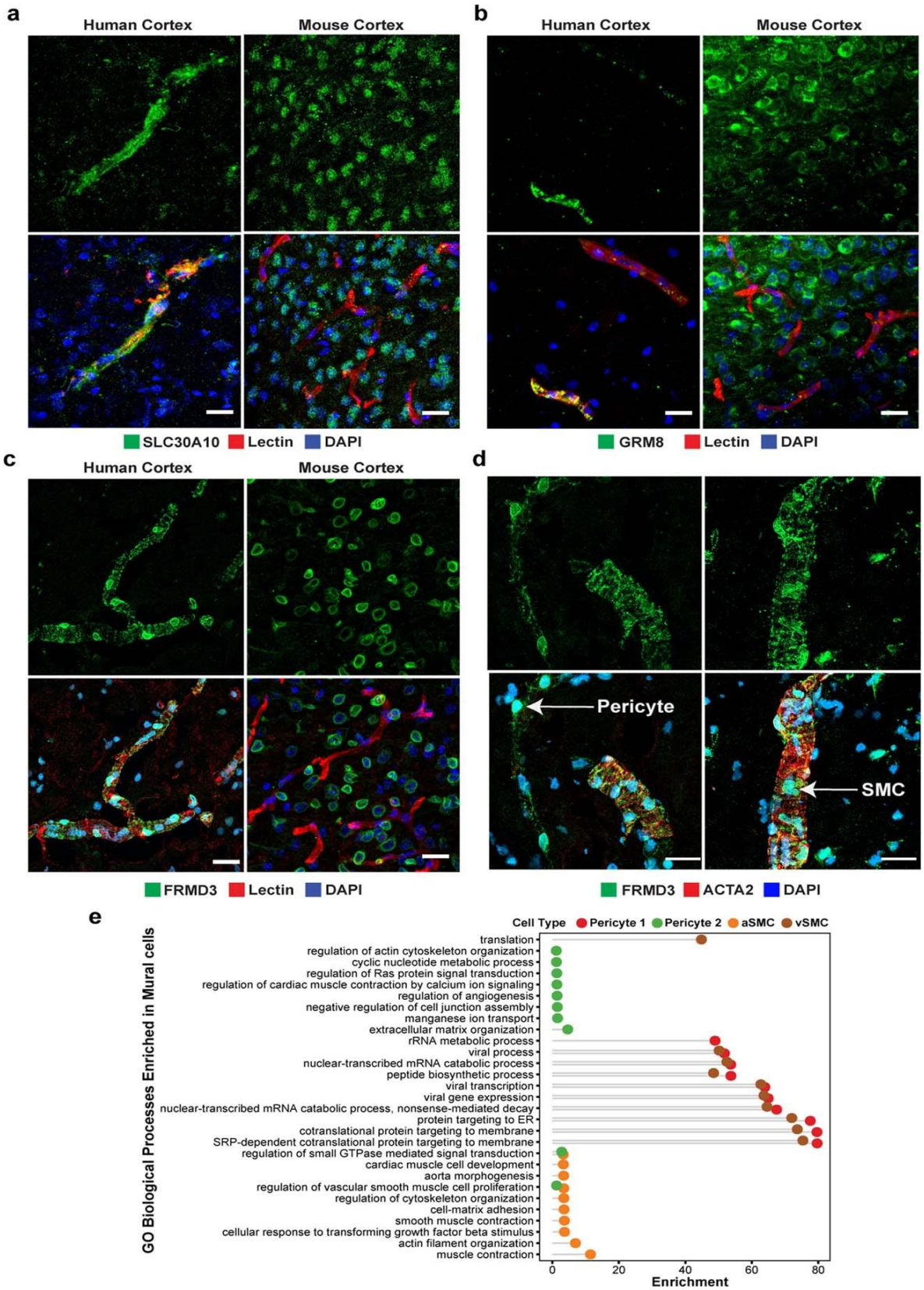

and pericytes are significantly shared. For example, the genes expressed at higher levels in

Extended Data Fig. 8. Zonation in human brain mural cells. a. Indirect immunofluorescence of SLC30A10 expression in human and mouse brain cortex. **b**. Indirect immunofluorescence of GRM8 expression in human and mouse brain cortex. **c**. Indirect immunofluorescence of FRMD3 expression in human and mouse brain cortex. **d**. Indirect immunofluorescence localization of FRMD3 on ACTA2+ (known SMC marker) vessels. **e**. Enriched Gene Ontology terms in mural zones. Representative images in **a–d** from $n = 3$ independent biological replicates for each marker. Brightness and contrast enhanced for visualization. Scale bar, 20 μm.

pericyte 1 were enriched in vSMCs. By contrast, genes expressed at higher levels in pericyte 2 were expressed at higher levels in aSMCs (**Fig. 3f** and **Extended Data Fig. 7c**).

We found zonated expression of several apolipoproteins in vSMCs, including those encoded by *APOD*, *APOE* and *APOO*. Failure of amyloid-β clearance in the perivenous space is thought to contribute to cerebral amyloid angiopathy and deficits of perivenous drainage in Alzheimer's disease (Morrone et al., 2020). Given the localized recruitment of immune cells to venules, the zonated expression of apolipoproteins, in particular that encoded by *APOE*, by vSMCs suggests a zonated functional role of amyloid-β clearance. In addition, our analysis revealed the expression of specific genes in human mural cells. We validated the expression of SLC20A2 and SLC30A10 and demonstrated these mural- and human-specific genes to exhibit expression wrapped around vessels but not co-localized with the endothelial marker lectin (**Fig. 3g** and **Extended Data Fig. 8a**). In pericytes and SMCs, we validated the zonated expression of GRM8 (**Extended Data Fig. 8b**) and FRMD3 by co-staining with the known aSMC marker ACTA2 (**Extended Data Fig. 8c, d**). We observed FRMD3 expression on large ACTA2+ vessels (**Extended Data Fig. 8d**), and on a subset of small microvessels with different morphologies, reminiscent of known pericyte heterogeneity. Furthermore, SLC20A2, SLC30A10, GRM8 and FRMD3 exhibited expression patterns in non-vascular cell types within the mouse posterior cortex, demonstrating the species-specific expression in human mural cells (**Fig. 3g** and **Extended Data Fig. 8a–c**).

Last, gene ontology and pathway analyses indicated that genes expressed at high levels in pericyte 2 and aSMCs were significantly enriched in SMC contraction and cardiac muscle cell action potential terms. Likewise, genes expressed at high levels in pericyte 1 and vSMC were significantly enriched in VEGF signalling pathway and immune responses terms (**Fig. 3h** and **Extended Data Fig. 8e**). The pathways enriched in pericyte 1 more closely resembled vSMCs, whereas pericyte 2 more closely resembled aSMCs, suggesting functional similarities between aSMC and pericyte 2 and between vSMC and pericyte 1. Together with gene expression profiling and immunostaining validation, our pathway analysis suggests that pericyte 2 represents the subclass of pericytes in closer proximity to arterioles, whereas pericyte 1 represents pericytes in closer proximity to venules.

Perivascular fibroblasts in human cortex

Endothelial cells, mural cells and astrocytes are notable components of the cerebrovasculature; however, recent studies in animal models have demonstrated a class of perivascular fibroblasts as being integral for vascular structure (Rajan et al., 2020; Saunders et al., 2018; Vanlandewijck et al., 2018). In particular, these perivascular fibroblasts, or stromal cells, express collagens and laminins, which are essential components of the extracellular matrix (ECM) (Muhl et al., 2020) and contribute to fibrotic scar formation after injury to the central nervous system (Fernández-Klett et al., 2013). Distinct fibroblast subtypes are present in mouse cerebrovasculature; however, the limited number has prevented characterization of their distinct transcriptional profiles and function (Vanlandewijck et al., 2018; Zeisel et al., 2018).

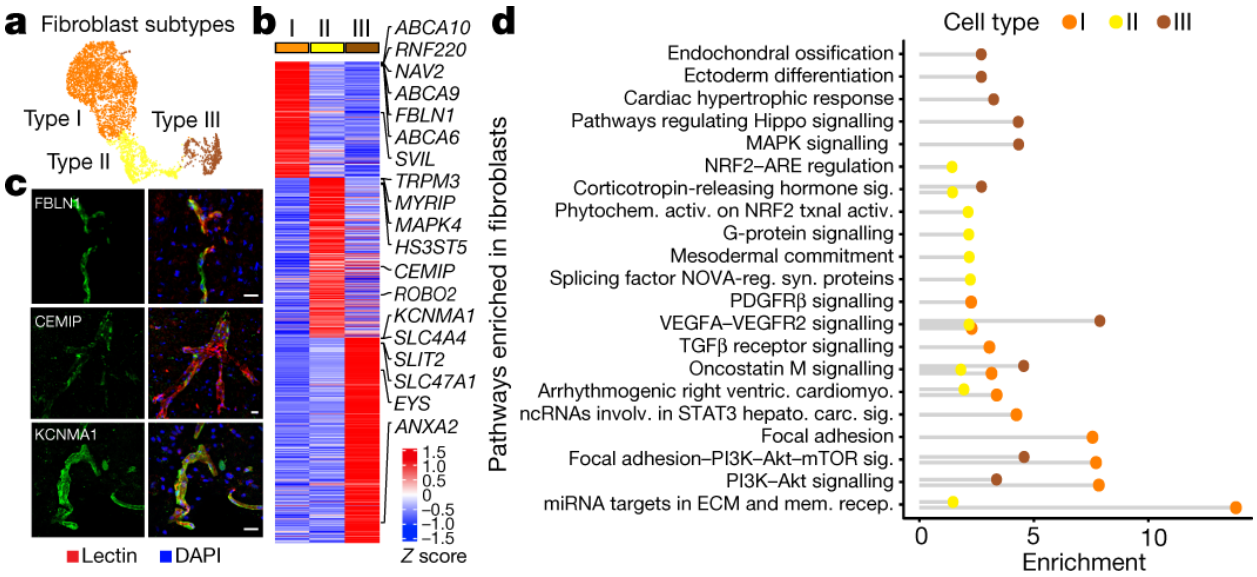

Fig. 4. Perivascular fibroblasts in the human cerebrovasculature. a, UMAP of integrated perivascular fibroblast subtypes from human *ex vivo* and *in silico*-sorted brains. **b**, Genes expressed at high levels in fibroblast subtypes. **c**, Indirect immunofluorescence of expression of the fibroblast markers FBLN1, CEMIP and KCNMA1. **d**, Enriched pathway analysis in perivascular fibroblast subtypes. Sig., signalling; reg. regulated; syn. synaptic; ventric., ventricular; cardiomyo., cardiomyocytes; involv., involved; hepato., hepatocellular; carc., carcinoma; mem., membrane; recep., receptor; activ., activation; phytochem., phytochemical. Representative images in **c** from $n = 3$ independent biological replicates for each marker. Brightness and contrast enhanced for visualization. Scale bars, 20 μm.

In our analysis, we uncovered three distinct subtypes of perivascular fibroblasts (**Fig. 4a**), two of which were consistent with those identified in mouse (types I and II). Type III fibroblasts shared expression of the mouse arachnoid barrier cell (ABC) marker (Zeisel et al., 2018) SLC47A1 ; however, several other markers of ABCs are not expressed in type III fibroblasts. As we did not expect to have ABCs, the human type III fibroblasts revealed by our analysis probably constitute a new human fibroblast subtype. Nevertheless, all subtypes expressed specific sets of genes (**Fig. 4b**), some of which are also expressed in mouse brain fibroblasts, although subtype-specific expression had not previously been assessed. We confirmed protein

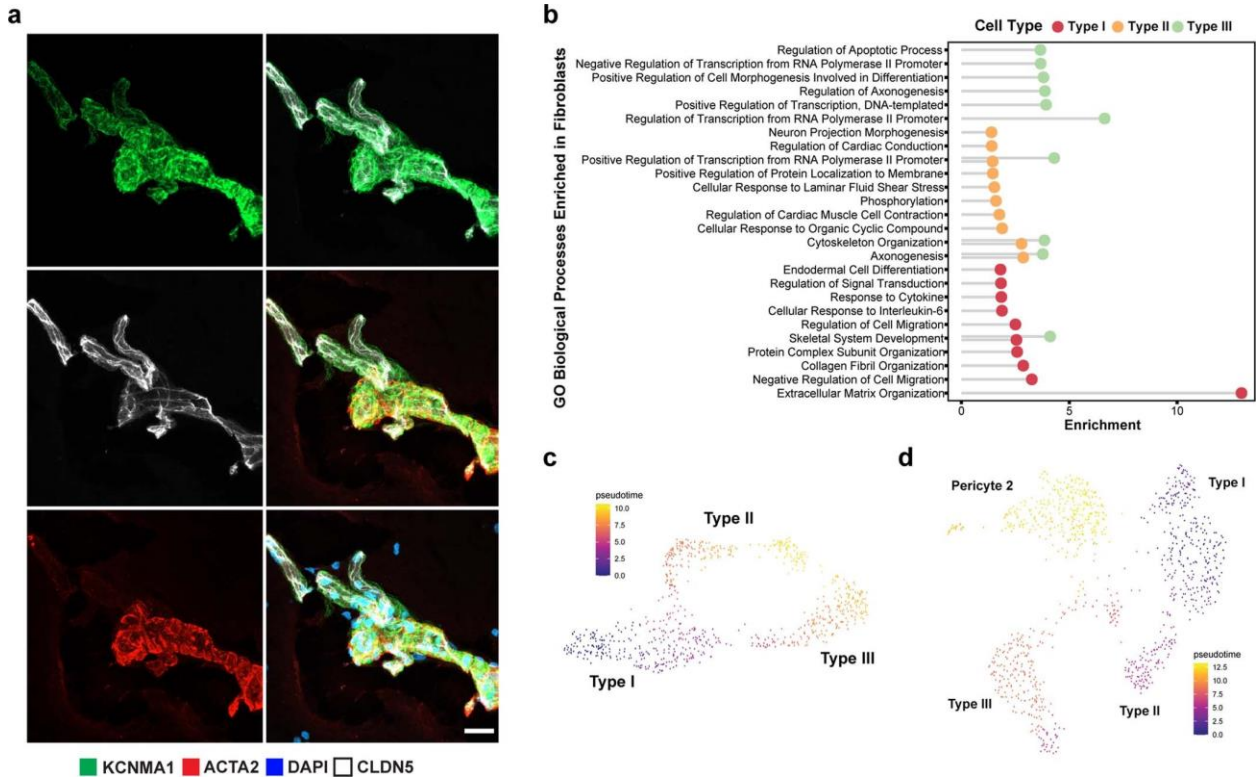

Extended Data Fig. 9. Validation and pathway analyses of perivascular fibroblast subtypes. a. Immunofluorescence staining of Type III fibroblast marker KCNMA1 on ACTA2+ vessels in human. **b**. Enriched Gene Ontology analysis in perivascular fibroblast subtypes. **c**. Pseudotime analysis of *ex vivo* fibroblast subtypes. **d**. Pseudotime analysis of *ex vivo* fibroblast subtypes and Pericyte 2 (note: Pericyte 1 not shown as it did not fall within any pseudotime trajectory). Representative image in **a**. from n = 3 independent biological replicates for each marker. Brightness and contrast enhanced for visualization. Scale bar, 20 μm.

level expression of FBLN1, CEMIP and KCNMA1, as markers for type I, II and III fibroblasts, respectively (**Fig. 4c** and **Extended Data Fig. 9a**).

Pathway and gene ontology enrichment analyses revealed distinct functional roles for each subtype (**Fig. 4d** and **Extended Data Fig. 9b**). Whereas all subtypes expressed genes involved in VEGF–VEGFR2 signalling, type I fibroblasts seem to be the main subtype involved in ECM organization. Given that fibrotic scars are predominantly composed of collagen I ECM protein (Dorrier et al., 2021), it is likely that type I fibroblasts are the contributing subtype to fibrosis during injury to the central nervous system. Type II and type III showed greater

significance in pathways related to cell fate, with type III showing expression of various growth factors, including that encoded by VEGFA. Pseudotime analysis of ex vivo fibroblasts revealed two gradients of gene expression from type I to type II and to type III, separately (**Extended Data Fig. 9c**). The type I to type II trajectory was continuous with pericyte 2 (**Extended Data Fig. 9d**), suggesting a lineage from type I to type II to pericytes and consistent with a study demonstrating the stem cell potential of fibroblasts to differentiate into pericytes (Rajan et al., 2020). This is in line with our evidence that the pericyte 2 type cells are in closer proximity to arterioles given that fibroblasts have been shown to be localized predominantly at the level of penetrating arterioles (Bonney et al., 2022). Therefore, type II fibroblasts probably represent an intermediate state exhibiting a transitional mural cell transcriptional phenotype.

Chapter 3: Molecular Profiling of the Human Cerebrovasculature in Huntington's Disease

The following text and figures have been adapted from previously published work by Francisco J. Garcia and co-authors. For original article, see [Garcia, Francisco J., et al. "Single-cell dissection of the human brain vasculature." Nature 603.7903 (2022): 893-899.]

HD vascular dysfunction

Several studies have noted cerebrovascular abnormalities across neurodegenerative diseases, which often precede more disease-specific pathological features (Sweeney, Kisler, et al., 2018). HD and HD-like syndromes including neuroferritinopathy (Chinnery et al., 2007) and primary familial brain calcification (Tadic et al., 2015) are autosomal-dominant neurodegenerative diseases caused by mutations in either the *HTT* gene (Macdonald, 1993) or in the vasculature-expressed genes *FTH1* (Chinnery et al., 2007) and *SLC20A2*, *PDGF* and *PDGFRB* (Tadic et al., 2015), respectively. In HD these abnormalities include increased BBB permeability, increased small vessel density, altered vessel morphology/cerebral blood volume, and activation of pericytes (J. J. Chen et al., 2012; Drouin-Ouellet et al., 2015; Harris et al., 1999; Hua et al., 2014). Although these changes have been shown to occur before the onset of HD-like phenotypes in the R6/2 (Di Pardo et al., 2017; Padel et al., 2018) and zQ175 (Liu et al., 2021) mouse models and also in pre-symptomatic stages of HD, the molecular bases of these alterations are not well understood.

To study cerebrovascular cells in the context of disease, we re-annotated 2,198 cells from our previously published post mortem neostriatal HD samples (H. Lee et al., 2020), and studied their gene expression changes. We corrected the annotation of 895 fibroblasts that we had previously identified as mural cells (**Extended Data Fig. 10a–c**). We also profile 1,747 additional cells from HD grade 1–4 and control cells purified with the BVE protocol on matched tissue samples from the caudate nucleus and putamen. Highlighting the importance of glia–

vasculature cell interactions, we found that genes expressed at high levels in one subcluster of astrocytes and one subcluster of microglia were significantly enriched in regulation of angiogenesis and blood vessel endothelial cell migration, suggesting that these glial cells may be specified functionally for vasculature regulation (**Extended Data Fig. 10d, e**). The numbers of astrocytes and microglia were significantly increased (**Fig. 5a**), suggesting that astrocytes and microglial cells associate more closely with the vasculature in HD.

We found 4,698 HD DEGs (hdDEGs) between control and HD for endothelial, mural and fibroblast cell types (**Supplementary Table 4**), some of which are known to be dysregulated in neurodegenerative conditions, including *ABCB1*, *ABCG2* and *SLC2A1* downregulation in endothelial cells. *PDGFRB, SLC20A2* and *FTH1* were all significantly downregulated in mural cells. Mutations in these genes are known to cause HD-like syndromes with primary pathology localized in the basal ganglia (Chinnery et al., 2007; Tadic et al., 2015), suggesting a link between vascular changes and regional vulnerability in HD. We also found significant endothelial downregulation of *MFSD2A,* which encodes a lipid transporter expressed in brain endothelial cells that restricts caveolae-mediated transcytosis (Ben-Zvi et al., 2014), suggesting that its dysregulation may underlie increased vesicular trafficking and BBB leakage. In addition, endothelial HD cells showed upregulation of genes associated with sprouting angiogenesis, endothelial cell migration and VEGF signalling (**Supplementary Table 4**), changes that may underlie the increased vessel density reported previously (Drouin-Ouellet et al., 2015). We predicted upstream regulators of hdDEGs using chromatin enrichment analysis (Methods) and found that *TCF4,* a regulator of the Wnt pathway, was both a top predicted regulator in HD endothelial cells, and itself upregulated in endothelial cells (Supplementary Table 4 and Extended Data Fig. 10f). Consistent with this, the Wnt signalling pathway is upregulated in brain

endothelial cell studies using induced pluripotent stem cells derived from patients with HD (R. G. Lim et al., 2017).

HD-upregulated genes in endothelial cells were enriched for many innate immune activation genes (**Extended Data Fig. 10g**), complementing our observation of innate immune activation in HD neostriatal spiny projection neurons (H. Lee et al., 2020), and being of interest given links between BBB dysregulation and innate immune activation (Daniels & Klein, 2015). Indeed, several key mediators of innate immune activation were upregulated in endothelial cells,

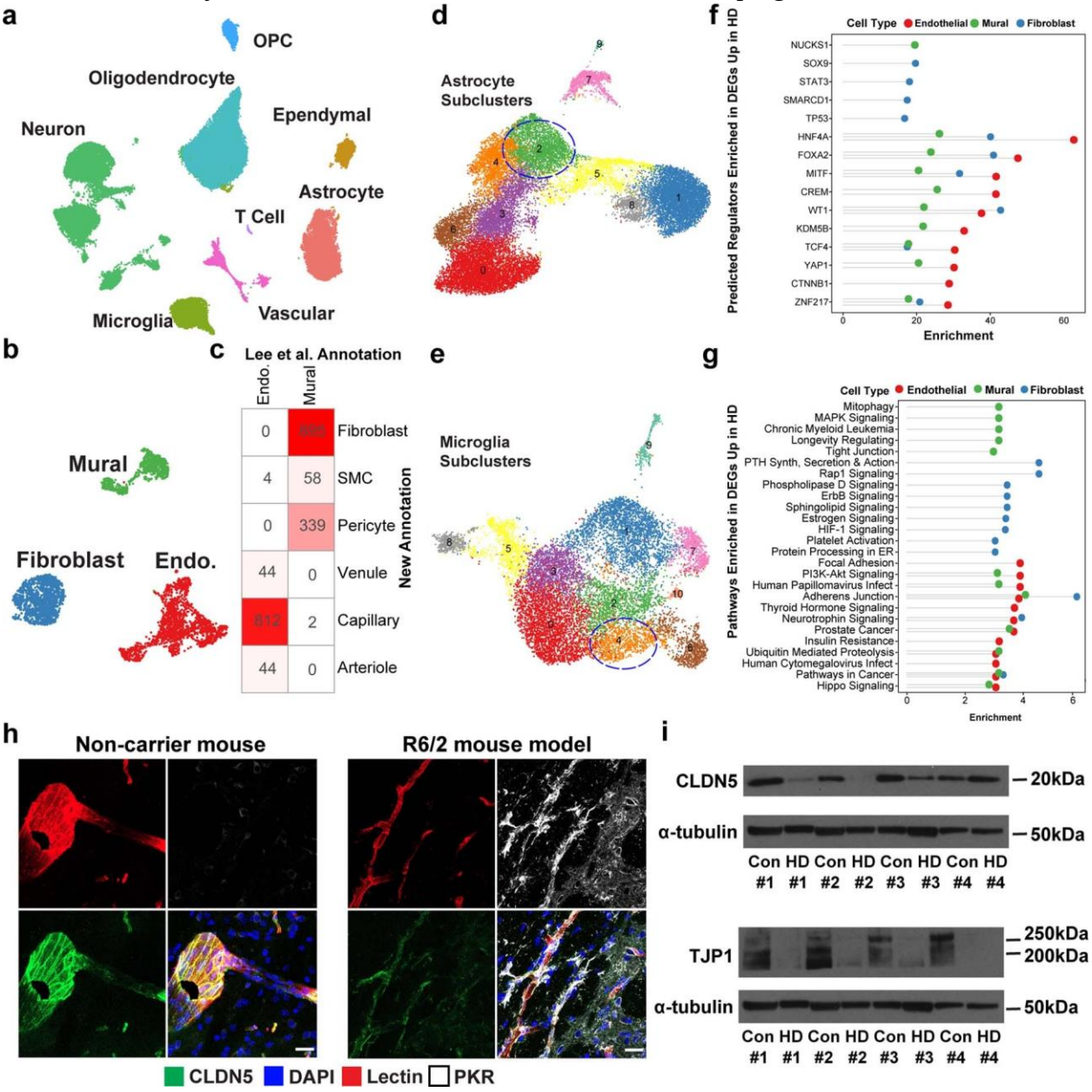

Extended Data Fig. 10. Cerebrovascular profiling in Huntington's disease. a. UMAP of integrated single nuclei from *post mortem* control and HD human patient samples. **b**. UMAP of integrated cerebrovasculature cells in *post mortem* control and HD human patients. **c**. Comparison of cerebrovasculature cell annotations (in cell numbers) in this study vs. Lee et al. **d**. UMAP analysis of astrocyte subclusters in HD. Vascular-related astrocytes outlined in blue. **e**. UMAP analysis of microglia subclusters in HD. Vascular-related microglia outlined in blue. **f**. ChEA prediction of top 10 regulators of upregulated genes in HD endothelial, mural, and fibroblasts cells. **g**. Pathway analysis of the top 10 enriched upregulated pathways in HD endothelial, mural, and fibroblasts cells. **h**. PKR immunoreactivity in the R6/2 HD mouse model engulfs blood vessels with low CLDN5 expression. **i**. Western blots for tight junction proteins CLDN5 and TJP1 from human HD and control samples. Representative images in **h**. from $n = 3$ independent biological replicates for each immunostaining. Brightness and contrast in immunofluorescence enhanced for visualization. Scale bar, 20 μm.

including *IKBKB*, *IRF2*/*3* and *STAT3* (**Supplementary Table 4**). We found that innate immune activation genes were also significantly upregulated in HD for both astrocytes and microglia, including *IRF3* and *TRAF3* (**Supplementary Table 5**). To validate this upregulation of innate immune signaling in astrocytes and microglia, we assessed expression of the innate immune sensor PKR in HD and HD mouse model tissue. In control tissue, some PKR expression is normally seen in the cerebrovasculature. We observed strong PKR upregulation in what seemed to be glial processes that engulfed blood vessels, in both human HD (**Fig. 5b**) and R6/2 HD mouse model samples (**Extended Data Fig. 10h**). These engulfed blood vessels were devoid of, or exhibited low levels of, the BBB tight junction protein CLDN5, and the engulfing processes were immunopositive for the astrocyte marker glial fibrillary acidic protein (GFAP), suggesting a correlation between endothelial and glial cell innate immune activation and a reduction of endothelial tight junction protein levels (**Fig. 5c** and **Extended Data Fig. 10h**). We further confirmed a significant reduction to overall levels of the BBB tight junction proteins CLDN5 and TJP1 (**Fig. 5d** and **Extended Data Fig. 10i**). As downregulation of CLDN5 and TJP1 levels is known to lead to the loss of BBB integrity, taken together these data provide evidence for a co-

occurrence of activation of innate immune signaling in endothelial cells/glial cells interacting with the vasculature and the loss of BBB integrity noted in HD.

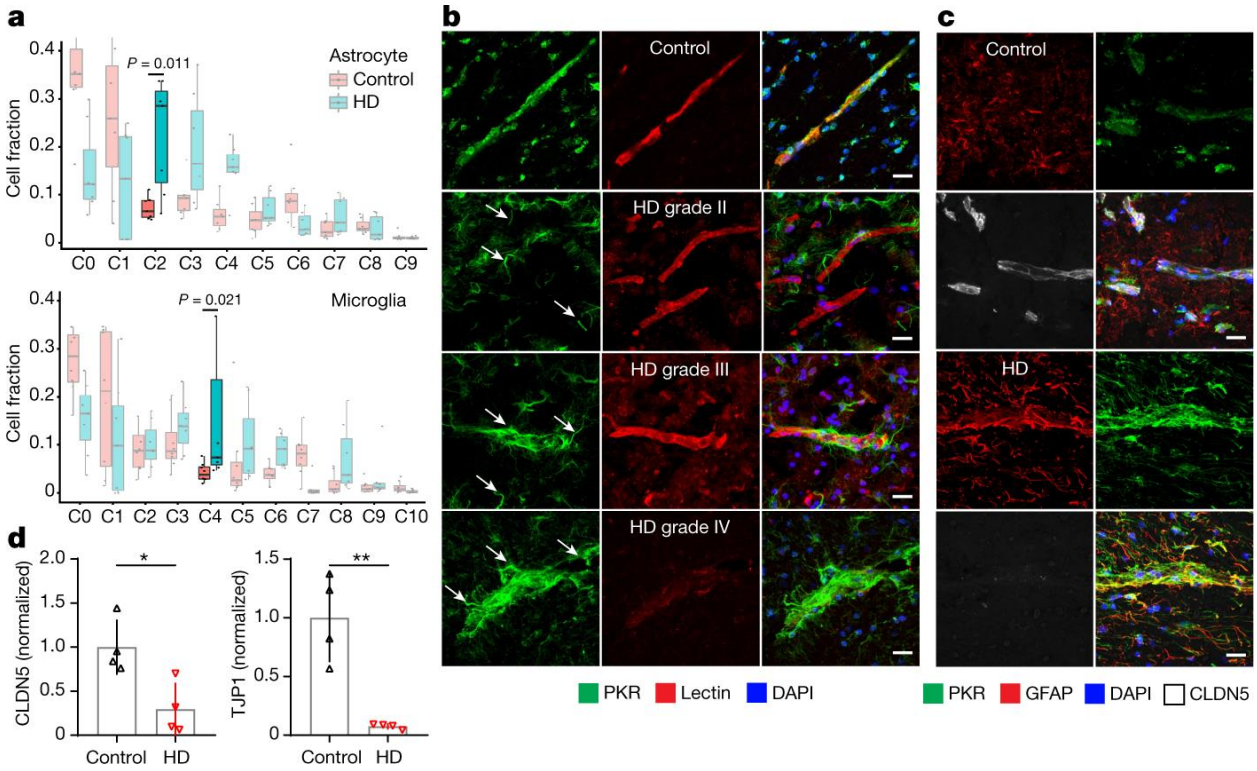

Fig. 5. Innate immune activation related to cerebrovascular dysfunction in HD. a, Cell fraction analysis of astrocyte (C0–C9) and microglia (C0–C10) subclusters; *P* value shown for highlighted clusters is calculated using the Wilcoxon rank sum test ($n = 8$ for each group). Centre line denotes the median; box limits denote the upper and lower quartiles; and whiskers denote the 1.5× interquartile range; dots denote individuals. **b**, PKR immunostaining in perivascular glial processes across various HD grades. PKR is normally detected in the vasculature in control samples; arrows indicate PKR-immunopositive glial processes that become apparent only in HD samples. **c**, PKR immunostaining co-localizes with GFAP and engulfs blood vessels with low expression levels of CLDN5. **d**, Western blot quantification for the tight junction proteins CLDN5 (left) and TJP1 (right). Two-tailed *t*-test, $*P = 0.0158$, $**P = 0.0025$. Error bars denote s.d. of the mean from $n = 4$ biologically independent samples from the caudate nucleus of controls and patients with HD. Representative images in **b** and **c** from $n = 3$ independent biological replicates for each immunostaining experiment. Brightness and contrast enhanced for visualization. Scale bars, 20 μm.

Chapter 4: Cell Type-Specific Lowering of Huntingtin in the Cerebrovasculature Delays Progression of Huntington's Disease *In Vivo*

Neurodegenerative diseases are characterized by dysfunction of specific neuronal populations in particular brain regions, a phenomenon known as selective or enhanced vulnerability (Fu et al., 2018). In many instances, accumulation of a pathological protein (e.g. amyloid-beta in Alzheimer's disease (AD), alpha-synuclein in Parkinson's disease (PD)) in these regions leads to neuronal toxicity and cell death. Despite this cell type and regional specificity, many of these diseases exhibit brain vasculature dysfunction, often at early stages preceding the onset of disease-specific phenotypes. The extent to which brain vasculature dysfunction contributes to disease pathology is not well understood. Furthermore, the feasibility of targeting the brain vasculature in neurodegeneration as a disease-modifying intervention has not been fully explored.

To assess the contribution of brain vasculature function on disease progression in HD, we developed an adeno-associated viral (AAV) approach to selectively lower huntingtin levels in the brain vasculature of animal models. We designed a construct encoding a microRNA (miR) targeting exon 1 of the *HTT* gene under the control of an abbreviated form of the CLDN5 promoter to drive expression specifically in brain endothelial cells. We demonstrate that systemic administration of a single viral dose at pre-symptomatic stages can delay the disease progression of HD *in vivo*. Our work highlights the importance of the brain vasculature in the disease course of neurodegenerative diseases and proposes a non-conventional approach for developing therapeutics to treat multiple brain diseases.

Development of a cerebrovasculature-targeting strategy for HD

Given the monogenic nature of HD, gene therapy approaches are of particular interest for the development of therapeutic interventions. In particular, many huntingtin-lowering strategies are currently in on-going clinical trials (Estevez-Fraga et al., 2022). However, recent setbacks in *HTT*-lowering ASO clinical trials have called into question many aspects of approaching therapeutic interventions for HD. Many of these strategies, including tominsersen developed by Roche, target the *HTT* gene non-selectively, meaning that both the wild-type and mutant alleles are affected. Given that normal HTT plays an important role in many biological processes, the loss of normal *HTT* could in part be contributing to the failure of these types of drugs. In addition, these trials enroll patients with early-stage disease, but many pathologies arise prior to the onset of disease symptoms. Therefore, it is possible the intervention is too late for proper efficacy (Kingwell, 2021). Most recently, UniQure and Voyager Therapeutics have begun clinical trials utilizing AAVs to deliver microRNAs for gene silencing of *HTT* and *mHTT*, respectively. These approaches hold great promise but also are invasive as delivery of the AAVs involves multiple stereotactic injections directly into the brain via MRI-guided neurosurgery.

Previous studies have shown that mHTT aggregates can be found in the cerebrovasculature (Drouin-Ouellet et al., 2015). Whether these aggregates originate from endothelial cells or are cleared as waste via transcytosis has not been addressed. Nevertheless, our own work has shown the brain endothelial cells do express *HTT*, suggesting that the brain vasculature could in principle contribute to the production of mutant protein and consequently, disease pathology (Garcia et al., 2022). To address the need of a non-invasive, targeted approach for lowering *HTT* in the brain, we developed a cerebrovasculature-targeting AAV that can be administered intravenously via retro-orbital injection into mouse models. To specifically drive

expression of transgenes using recombinant AAVs (rAAVs), we utilized recently developed human DNA MiniPromoters (MiniPs) that drive cell type-specific expression in CNS cells (de Leeuw et al., 2014, 2016; Portales-Casamar et al., 2010). In particular, the Ple34 MiniP contains *CLDN5* regulatory regions for specific expression in brain endothelial cells. We designed a rAAV plasmid containing the Ple34 *CLDN5* MiniP to drive expression of EGFP (pAAV-*CLDN5*::EGFP, **Fig. 6a**) and utilized the AAV9 capsid serotype for production of rAAVs. To validate expression in brain endothelial cells, we injected 6 week old wild-type C57BL6/J mice with AAV9-*CLDN5*::EGFP via retro-orbital administration at a dose of $8x10^{11}$ viral genomes (vg), as previously published (de Leeuw et al., 2016). 4 weeks after viral incubation, we confirm expression of the transgene by immunofluorescent co-localization of EGFP labeling with lectin (**Fig. 6b**).

Next, we designed a rAAV construct for lowering of *HTT* in a cell type-specific manner. To make use of the cell type-specificity afforded by the *CLDN5* MiniP we used a microRNA embedded in a reporter gene intron. The *HTT*-targeting sequence, miH12-451, contains both an optimized scaffold and guide sequence and is currently being developed for HD clinical trials by UniQure (Miniarikova et al., 2018, 2016). Furthermore, to drive increased expression we included a chimeric intron sequence (CIS), derived from the human β-globin gene, downstream of the promoter sequence (Huang & Gorman, 1990). We constructed both pAAV-*CLDN5*::EGFP-miH12-451 (hereto referred to as pAAV-*CLDN5*::EGFP-miR) for targeting *HTT* and pAAV-*CLDN5*::EGFP-scrambled (derived from the miR-155 sequence) as a non-targeting control (**Fig. 6c**). These plasmids were subsequently used for viral packaging using the AAV9 serotype.

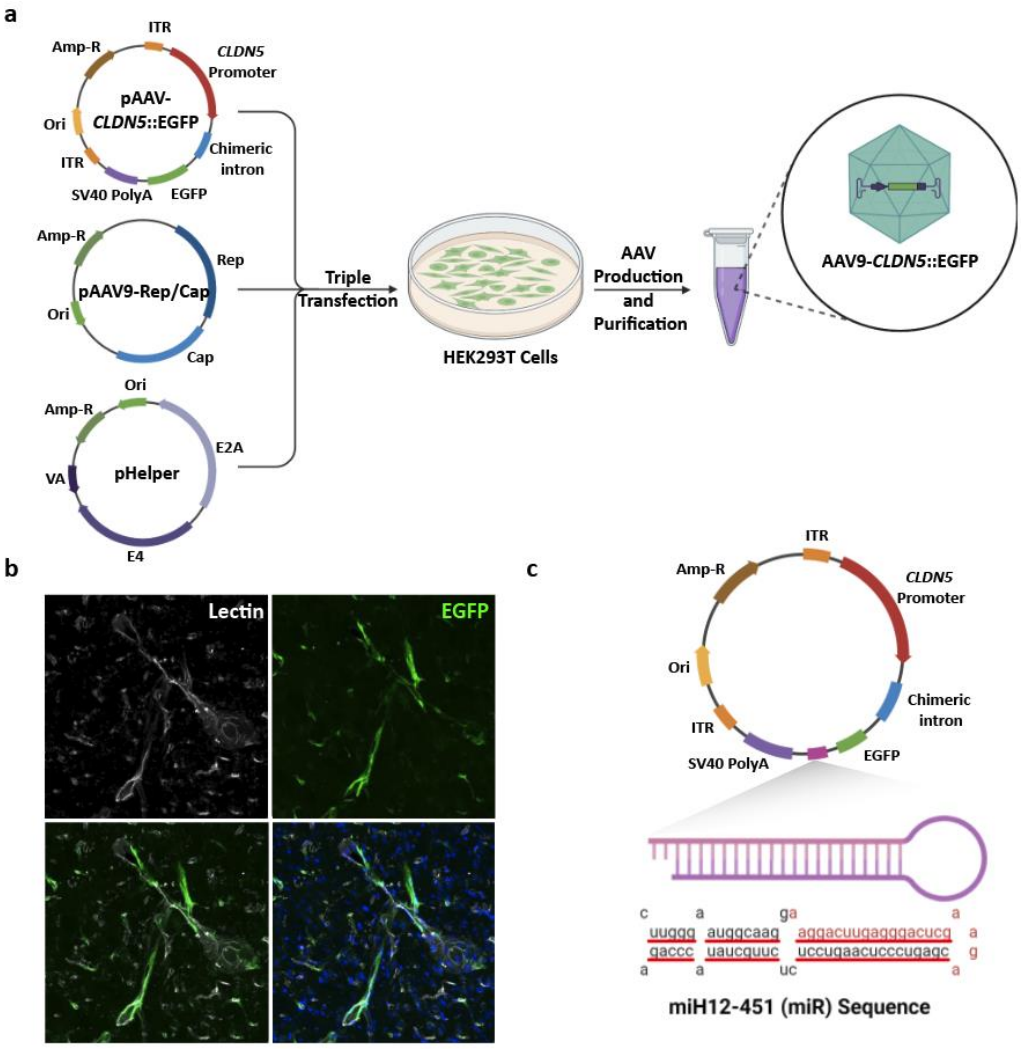

Fig. 6 Design and production of brain vasculature targeting-AAVs. a, Plasmid design and AAV production schematic. pAAV design includes cell type-specific MiniP (*CLDN5*), chimeric intron, EGFP coding sequence, and SV40 polyadenylation signal all flanked by AAV2 ITRs. AAV production utilizing triple transfection method. **b,** Immunofluorescence image of mouse cortex 4 weeks after transduction with AAV9-*CLDN5*::EGFP at 8 x 10^{11} Vg. **c,** Plasmid design for pAAV-*CLDN5*::EGFP-miR encoding a non-allele-specific microRNA targeting exon 1 of the *HTT* gene.

AAVs modulate behavioral phenotypes in the zQ175DN mouse model of HD

To test the role of brain endothelial-derived huntingtin in the disease progression of HD, we administered AAV9-*CLDN5*::EGFP-miR and -scrambled via retro-orbital injection into commonly used human *HTT* knockin mouse lines, zQ175 (Menalled et al., 2012), without its

neomycin cassette, zQ175 delta neo (zQ175DN). This mouse model of HD has been shown to exhibit transcriptional dysregulation and mitochondrial dysfunction in affected SPNs as early as 6 months of age (H. Lee et al., 2020) and precedes some behavioral abnormalities, particularly those observed by rotarod performance at 30 weeks of age (~7.5 months) (Menalled et al., 2012). More recently, arteriolar cerebral blood volume as well as expression of GLUT1 on blood vessels in the striatum has been demonstrated to be significantly increased in heterozygous zQ175DN mice at 3 months of age (Liu et al., 2021), much earlier than reported transcriptional changes in neurons. Given the documented changes to the cerebrovasculature of the striatum in zQ175DN mice at 3 months of age, we administered *HTT*-lowering and non-targeting AAVs ($1x10^{12}$ vg per mouse) at 4 weeks of age (~1 month) into both female heterozygous and non-carrier mice (n=6 mice per group) and performed a battery of behavioral assays, including open-field testing, rotarod, burrowing, rearing and climbing, at specified time points beginning at 5 weeks of age (**Fig. 7a**).

Open-field testing was performed at 9, 21, 24, 29, and 52 weeks of age based on previous behavioral characterization performed on the zQ175 model (Menalled et al., 2012). Consistent with previous studies, we observed no significant differences in ambulatory behaviors (time and distance) at 9 weeks of age across groups. At 21 and 24 weeks of age but not 29 weeks of age, we observed a significant improvement in ambulatory time ($p = 0.0243$, $p = 0.0174$, and $p = 0.3822$ at 21, 24, and 29 weeks of age, respectively) and distance ($p = 0.0702$, $p = 0.0092$, and $p = 0.4235$ at 21, 24 and 29 weeks of age, respectively) between heterozygous mice administered with miR AAV compared to scrambled AAV (**Fig. 7b**). This behavior was exacerbated in the first 10 minutes of the open-field testing session for both ambulatory time ($p = 0.0024$ and $p = 0.0276$ at 21 and 24 weeks of age, respectively) and distance ($p = 0.0047$ and $p = 0.0469$ at 21

and 24 weeks of age, respectively), and though not significant, a trend for improvement was observed at 29 weeks of age ($p = 0.0760$ and $p = 0.0582$ for ambulatory time and distance, respectively) (**Fig. 7c**). The lack of significance at 29 weeks of age could have occurred due to decreased efficacy of the AAV or some other factor like age or testing parameters. Given that previous zQ175 behavioral characterization displayed significance between genotypes during the dark phase, whereas our study measured open-field behaviors during the light phase, we performed open-field testing at 52 weeks of age (12 months of age) during the dark phase. At this age, zQ175DN heterozygous mice administered with the miR AAV demonstrated significantly improved ambulatory time ($p = 0.0087$) and ambulatory distance ($p = 0.0258$). Consistent with previous time points assessed, this behavior pattern was exacerbated during the first 10 minutes of the open-field testing session ($p = 0.0019$ and $p = 0.0098$ for ambulatory time and distance, respectively).

Rotarod performance was assessed at 5 and 54 weeks of age. At 5 weeks, we observed no significant differences between zQ175DN heterozygous mice administered with the miR AAV compared to scrambled AAV at any of the days tested. However, at 54 weeks of age, we observed a significant improvement in latency to fall across these two groups on each of days of testing ($p = 0.0006$, $p = 0.0029$, and $p = 0.0010$ on days 1, 2, and 3 of testing, respectively) (**Fig. 7d**). Furthermore, given the long intermittent time between testing periods, we performed re-training on all mice prior to testing at 54 weeks of age. Interestingly, though not significant ($p = 0.0767$), we observed a positive trend in learning behavior of the rotarod in zQ175DN heterozygous mice administered with the miR AAV compared to scrambled AAV as measured by average number of falls across three trials during the testing period (**Fig. 7e**).

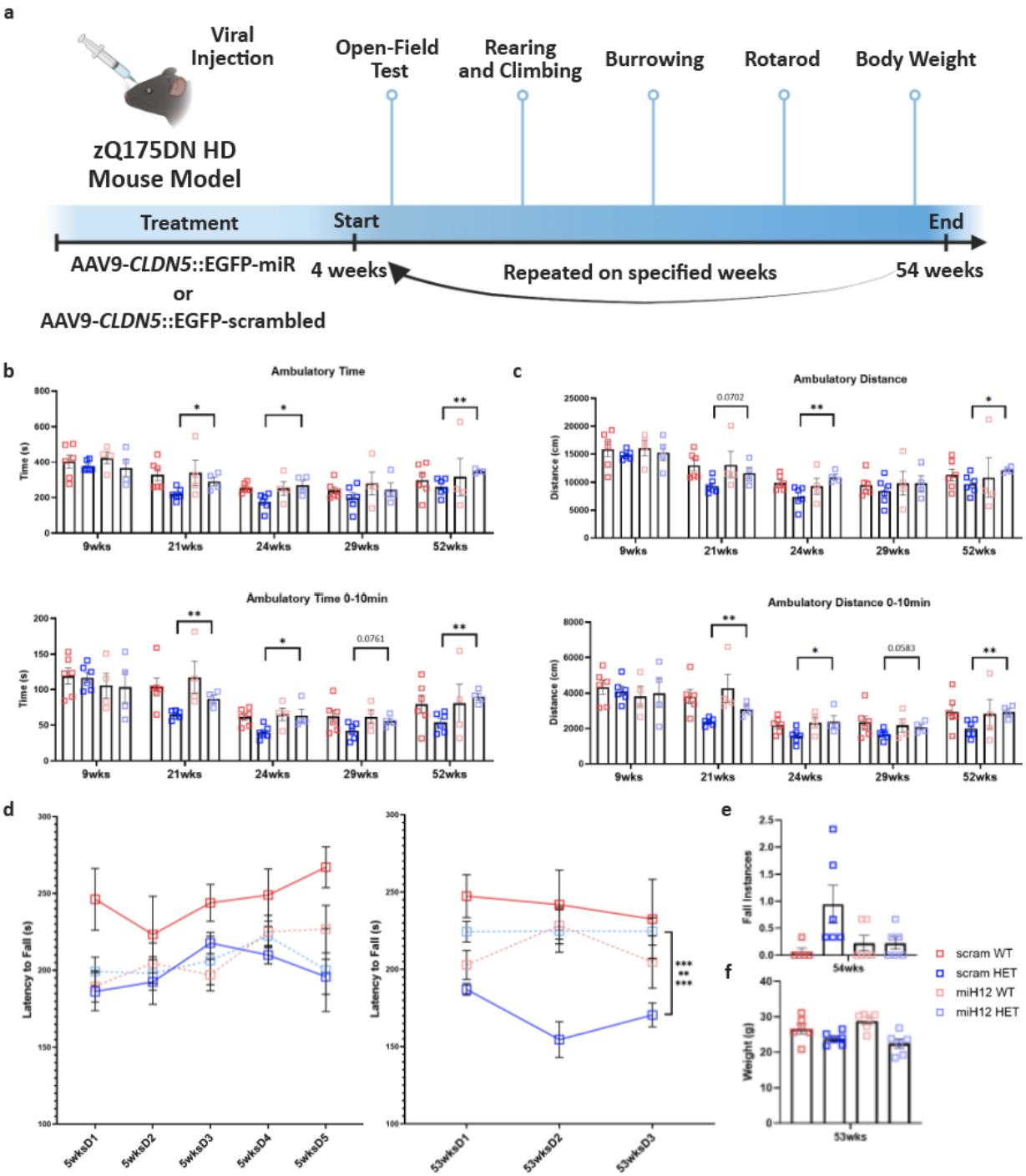

Furthermore, the improvement in locomotor behavior as assessed by both open-field testing and rotarod performance was not due to weight differences across heterozygous mice, as both treated groups showed no significant difference in weight (**Fig. 7f**).

Fig. 7. Behavior performance in zQ175DN mice treated with brain vasculature-targeting AAV. a, Experimental schematic of behavioral assays. **b-c,** Ambulatory time, **b,** and distance, **c,** performance as measured by open field test. Data shown for full 60 min of testing (top) and first 10 min of testing (bottom). **d,** Rotarod performance measured as latency to fall (in seconds) at 5 weeks of age (left) and 54 weeks of age (right). Data for each week represented as average of all mice within a group, with the average of each mouse calculated from 3 trials. **e,** Fall instances at 54 weeks of age. **f,** Weight (measured in grams). Statistical analysis shown as unpaired two-tailed t-tests for all behaviors. Error bars represent stand error of the mean (s.e.m.). Open-field testing on week 52 performed in the dark phase.

Burrowing assay was performed at 29, 52, and 54 weeks of age. At all tested ages, no significance was found across all treated groups in percentage of food pellets burrowed (**Fig. 8a**). Similarly, we performed the rearing and climbing assay at 21 and 52 weeks of age and found no significance in either rearing or climbing behavior across all treated groups (**Fig. 8b-c**).

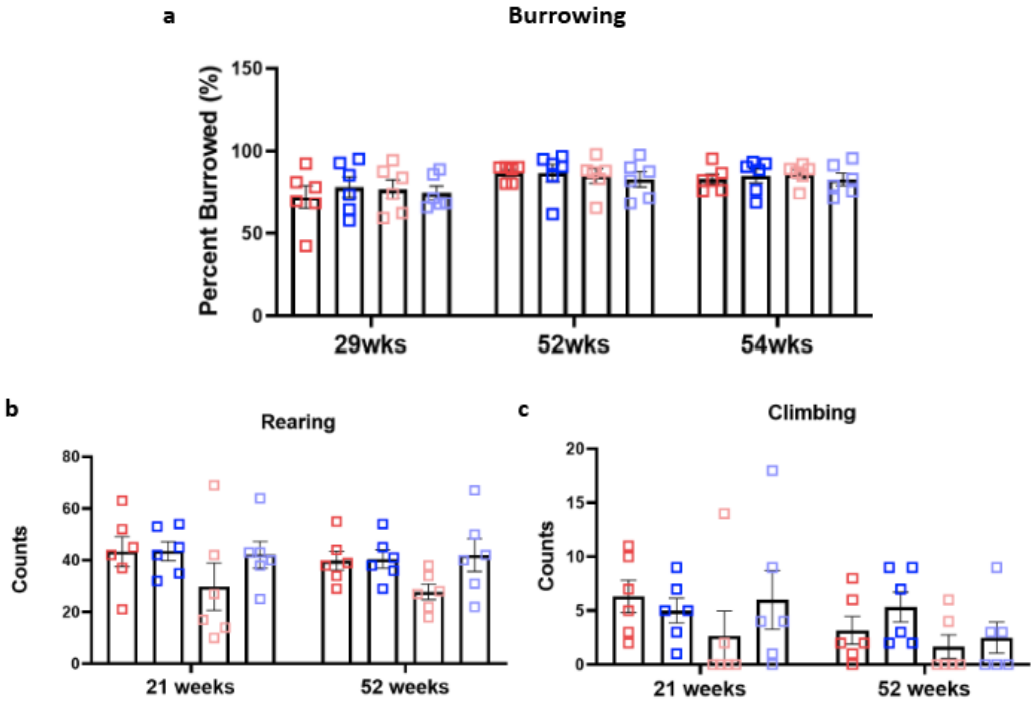

Fig. 8. Burrowing, rearing, and climbing performance in zQ175DN mice treated with brain vasculature-targeting AAV. a, Percent burrowed food pellets at 29, 52, and 54 weeks of age. **b-c,** Rearing and climbing counts measured at 21 and 52 weeks of age. Statistical analyses performed as unpaired two-tailed t-tests for all behaviors. No significance found in any behavioral test shown. Error bars represent stand error of the mean (s.e.m.).

Collectively, these behavioral tasks demonstrate that cell type-specific lowering of *HTT* in the brain endothelium is sufficient to modulate locomotor behaviors in the zQ175DN mouse

model of HD. Importantly, this AAV gene therapy was administered at a pre-symptomatic stage prior to the onset of overt degenerative and cerebrovascular phenotypes. While we did not observe significance in burrowing, rearing, or climbing behaviors, it is important to note that the behavioral phenotypes of the zQ175DN model are mild, and it is likely the assay is not sensitive enough to capture significant differences. Indeed, the burrowing assay in particular was not able to discriminate heterozygous versus non-carrier mice even at the late 54 weeks of age time point where known motor deficits have been extensively documented.

AAVs modulate behavioral phenotypes in the R6/2 mouse model of HD

We repeated AAV-mediated *HTT*-lowering experiments on the R6/2 mouse model of HD, which exhibits a faster progression of disease phenotypes with increased severity (Cepeda-Prado et al., 2012) and demonstrate BBB disruption as early as 6-weeks of age (Di Pardo et al., 2017). AAVs were administered ($1x10^{12}$ vg per mouse) at 4-weeks of age into both male hemizygous and non-carrier mice (n=10 mice per group) with behavioral testing performed every week beginning at 4-weeks of age (1-day post-injection) (**Fig. 9a**).

Open-field testing was performed every week starting at 4 weeks of age. Though we did not observe any significant differences between R6/2 hemizygous mice administered with the miR AAV compared to scrambled AAV at any of the weeks tested, we did observe a trend towards improvement in the last 10 minutes at 8.5 weeks of open field testing in both ambulatory time ($p = 0.1177$) and distance ($p = 0.2067$) (**Fig. 9b-c**).

Rotarod testing was performed at 5, 7, and 8 weeks of age. At 5 weeks of age, all genotypes and conditions performed at equal levels (**Figure 9d**). No significance in number of

falls during training was found across groups, demonstrating that no group had baseline higher performance prior to learning (**Figure 9e**). At 7 weeks of age, hemizygous mice dropped significantly in performance, including both miR and scrambled AAV injected groups. However, consecutive days of testing at 7 weeks of age demonstrated an improvement in rotarod performance in miR-injected hemizygous mice compared to scrambled-injected on Day 3 of testing ($p = 0.0436$). This trend was maintained but not significant at 8 weeks of age, with both groups overall dropping in performance (i.e. decreased latency to fall) but with miR injected mice performing on average better compared to scrambled injected mice. Similar to the zQ175DN, this difference in rotarod performance in R6/2 mice was not due to weight differences across groups, as hemizygous mice in both groups exhibited no significant differences in weight (**Figure 9f**).

Interestingly, unlike the zQ175DN, R6/2 non-carrier mice compared to hemizygous mice displayed decreased performance on the burrowing assay at 8.5 weeks of age. Though not significant, R6/2 hemizygous mice injected with miR AAV demonstrated at trend of improved burrowing compared to hemizygous mice injected with scrambled AAV ($p = 0.1218$) (**Fig. 9g**).

Collectively, these behavioral tasks demonstrate that cell type-specific lowering of *HTT* in the brain endothelium is sufficient to modulate locomotor behaviors in the R6/2 mouse model of HD, though not to the same extent as the zQ175. It is worth noting that this AAV gene therapy was administered also at a pre-symptomatic stage prior to the onset of overt degenerative and cerebrovascular phenotypes. While we did not observe significance in most assays, there are many positive trends in performance which are typically not seen in this mouse model given the fast disease progression. Given that AAV expression does not reach sufficient levels until about 2 weeks post-transduction, it is very possible that the AAV intervention effects would not begin

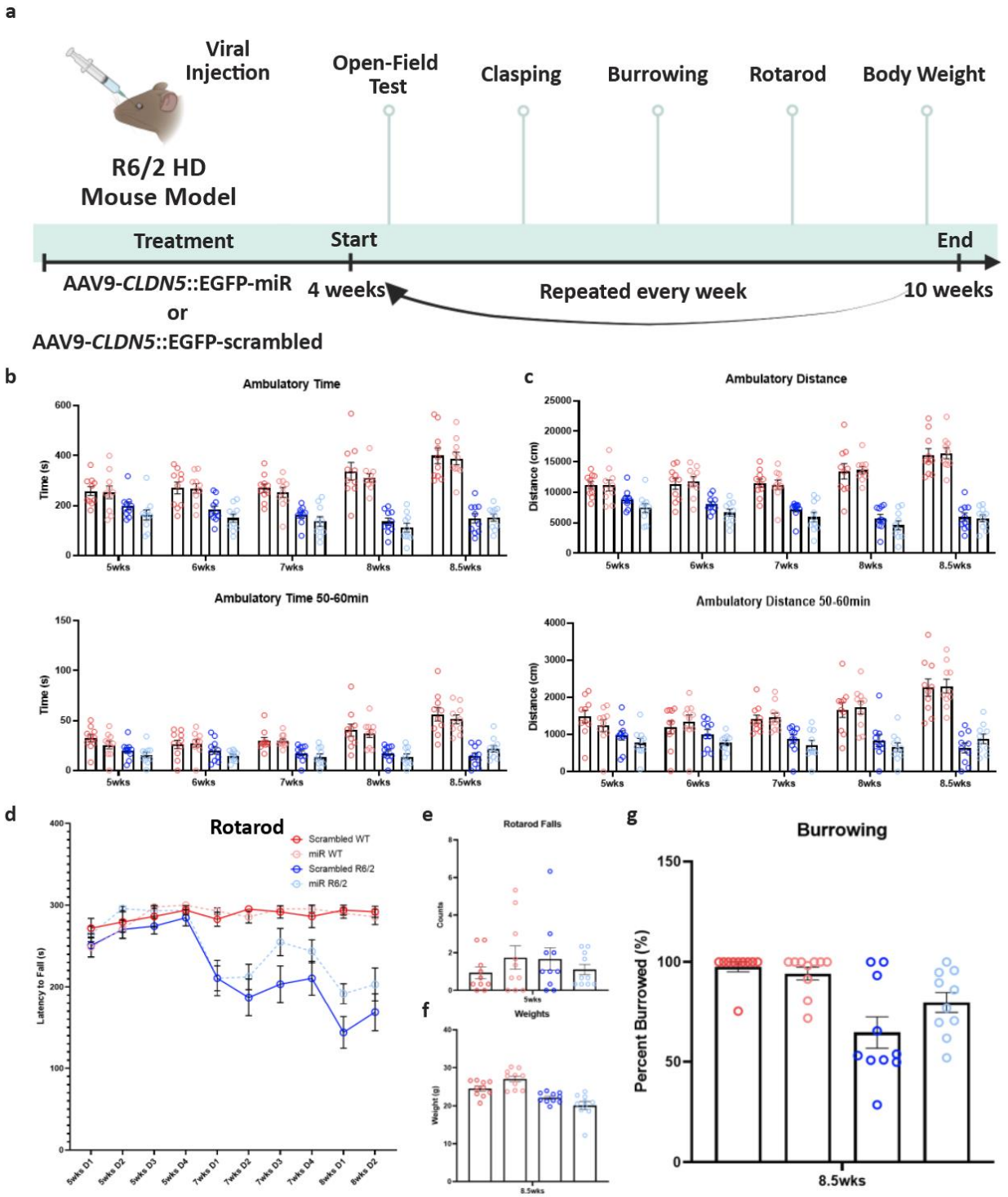

until approximately 6 weeks of age when cerebrovascular changes have already been reported to be present (Di Pardo et al., 2017). Therefore, the mild improvement in motor performance of R6/2 mice that received the miR intervention could be due to the fast disease progression and

Fig. 9. Behavior performance in R6/2 mice treated with brain vasculature-targeting AAV. a, Experimental schematic of behavioral assays. **b-c,** Ambulatory time, **b,** and distance, **c,** performance as measured by open field test. Data shown for full 60 min of testing (top) and last 10 min of testing (bottom). **d,** Rotarod performance measured as latency to fall (in seconds) at 5, 7, and 8 weeks of age. Data for each week represented as average of all mice within a group, with the average of each mouse calculated from 3 trials. **e,** Fall instances at 5 weeks of age. **f,** Weight (measured in grams). **g.** Burrowing assay performance demonstrated as percentage of food pellets burrowed. Statistical analysis shown as unpaired two-tailed t-tests for all behaviors. Error bars represent stand error of the mean (s.e.m.).

onset of cerebrovascular dysfunction around the same time that miR expression begins to reach therapeutic levels.

Chapter 5: Strategies for Interrogating Mechanisms of Cerebrovasculature Cell Types

Neurons and glia are known to interact extensively with the vasculature. Endothelial cells have been shown to synthesize BDNF as a guidance cue for neuronal precursors to migrate along the vasculature in the adult forebrain (Snapyan et al., 2009). Similarly, astrocytes have been shown to provide complementary scaffolds for neuroblasts (Whitman et al., 2009), and microglia migrate postnatally along the vasculature to occupy perivascular regions devoid of astrocytic end-feet (Mondo et al., 2020). How these particular subsets of neuronal and glial cell types are coupled to the vasculature and how their transcriptional profiles differ from non-coupled cells remain unanswered questions.

Furthermore, it is well established that there is regional heterogeneity in gene expression across neuronal and glial cell populations (Hodge et al., 2019; Saunders et al., 2018). Whether this extends to cerebrovascular cell types is unclear; however, evidence from functional and disease studies suggests there to likely be regional differences. For example, nitric oxide (NO), an important vasodilator, is normally produced through the catalytic activity of nitric oxide synthase (NOS) expressed in brain endothelial cells, eNOS. However, in the hippocampus, the main source of NO is produced through the activity of neuronal NOS, nNOS. Nerve fibers in close proximity to hippocampal arterioles contain nNOS to generate NO that can influence vascular tone. In addition, experiments using L-NAME (NG-nitro-L-arginine methyl ester), an inhibitor of NOS, have shown that while large arteries that feed into the hippocampus (i.e. posterior cerebral artery) and cortical arterioles undergo vasoconstriction after L-NAME treatment, hippocampal arterioles are unaffected, suggesting that the endothelium does not produce NO, and thus, the basal activity of NOS-mediated regulation of myogenic tone is different in the hippocampus (Johnson, 2023).

As another example, the basal ganglia is a region particularly vulnerable to infarcts and lesions, in part thought to be because of how it is vascularized. Anatomical studies have shown that the main vascular supply of the basal ganglia stems from the lenticulostriate arteries (LSAs) and the recurrent artery of Heubner (RAH). Functional compartments of the basal ganglia overlap with microvascular territories and contain a large number of non-anastomotic vessels, thereby compartmentalizing the blood supply to each of the sub-regions. In considering the origins from the Circle of Willis, the LSAs branch from the middle cerebral artery whereas the RAH branches from the anterior cerebral artery (Feekes & Cassell, 2006; Kirst et al., 2020). Therefore, the sources of CBF into the basal ganglia are distinct and could impact not only their predisposition to insults but also their baseline gene expression profiles.

Together with evidence from the basal ganglia, hippocampus, and cortex, it is likely that gene expression patterns of cerebrovascular cell types are distinct across brain regions and that these profiles are also likely to have functional consequences on brain dynamics, such as neurovascular coupling. In this chapter, I present preliminary evidence both supporting the existence of vasculature-coupled (vc) cell types in the mouse and human brain, as well as tools for beginning to dissect the underlying mechanisms in a region-specific manner.

Vasculature-coupled cell types in the human brain

In our *ex vivo* human samples, as expected by physical BVE protocol co-purification, we found vasculature-coupled (vc) neuronal and glial cells with distinct expression profiles from the corresponding canonical cell types. Despite showing features of both canonical and vascular cells, we confirmed vasculature-coupled cells do not stem from ambient RNA or doublets, as they were unaffected by two rounds of doublet exclusion at the cluster and cell levels and

ambient RNA removal steps (**Extended Data Fig. 11a-b**). Furthermore, to rule out the possibility of vascular cell contamination, we performed a computational subtraction analysis of canonical cell signatures from their corresponding vasculature-coupled pairing, and demonstrated that the residual signatures did not cluster with any vascular cell type, indicating that these cells do not represent doublets but harbor unique gene expression profiles (**Extended Data Fig. 11c**). Hundreds of specifically expressed genes in these vasculature-coupled cells, when compared to canonical cell types, included significant enrichment in the regulation of angiogenesis, metal ion transport, and protein localization terms (**Extended Data Fig. 11d-e**). In particular, vc-astrocytes and vc-microglia showed increased expression of genes involved in the negative regulation of cell migration and cell junction assembly, suggesting these cell types exhibit more stationary behavior (e.g. less dynamic processes) when coupled to the vasculature (**Extended Data Fig. 11f**).

We validated the snRNA-seq observed proportion of vc-cell types by utilizing known markers to calculate proportions of different cell types in immediate proximity of blood vessels (see Methods), and used novel markers to specifically label these coupled cells. In particular, we performed indirect immunofluorescence staining for OLIG2, GFAP, and NeuN to label all oligodendrocytes, astrocytes, and neurons, respectively, and then counted the proportion in direct contact with the vasculature in tissue sections. Cell counting proportions for these vc-cell types across multiple samples were consistent with proportions obtained by snRNA-seq (**Extended Data Fig. 11g**).

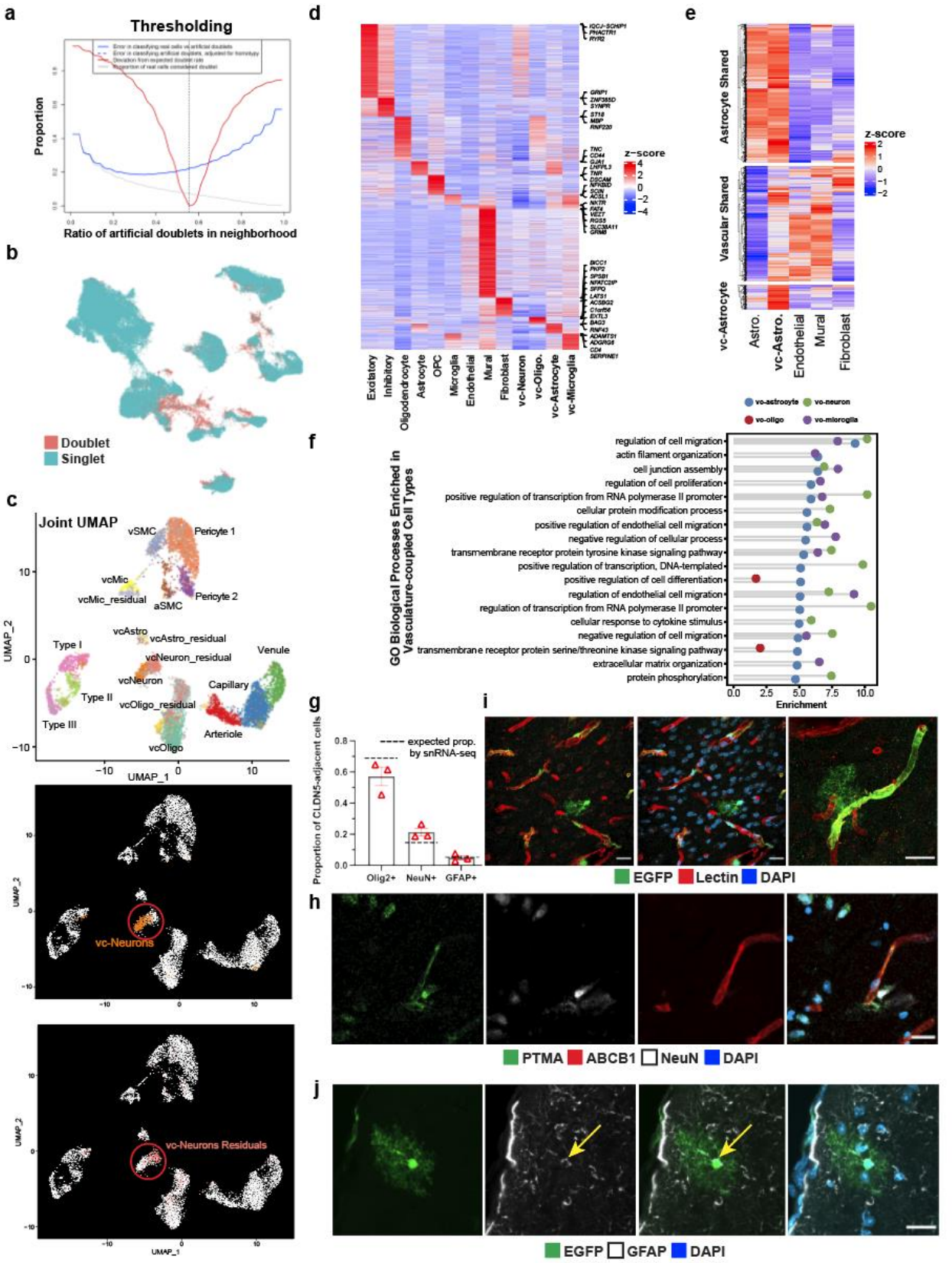
a
Thresholding
Proportion
Ratio of artificial doublets in neighborhood
b
Doublet
Singlet
c
Joint UMAP
vSMC
Pericyte 1
vcMic
vcMic_residual
aSMC
Pericyte 2
vcAstro
vcAstro_residual
Type I
vcNeuron_residual
Venule
vcNeuron
Capillary
Type II
vcOligo_residual
Type III
Arteriole
vcOligo
UMAP_1
UMAP_2
vc-Neurons
vc-Neurons Residuals
d
z−score
Excitatory
Inhibitory
Oligodendrocyte
Astrocyte
OPC
Microglia
Endothelial
Mural
Fibroblast
vc-Neuron
vc-Oligo.
vc-Astrocyte
vc-Microglia
e
Astrocyte Shared
Vascular Shared
vc-Astrocyte
z-score
Astro.
vc-Astro.
Endothelial
Mural
Fibroblast
vc-astrocyte
vc-neuron
vc-oligo
vc-microglia
f
GO Biological Processes Enriched in Vasculature-coupled Cell Types
regulation of cell migration
actin filament organization
cell junction assembly
regulation of cell proliferation
positive regulation of transcription from RNA polymerase II promoter
cellular protein modification process
positive regulation of endothelial cell migration
negative regulation of cellular process
transmembrane receptor protein tyrosine kinase signaling pathway
positive regulation of transcription, DNA-templated
positive regulation of cell differentiation
regulation of endothelial cell migration
regulation of transcription from RNA polymerase II promoter
cellular response to cytokine stimulus
negative regulation of cell migration
transmembrane receptor protein serine/threonine kinase signaling pathway
extracellular matrix organization
protein phosphorylation
Enrichment
g
Proportion of CLDN5-adjacent cells
expected prop. by snRNA-seq
Olig2+
NeuN+
GFAP+
i
EGFP
Lectin
DAPI
h
PTMA
ABCB1
NeuN
DAPI
j
EGFP
GFAP
DAPI

Extended Data Figure 11. Vascular-coupled (vc) cell types in the *ex vivo* snRNA-seq data. a. Thresholding parameters for doublet detection. **b.** UMAP of determined singlet/doublets in human *ex vivo* samples. **c.** UMAPs of joint (top), vc-neurons (orange) and vc-neuron residuals (pink) after subtraction of canonical neuron signature. **d.** Heatmap of DEGs in canonical, vascular, and vascular-coupled cell types. **e.** Heatmap of DEGs in all astrocytes (top), shared between vc-astrocytes and vascular cell types (middle), and vc-astrocytes only (bottom). **f.** Gene ontology enrichment in vc-cell types. **g.** Quantification of vc-cell types in direct contact with the vasculature by indirect immunofluorescence staining and cell counting in tissue. Dashed lines represent proportions reported by snRNA-seq. **h.** Indirect immunofluorescence staining of a PTMA-expressing vc-neuron that is on the vasculature. **i.** Virally transduced *CLDN5*::EGFP expression in mouse brain vc-astrocytes and endothelial cells. **j.** Co-localization of a non-vessel, *CLDN5*::EGFP-expressing cell with the astrocyte marker GFAP. Yellow arrow depicts EGFP+/GFAP+ astrocyte. Scale bar, 20μm.

As migrating neuroblasts have been shown to use the vasculature as a scaffold during adult neurogenesis in mouse, we predicted that vc-neurons may represent this population of immature interneurons. Indeed, vc-neurons were highly enriched for LATS1, TIMP2, and PTMA compared to all canonical neurons, with all three genes previously shown to play roles in neuronal differentiation (X. Cao et al., 2008; Halder & Ueda, 2012; Pérez-Martínez & Jaworski, 2005; Ueda et al., 2017). We validate that a small number of NeuN/RBFOX3-expressing neurons co-express LATS1 and PTMA and can be found immediately adjacent, seemingly coupled, to blood vessels (**Fig. 10a, Extended Data Fig. 11h**). We further investigated this in vivo by utilizing the thymidine analogue, ethynyl deoxyuridine (EdU), to label dividing cells in the adult mouse brain. After 30 days of EdU administration, we found that compared to NeuN+/EdU- cells (23.8%), NeuN+/EdU+ cortical neurons (42.8%) were significantly more likely to be localized on the vasculature (**Fig. 10b**). These results are consistent with those found in humans and suggest that vc-neurons most likely represent a population of immature interneurons along the vasculature which exhibit distinct transcriptional programs.

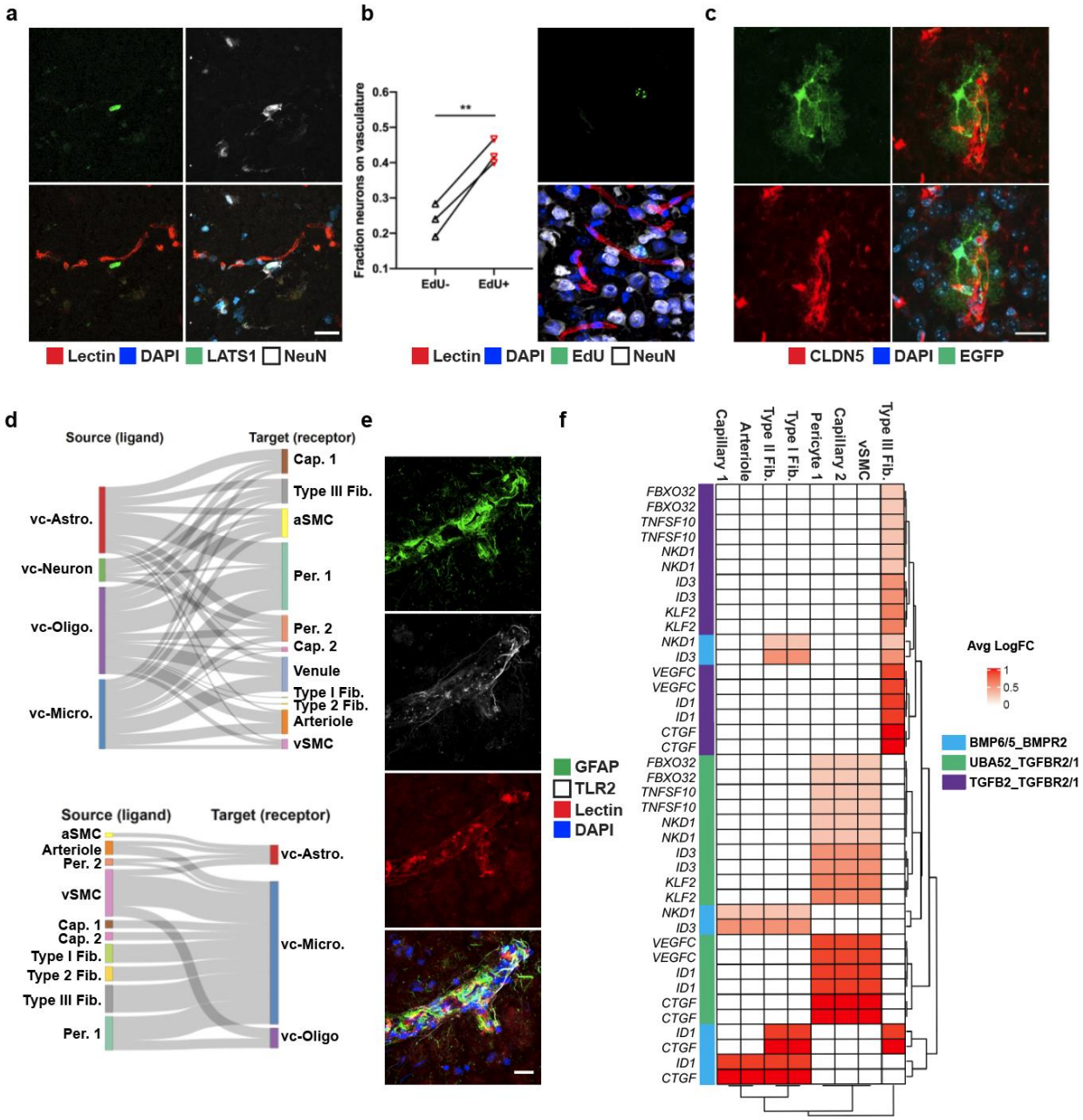

Fig. 10. Cell types coupled to the human cerebrovasculature. a. Co-localization of vc-neuron expressing LATS1/NeuN along the vasculature. **b.** Quantification of EdU and NeuN cells along the vasculature. Indirect immunofluorescence showcases an EdU+/NeuN+ cell along the vasculature. **c.** Virally transduced *CLDN5*::EGFP expression in mouse brain vc-astrocytes and endothelial cells. **d.** Cell-cell interaction Sankey plots between vascular cell types (endothelial, mural, fibroblast) and canonical cell types (astrocyte, neurons, microglia, oligodendrocytes). **e.** Indirect immunofluorescence of GFAP/TLR2 expressing astrocytes coupled with the cerebrovasculature. **f.** Heatmap of ligand-receptor pairings in vascular cells (ligand) and microglia (receptor) and downstream target. Scale bar, 20µm. **p < 0.01

Astrocytes have been shown to express cell junction proteins, including members of the claudin family (e.g. CLDN1, CLDN2, CLDN4, CLDN11) (Horng et al., 2017; Romanitan et al., 2010). Interestingly, a subset of astrocytes in the frontal cortex has also been shown to express CLDN5 (Romanitan et al., 2010), a marker gene for brain endothelial cells. We found that vc-astrocytes in particular, when compared to canonical astrocytes, displayed enriched expression of CLDN5. To validate the expression of CLDN5 in astrocytes, we performed viral-mediated transduction using an adeno-associated virus injected intravenously engineered to allow expression of EGFP under the CLDN5 promoter, as described previously. We observed brain-wide transduction of blood vessels (**Extended Data Fig. 11i**), and, as predicted by our snRNA-seq data for vc-astrocytes, a subpopulation of astrocytes expressing EGFP (**Fig. 10c**). We validated these non-endothelial CLDN5-expressing cells to be vc-astrocytes by virtue of their expression of the astrocyte marker GFAP (**Extended Data Fig. 11j**). Though not all GFAP+ astrocytes were EGFP+, transduced EGFP+ astrocytes were found across the whole brain, including cortex, striatum, hippocampus, and midbrain, and in close proximity to the vasculature, with their soma in close proximity to blood vessels. Together, our functional enrichment analysis and *in vivo* experiments using cell type-specific viral transduction suggest vc-astrocytes represent a subpopulation of astrocytes closely coupled to the vasculature.

Furthermore, to reveal mechanisms of communication between vasculature-coupled and vascular cell types, we computationally integrated cell type-specific ligand, receptor, and downstream target gene expression in a statistical permutation framework (see Methods). We found that vc-astrocytes, vc-oligodendrocytes, and vc-microglia all interact extensively with Pericyte 1 cells, as a major signal-receiving vascular cell type (**Fig. 10d**). We confirm TLR2 enrichment in vc-astrocytes by indirect immunofluorescence staining to demonstrate that a

subset of GFAP-expressing astrocytes in proximity to the vasculature express TLR2, whereas GFAP-expressing astrocytes not in proximity to blood vessels do not express TLR2 (**Fig. 10e**). Lastly, we found vc-microglia receive signals from many vascular cell types, including vSMCs, all fibroblast subtypes, and pericytes, indicating that they may act as central hubs for vasculature interactions. Predicted receptors TGFBR1, TGFBR2, and BMPR2 were highly expressed in vc-microglia, indicating they may act as mediating receptors. These receptors activate downstream targets ID1, VEGFC, and ID3, which were also highly expressed in vc-microglia (**Fig. 10f**).

Improved design of genetic tools for profiling cerebrovasculature cell types *in vivo*

Despite the high specificity of our previously developed AAV plasmids for targeting the cerebrovasculature, a constraint of AAVs is the packaging capacity which is typically between 4.5-4.8kb from 5' ITR to 3' ITR and includes the ITRs. Given the size of the MiniP for *CLDN5* used in previous experiments (2976bp), the usage of this AAV for overexpression constructs is very limited. Furthermore, the development of improved AAV capsids derived from AAV9 using directed evolution methods has enabled for packaging of constructs into AAVs with increased tropism towards brain endothelial cells (Ravindra Kumar et al., 2020). However, this improved capsid targeting brain endothelial cells, PHP.V1, has also shown to transduce ~60% cortical astrocytes.

To improve upon this system, we combined the specificity of a new generation of *CLDN5* MiniP (Ple261) with a shorter size (1670bp) with the increased tropism of the PHP.V1 capsid to transduce brain endothelial cells. Using previously developed methods for generation of rAAVs, we produced viral particles of PHP.V1-*sCLDN5*::EGFP ("*sCLDN5*" for short *CLDN5*

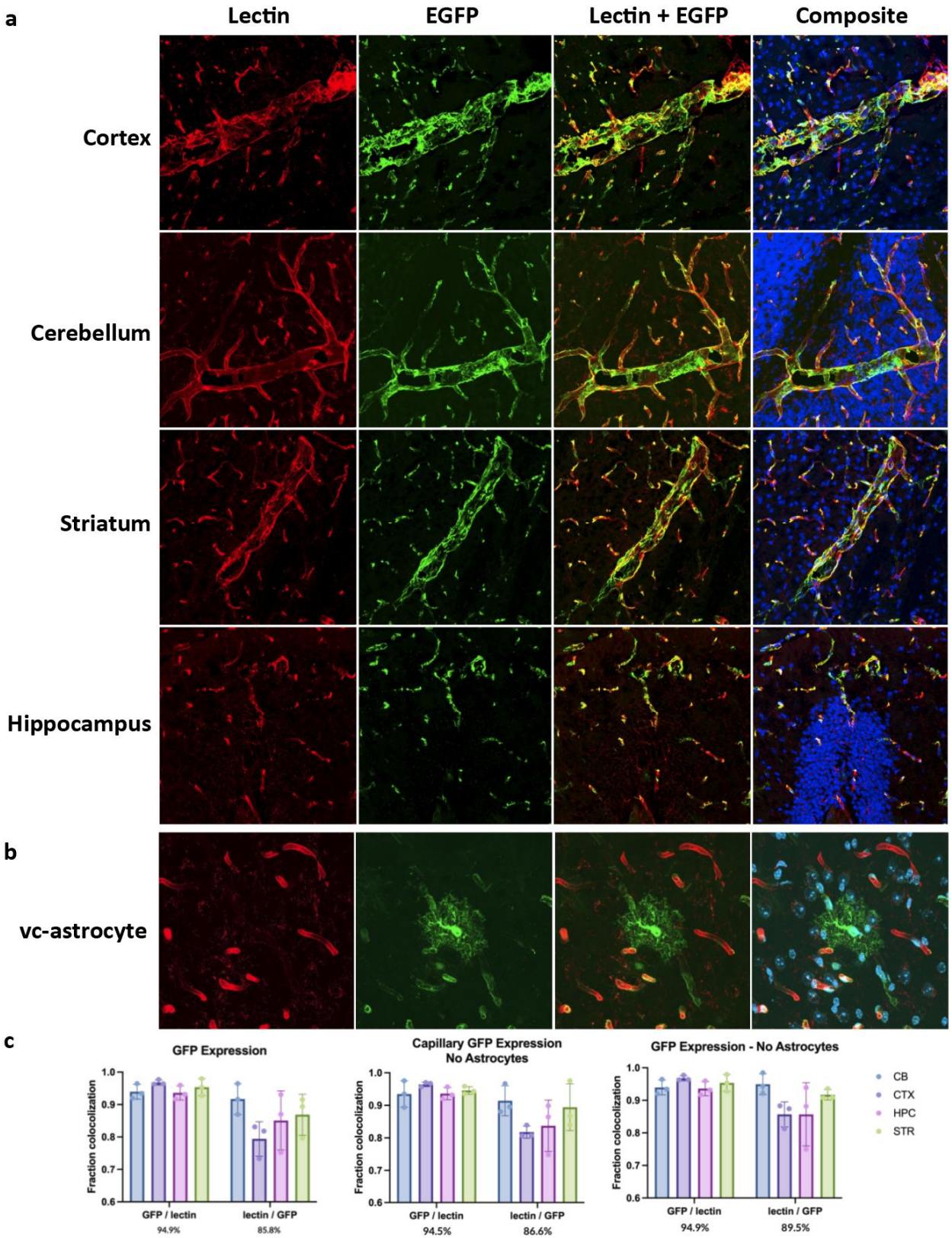

to distinguish from previous iteration of the *CLDN5* MiniP) for intravenous injection into wild-type C57BL6/J mice.

Fig. 11. Transduction efficiency of PHP.V1-s*CLDN5*::EGFP in wild-type mice. a. Immunohistochemical images of 6-week-old C57BL6/J mice injected with AAV by retro-orbital injection. Representative images 4 weeks post-transduction shown across multiple brain regions including cortex, cerebellum, striatum, and hippocampus. **b,** Expression of EGFP in vc-astrocytes. **c,** Quantification of transduction efficiency across multiple brain regions. Each dot represents individual biological replicates (n = 3) calculated as average expression of GFP/lectin across 3 images. CB = cerebellum, CTX = cortex, HPC = hippocampus, STR = striatum.

We performed immunohistochemical analysis on 6 week old wild-type mice 4 weeks post-transduction of injected PHP.V1-s*CLDN5*::EGFP at a dose of 1 x 10^{12} vg per mouse. We

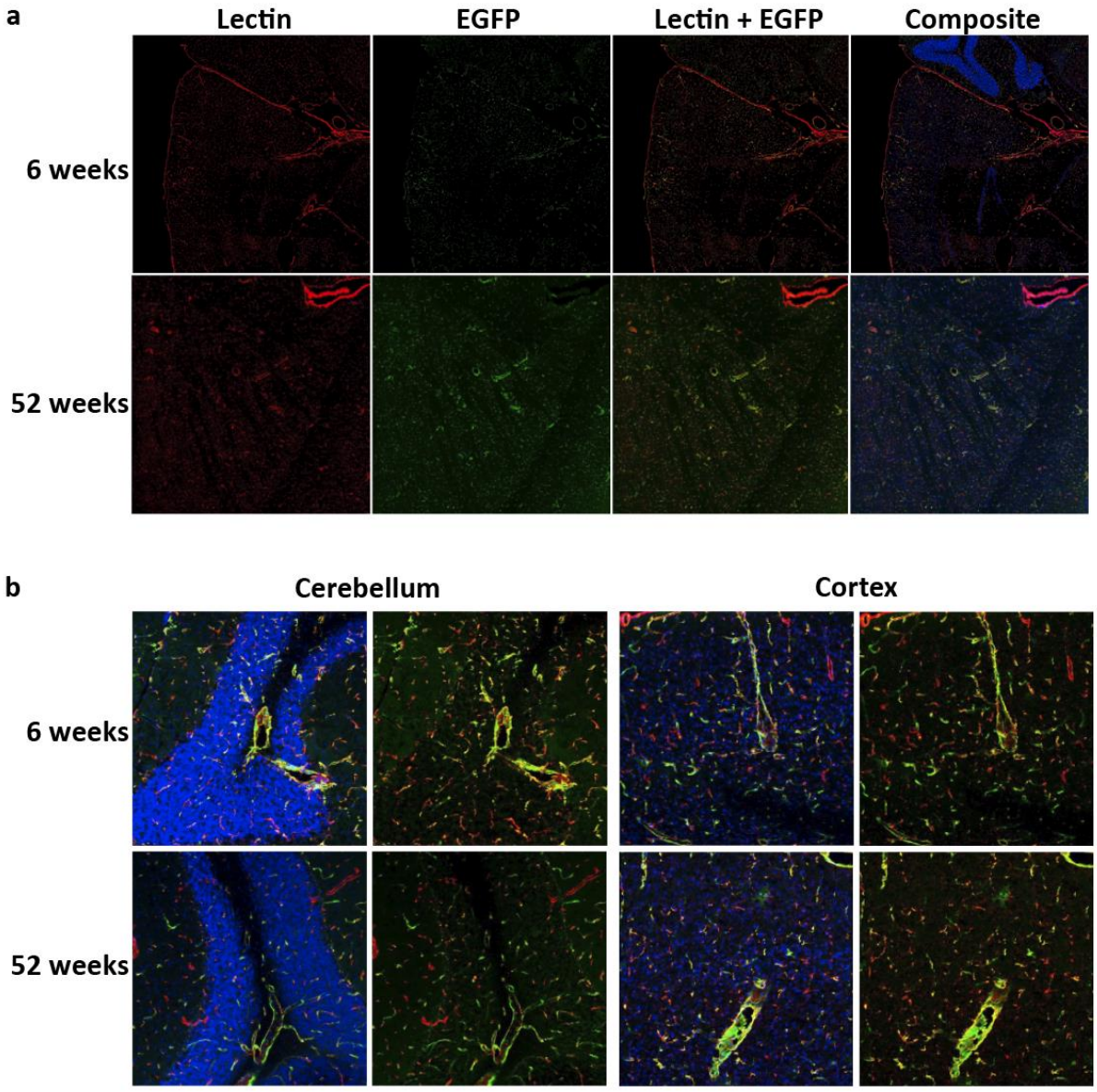

Fig. 12. Transduction efficiency of PHP.V1-s*CLDN5*::EGFP in young and aged mice. a. Immunohistochemical images of 6-week-old and 52-week-old C57BL6/J mice injected with AAV by retro-orbital injection. Representative images 4 weeks post-transduction shown across multiple brain regions including cortex and cerebellum (top) and striatum (bottom). **b,** Zoomed in view of transduction efficiency in 6-week-old and 52-week-old mice across cerebellum (left) and cortex (right).

found specific, brain-wide transduction of both large and small parenchymal vessels (**Fig. 11a**) as well as a small population of transduced astrocytes which likely represent the previously described vc-astrocytes in close proximity to the vasculature (**Fig. 11b**). We quantified the transduction efficiency across multiple brain regions including cortex, cerebellum, striatum, and hippocampus and found that across brain regions we transduce on average 94.9% of blood vessels when normalized to lectin staining (**Fig. 11c**).

Interestingly, we observed no expression of EGFP in either pial vessels on the surface of the parenchyma or in choroid plexus epithelial cells (**Fig. 12a**). Furthermore, when injected into aged, 52-week-old, mice, we also observed similar phenomenon and brain-wide transduction (**Fig. 12a-b**), demonstrating the feasibility of using this viral tool for aging studies. We further confirmed the specificity by analyzing other organs and observed no transduction in either heart or liver vasculatures (data not shown).

To further illustrate the utility of this viral tool for targeting brain endothelial cells, we developed constructs for interrogating different aspects of the cerebrovasculature. In particular, we designed AAVs for profiling the translatome of the vc-astrocyte population via administration into *Aldh1l1*-Cre mice of a PHP.V1-s*CLDN5*::DiO-TRAP virus driving expression of the TRAP construct in a double-inverted orientation (data not shown). Furthermore, we designed AAVs for profiling mitochondrial proteome by administration of a PHP.V1-s*CLDN5*::MITO-Tag virus driving expression of a MITO-Tag construct (Bayraktar et

al., 2019) to label the mitochondria in brain endothelial cells (data not shown). Lastly, we designed AAVs for overexpression of essential BBB genes by administration of PHP.V1-s*CLDN5*::MFSD2A-3xHA to drive expression of MFSD2A (data not shown) which has been shown to be significantly downregulated across multiple neurodegenerative diseases. Altogether, these tools demonstrate the feasibility of using AAV approaches not only for gene therapy applications, but also interrogating different aspects of cerebrovascular biology.

Chapter 6: Discussion

The following text and figures have been adapted from previously published work by Francisco J. Garcia and co-authors. For original article, see [Garcia, Francisco J., et al. "Single-cell dissection of the human brain vasculature." Nature 603.7903 (2022): 893-899.]

Single-cell profiling of the human brain vasculature in health and disease

Interrogating cell types of the cerebrovasculature in humans at a molecular level has been challenging owing to a lack of a high-throughput methodology to capture these cell types for genome-wide gene expression analyses. Species-specific patterns of expression between mouse and human brain microvessels have been noted, but the lack of cellular specificity has prevented a thorough mapping of their molecular composition (Song et al., 2020). Here, by developing independent experimental and in silico sorting methodologies for the enrichment and compatibility with snRNA-seq, we catalogued the transcriptional profiles of thousands of single nuclei comprising the human cerebrovasculature. Included are profiles generated from fresh human cortex surgical resections that eliminate any possibility of transcriptional alterations associated with the post mortem interval. These profiles reveal human-specific characteristics of the cerebrovasculature. We observe that vascular zonation is an evolutionarily conserved phenomenon when comparing mice to humans despite notable gene expression differences along the arteriovenous axis. We observed similar degrees of diversity and specificity in the gene expression patterns of mural cells, which until now have remained ill-defined, and validated the expression of new marker genes, confirming the cell-type-specific expression at the protein level. In addition, we identified three subtypes of perivascular fibroblasts. Last, in our ex vivo enriched dataset, we found subpopulations of neuronal and glial cells co-clustering with vascular cell types. We excluded these cells from analysis here, owing to the possibility of nuclei doublets, but they may represent bona fide populations of vasculature-coupled cells, as recently reported for

both microglia and adult-born immature neurons (Fujioka et al., 2019; Mondo et al., 2020), and future work will be needed to elucidate their identity and functions.

Understanding the normal cellular and molecular characteristics of the cerebrovasculature is crucial for studying mechanisms of its dysfunction. Thus, we also conducted cell-type-specific differential gene analysis of cerebrovascular cells in the context of HD to elucidate potential mechanisms of dysfunction. In addition to the previously studied Wnt signalling pathway (R. G. Lim et al., 2017), our work reveals the activation of the innate immune signalling, which we have recently reported to occur in striatal neurons (H. Lee et al., 2020; R. G. Lim et al., 2017), as also occurring in endothelial cells and vascular-interacting astroglial and microglial cells in the HD brain. Our work reveals that this innate immune activation co-occurs with loss of endothelial tight junction protein expression, suggesting that blockade of innate immune activation in the HD brain could prevent loss of BBB integrity. Future studies in mouse models will provide further insights into the therapeutic potential of targeting these gene alterations in the cerebrovasculature. Further investigating large intracranial vessels will be of great importance given their prominent role in other neurological diseases (Wingo et al., 2020).

Viral tools for gene therapy and profiling cerebrovascular biology

Advances in single-cell technologies has demonstrated the differential roles of cell types in health and disease. It has been noted that specific neuronal populations in the brain are particularly vulnerable across different neurodegenerative diseases (Fu et al., 2018), demonstrating the need to develop targeted therapeutics that not only cross the BBB but also selectively affect only specific populations of cells. Development of gene therapy strategies are promising approaches but are costly and time-consuming. Rather than developing gene therapy interventions for specific diseases, development of gene therapy interventions to target a

common phenotype across multiple neurological disorders may demonstrate promise for delaying disease progression. The cerebrovasculature has recently been shown to exhibit dysfunction early in the disease progression of multiple neurodegenerative disorders. Furthermore, given the accessibility through the circulatory system, administration of gene therapy strategies intravenously provides a non-invasive route for drug delivery.

By targeting the causative gene in a monogenic, neurodegenerative disease, namely, Huntington's disease, we demonstrate that targeting the cerebrovasculature to lower levels of *HTT* is sufficient to delay the progression of behavioral phenotypes in two mouse models. These proof-of-principle experiments highlight the potential of using non-immunogenic AAVs to treat multiple neurological disorders, in particular those with know genes that induce brain pathologies (e.g. amyloid-β, α-synuclein, etc.).

Furthermore, we also demonstrate that by improving the specificity and design of the AAV plasmid, we can develop an assortment of viral tools for studying various biological mechanisms of the cerebrovasculature, including but not limited to, regional heterogeneity in gene expression, vasculature-coupled cell types, mitochondrial diversity, and BBB function.

Combined with our high-resolution profiling of the human brain vasculature, our studies demonstrate the importance of studying the cerebrovasculature to further understand mechanisms of normal brain function and alterations in disease. Future studies will shed important insights into the utility of these transcriptomic datasets and gene therapy tools not only for our understanding of basic cerebrovascular biology but also for the potential to treat incurable brain diseases.

Chapter 7: Methodology

Animal use

All animal experiments were approved by the MIT Committee on Animal Care. Mice were grouped housed with food and water provided ab libitum on a standard 12 h light/12 h dark cycle. Male 6-week-old C57BL/6J wild-type mice (Jackson Laboratories stock number 000664) were used for snRNA-seq and immunofluorescence experiments. Male 4- and 9-week-old B6CBA-Tg(HDexon1)62Gpb/1J mice (CAG repeat length 160 ± 5; Jackson Laboratories stock number 002810) and non-carrier controls were used for R6/2 experiments. Female 4-week-old B6J.zQ175DN (Jackson Laboratories stock number 370832) knock-in congenic and non-carrier C57BL/6J mice were used for zQ175 experiments. Male 4-week-old B6;FVB-Tg(Aldh1l1-cre)JD1884Htz/J (Jackson Laboratories stock number 023748) mice were used for PHP.V1-sCLDN5::DiO-TRAP experiments. No prior procedures were performed on any animal before experiments. Randomization and blinding of animals was not necessary in this study given the unbiased experimental approach. All brain dissections were performed on dry ice after cooling the head in liquid nitrogen for 3 s. Dissected whole brain or posterior cortex were subsequently flash frozen in liquid nitrogen and stored at −80 °C until further use.

Human tissue

Human tissue analyses were conducted as exempt human research, as this was secondary research using biological specimens not specifically collected for this study. All samples were obtained from biobanks/repositories as follows, using appropriate de-identification and under consent. All resected ex vivo human tissue was originally obtained fresh or fresh-frozen from the Boston Children's Hospital through the Phenotyping and Banking Core of Neurological

Disorders (protocol 09-02-0043 approved by the Boston Children's Hospital Institutional Review Board (IRB), under which samples are collected for the use of Boston Children's Hospital investigators and their collaborators). On surgical resection, tissue was examined by a licensed neuropathologist and allocated for clinical or research purposes. Non-pathologically deemed tissue was then either used immediately or stored fresh frozen at −80 °C until further use. All selected samples were from patients aged between 11 and 22 years with a primary diagnosis of medically refractory epilepsy with no known genetic mutations (that is, spontaneous epilepsy). Individuals with known arteriovenous malformations were also excluded from the study. In silico data were derived from 12 pathologically normal donor samples obtained from the Religious Orders Study and Rush Memory and Aging Project (ROSMAP), and data were obtained from the Rush Alzheimer's Disease Center Repository following guidelines approved by the IRB of the Rush University Medical Center. For these samples, all participants signed a Repository Consent form in addition to Informed Consent and an Anatomic Gift Aid. These ROSMAP samples included 7 brain regions: prefrontal cortex, mid-temporal cortex, angular gyrus, entorhinal cortex, thalamus, hippocampus and mammillary body. HD profiling data were derived from 8 HD and 8 age-matched unaffected control post mortem tissue samples, which were acquired through the National Institutes of Health (NIH) NeuroBioBank or the University of Alabama at Birmingham.

Indirect immunofluorescence staining

Brain tissue was collected from the HD R6/2 model and the control mice following transcardial perfusion with 4% PFA in 1× PBS. Human and mouse brain tissue samples were cryoprotected and cryosectioned onto glass slides at 20 µm thickness. Sections were fixed for 10 min using cold

acetone (human alone) under gentle agitation, washed with 1× TBS, permeabilized with 1× TBS-T (1× TBS with 0.05% Tween20) and blocked with blocking buffer (2% heat-inactivated donkey serum, 0.1% fish gelatin in 1× TBS-T) for 1 h at room temperature. Slides were subsequently incubated with primary antibody in blocking buffer at specified dilutions (Supplementary Table 6) overnight at 4 °C. Slides were then washed with 1× TBS-T, incubated with secondary antibody (1:5,000 dilution of specified fluorophore as described in Supplementary Table 6) in blocking buffer for 1 h at room temperature, washed again with 1× TBS-T followed by 1× TBS, stained with DAPI and mounted with ProLong Gold antifade mounting medium (ThermoFisher Scientific). For post mortem human tissue sections, autofluorescent signal arising from endogenous lipofuscin was quenched with a 30-s exposure to TrueBlack Lipofuscin Autofluorescence Quencher (Biotium) and washed with 1× -TBS before mounting. A Zeiss LSM700 or LSM900 confocal microscope (Carl Zeiss AG) with a 20× and 40× objective lens was used for imaging. All image processing was performed using ImageJ software.

BVE for snRNA-seq

The BVE protocol was adapted from refs. 7,8. All procedures were performed on ice. Ex vivo human, post mortem human and dissected mouse cortical tissue were homogenized in 5 ml MCDB 131 medium containing 0.5% (wt/vol) endotoxin-, fatty-acid- and protease-free BSA and 10 U µl−1 recombinant RNase Inhibitors using ten strokes with the loose pestle followed by ten strokes with the tight pestle in a 7-ml KIMBLE Dounce tissue grinder. Homogenized tissue was transferred into 15-ml conical tubes and centrifuged at 2,000g for 5 min at 4 °C using a fixed-angle rotor. Cell pellet was resuspended in 2 ml 17% (wt/vol) 70-kDa dextran solution (in 1× PBS + 10 U µl−1 recombinant RNase Inhibitors) and ultracentrifuged at 10,000g for 15 min at

4 °C in a swing-bucket rotor. Myelin and cellular debris were carefully removed before decanting supernatant. Resultant pellet or fresh-frozen tissue was homogenized in 700 µl homogenization buffer (320 mM sucrose, 5 mM CaCl2, 3 mM Mg(CH3COO)2, 10 mM Tris HCl pH 7.8, 0.1 mM EDTA pH 8.0, 0.1% NP-40, 1 mM β-mercaptoethanol and 0.4 U µl−1 SUPERase In RNase Inhibitor (ThermoFisher Scientific)) with a 2-ml KIMBLE Dounce tissue grinder (MilliporeSigma) using ten strokes with the loose pestle followed by ten strokes with the tight pestle. Homogenized tissue was filtered through a 40-µm cell strainer and mixed with 450 µl of working solution (50% OptiPrep density gradient medium (MilliporeSigma), 5 mM CaCl2, 3 mM Mg(CH3COO)2, 10 mM Tris HCl pH 7.8, 0.1 mM EDTA pH 8.0 and 1 mM β-mercaptoethanol). The mixture was then slowly pipetted onto the top of an OptiPrep density gradient containing 750 µl of 30% OptiPrep Solution (134 mM sucrose, 5 mM CaCl2, 3 mM Mg(CH3COO)2, 10 mM Tris HCl pH 7.8, 0.1 mM EDTA pH 8.0, 1 mM β-mercaptoethanol, 0.04% NP-40 and 0.17 U µl−1 SUPERase In RNase Inhibitor) on top of 300 µl of 40% OptiPrep Solution (96 mM sucrose, 5 mM CaCl2, 3 mM Mg(CH3COO)2, 10 mM Tris HCl pH 7.8, 0.1 mM EDTA pH 8.0, 1 mM β-mercaptoethanol, 0.03% NP-40 and 0.12 U µl−1 SUPERase In RNase Inhibitor) inside a Sorenson Dolphin microcentrifuge tube (MilliporeSigma). Nuclei were pelleted at the interface of the OptiPrep density gradient by centrifugation at 10,000g for 5 min at 4 °C using a fixed-angle rotor (FA-45-24-11-Kit). The nuclear pellet was collected by aspirating ≈100 µl from the interface and transferring to a 2.5-ml low-binding Eppendorf tube. The pellet was washed with 2% BSA (in 1× PBS) containing 10 µl−1 SUPERase In RNase Inhibitor. The nuclei were pelleted by centrifugation at 300g for 3 min at 4 °C in a swing-bucket rotor (S-24-11-AT). Nuclei were washed two times with 2% BSA and centrifuged under the same conditions.

The nuclear pellet was then resuspended in ≈100 µl of 2% BSA and manually counted using a haemocytometer and microscope as well as being inspected for cellular debris.

Immunofluorescence Cell Counting

Three human cortical tissue samples were sectioned and stained for OLIG2, NeuN, GFAP, CLDN5, and DAPI as described in the indirect immunofluorescence methods section. For each sample, 10 40X confocal images from random regions containing blood vessels were acquired. DAPI+ cells located on or touching the CLDN5 stain were counted and identified using respective marker genes for oligodendrocytes, neurons, and astrocytes. Endothelial and mural cells were excluded from the total cell count and the calculation of the proportion of vc-cell types. Identification of endothelial and mural cells was estimated by either elongated (endothelial) or "bump-on-a-log" nuclei morphology (mural) and which were not co-labelled with any stain other than CLDN5 and DAPI.

Quantitative real-time PCR

Mouse posterior cortex was disrupted for RNA isolation using the TissueLyser (QIAGEN) for 2 × 2 min at 20 Hz as recommended by the manufacturer. Enriched blood vessel pellets from the BVE protocol were disrupted using QIAGEN Buffer RLT. RNA was then isolated using the RNeasy Lipid Tissue Mini Kit (QIAGEN). For qRT–PCR, the TaqMan Universal Master Mix (ThermoScientific) was used, and PCR reactions were run on a StepOnePlus system (ThermoScientific).

Western blotting

Human post mortem caudate nucleus tissue samples from patients with HD and age-matched unaffected controls were homogenized in 1 ml RIPA lysis buffer (ThermoScientific) containing a protease inhibitor cocktail (MilliporeSigma). Approximately 10 μg of protein in 1× LDS was loaded onto 4–12% Bis-Tris gels and run using MOPS Running Buffer at 175 V for 1 h. Protein samples were then transferred onto PVDF membranes (Bio-Rad) using 10% methanol in 1× transfer buffer at 50 V for 1.5 h. Membranes were then washed in 1× TBS-T (1× TBS with 0.05% Tween20), blocked with 5% milk for 1 h at room temperature, and subsequently incubated with primary antibodies (Supplementary Table 6) in 5% milk at 4 °C overnight under gentle agitation. Membranes were then washed again with 1X TBS-T, and incubated with HRP secondary antibodies for 1 h at room temperature, and substrate (Pierce ECL Plus) was applied for chemiluminescent detection. Immunoblots were quantified using ImageJ software. Two-tailed paired t-tests were performed for statistical analysis.

snRNA-seq and associated analysis

Droplet-based snRNA-seq libraries were prepared using the Chromium Single Cell 3′ Reagent Kit v3 (10x Genomics) according to the manufacturer's protocol and sequenced on an Illumina NovaSeq6000 at the MIT BioMicro Center. Raw sequencing reads were aligned to the pre-mRNA annotated Mus musculus reference genome version GRCm38 or Homo sapiens reference genome version GRCh38 and counts were estimated using Cellranger 3.0.1 (10x Genomics). The generated cell-by-gene unique molecular identifier (UMI) count matrix was analysed using the Seurat R package v.3.2.0 (Butler et al., 2018). We kept only the cells expressing at least 500 genes and genes with expression in at least 50 cells. The cells were also filtered by the maximum of 8,000 expressed genes and of 10% mitochondrial genes. The UMI counts were then

normalized for each cell by the total expression, multiplied by 10,000 and log transformed. We used Seurat's default method to identify highly variable genes and scale data for regressing out variation from UMI and mitochondrial genes. The scaled data with variable genes were used to perform principal component analysis. The top 30 principal components were chosen for further analysis, including clustering to identify cell populations. UMAPs were calculated in the Seurat R package using the top 30 PCs and min_dist = 0.75. Harmony was used to perform batch-effect correction.

Doublet removal

To remove the potential doublets in the dataset, we first used DoubletFinder with the parameter of 7.5% doublet formation rate on the basis of the recommendation of 10x Genomics at the single-cell level to identify the most likely doublets (McGinnis et al., 2019). Then, clusters of cells showing higher expression of marker genes corresponding to two or more cell types were excluded from further analysis.

Cell-type annotation and marker-gene identification

To annotate the cell type for each cluster, we identified the marker genes using the Wilcoxon rank sum test by comparing one cluster with the others. Next, we checked the canonical markers (excitatory neuron: NRGN, SLC17A7 and CAMK2A; inhibitory neuron: GAD1 and GAD2; astrocyte: AQP4 and GFAP; oligodendrocyte: MBP, MOBP and PLP1; microglia: CSF1R, CD74 and C3; oligodendrocyte precursor cell: VCAN, PDGFRA and CSPG4; endothelial: FLT1 and CLDN5; pericyte: AMBP) in each cluster to determine the cell type. Finally, we performed gene set enrichment analysis by testing the significance of overlapping genes between marker

genes that we identified and the published marker-gene sets (Wang et al., 2018) to further confirm the cell type of each cluster.

In silico sorting approach

For the full snRNA-seq datasets with all cell types in the brain (excitatory and inhibitory neurons, astrocytes, oligodendrocytes, oligodendrocyte precursor cells, microglia and vascular cells), we first performed clustering and annotated the cell type for each cluster on the basis of the canonical markers of vascular cell types and then calculated the cell-type score for each cell on the basis of the average expression of a set of vascular markers (Wang et al., 2018). The cells with the specific high score of vascular cell types were kept for further integrative analysis (twofold higher than the second score).

Integrative analysis of human fresh, frozen and mouse single-cell RNA-seq datasets

The homologue genes of human and mouse were kept for integration. Canonical correlation analysis in Seurat41 was used to integrate human snRNA-seq data from fresh and frozen samples and mouse single-cell RNA-seq data (Vanlandewijck et al., 2018). To compare the difference between human fresh and frozen samples, we applied MAST in R to identify the DEGs (tsDEGs) by considering age and sex as the covariates (Finak et al., 2015). We used the Wilcoxon rank sum test to identify the DEGs between human and mouse data (two comparisons: human fresh versus mouse; human frozen versus mouse) and tested the significance of agreement between two comparisons by Fisher's exact test.

Functional enrichment analysis

Enrichr in R (E. Y. Chen et al., 2013; Kuleshov et al., 2016; Xie et al., 2021) was used to perform functional enrichment analysis based on the following databases: Gene Ontology 2018 (Ashburner et al., 2000; The Gene Ontology Consortium, 2019), KEGG/WikiPathways 2019 Human and ChIP Enrichment Analysis 2016. False discovery rate (FDR) < 0.05 was used as a threshold to select the significant enrichment.

Endothelial and mural zonation analysis

The cell orders along the endothelial and mural zonation were determined by the pseudotime analysis using Monocle3 (J. Cao et al., 2019). We next built a quadratic linear regression model to identify the zonation-related genes, smoothed the gene expression along the predicted zonation axis by fitting a smoothing spline in R, and clustered those genes into eight distinct expression patterns.

Differential gene expression analysis

We identified DEGs between control and HD samples (hdDEGs) using a multiresolution method in ACTIONet v2.1.9 (Mohammadi et al., 2020). In brief, the pseudobulk gene expression matrix for each sample is generated on the basis of a number of multiresolution bins (by default is 25). The single-cell variance in pseudobulk data is also considered as a covariate when limma (Ritchie et al., 2015) is applied for differential analysis. In addition, age, sex and PMI are also controlled as covariates in the model. Genes with FDR < 0.05 and log2[foldchange] > 0.05 were used for subsequent functional enrichment analysis as described above.

Cell-Cell Interaction Analysis

We build a computational framework to predict the interaction between vascular cell types and vasculature-coupled cell types. Specifically, we first integrated the information of the ligand-receptor pairs from (Ramilowski et al., 2016) and the target genes from KEGG 2019 signaling pathways. We then filtered the ligand, receptor and target genes by the cell type-specific expression. For each pair of cell types, we calculated a score for each ligand-receptor pair to evaluate the probability of interaction between two cell types and mediated pathway by the ratio of number multiplication of cells with the expression of ligand and receptor to the universal set. To test the significance of each ligand-receptor pair, we permuted the cell ID in the gene expression matrix and calculated the *p*-value of the score.

Plasmid cloning for AAV production

A *cis* rAAV genome plasmid with AAV2 inverted terminal repeats was utilized for cloning of a *CLDN5* MiniPromoter and EGFP reporter using restriction enzymes. Ple34(CLDN5) containing the *CLDN5* MiniPromoter pEMS1982 was a gift from Elizabeth Simpson (Addgene plasmid # 49113). The transgene construct was subsequently packaged into an AAV9 serotype followed by purification via advanced 2xCsCl ultracentrifugation and qPCR titration. Cloning and viral packaging was performed by SignaGen Laboratories (Frederick, MD). The rAAV-*CLDN5*::EGFP virus was injected into 6 week old male C57BL/6J mice (*n*=3) via retro-orbital injection at a titer of 8×10^{11} vg per mouse, as previously described (de Leeuw et al., 2016). Mice were harvested 3 months after injection and evaluated for transduction efficiency using anti-GFP and anti-CLDN5 antibodies as described in the indirect immunofluorescence methods section. miR sequence targeting exon 1 of the huntingtin gene was obtained from previously published work (Miniarikova et al., 2016) and synthesized by Virovek Inc. Plasmids containing the CLDN5 MiniPromoter sequences (Ple34, “CLDN5” and Ple261, “sCLDN5”) were obtained

from Addgene. Cloning of pAAV9-CLDN5::EGFP-scrambled and pAAV9-CLDN5::EGFP-miR was performed by Virovek Inc. Construction of plasmids containing the sCLDN5 promoter were performed in-house using restriction digest or In-Fusion Snap Assembly (Takara Bio).

AAV production

Production of AAV9-CLDN5::EGFP-scrambled and AAV9-CLDN5::EGFP-miR was performed by Virovek Inc. utilizing their patented BAC-TO-AAV technology to generate recombinant baculovirus followed by AAV production at a titer concentration of 1.0E+13 vg/mL. For production of PHP.V1-sCLDN5::EGFP and all other plasmids containing the PHP.V1 capsid, AAV production was performed in-house utilizing a previously published protocol (Challis et al., 2019). In brief, triple transfection of HEK293T cells was performed on 90-95% confluent cells in DMEM containing glutamax supplemented with 5% FBS and non-essential amino acids. Fresh, warm media was replaced 12h post-transfection. Media was collected 72h post-transfection. Media and cells were collected 120h post-transfection and combined with previous fraction. Cells and media were centrifuged at 2,000g for 15min at room temperature. Supernatant was collected in a separate bottle and combined with 40% (wt/vol) PEG (final concentration 8% wt/vol PEG) and incubated on ice for 2h before transferring to 4^{o}C overnight. Cell pellet was re-suspended in buffer containing salt-active nuclease (SAN) and incubated at 37^{o}C for 1h before transferring to 4^{o}C overnight. PEG-media was centrifuged at 4,000g for 30min at 4^{o}C. After centrifugation, supernatant was bleached and discarded. PEG pellet was resuspended in SAN+SAN buffer, combined with previous fraction, and incubated at 37^{o}C for an additional 30min. Lysate was centrifuged at 2,000g for 15min at room temperature and supernatant was loaded onto an iodixanol gradient (15%, 25%, 40%, and 60% fractions). Gradients were

transferred to an ultracentrifuge using a Type 70 Ti rotor set at 350,000g for 2h and 25min at 18^{o}C. AAV particles were collected from the 40/60% interface, washed in 1X PBS, and concentrated using an Amicon filter device with a 100kDa cutoff. AAV titration was performed using the AAVpro Titration Kit (for Real Time PCR) Ver.2 (Takara Bio).

Retro-orbital injections

Mice were anesthetized under 2% isoflurane. Prior to injection, topical ophthalmic solution of 0.5% proparacaine was administered to the eye to be injected. While under anesthesia, 100uL of AAV particles at a concentration of 1 x 10^{10} Vg/uL were injected using a 27.5-gauge insulin needle into the retro-orbital sinus. After injection, lubricant was applied to the injected eye to prevent corneal drying and injury.

Open-field test

Open field testing was performed in 60-min sessions per mouse using an infrared (IR) photobeam open field (17″ × 17″ × 12″) with 16 IR beams spaced regularly along the x, y, and z axes (#MED-OFAS-RSU, Med Associates, St. Albans, VT). Unless specified, all testing was performed during the light phase starting at 7am and never past 1pm. For larger cohorts, testing was split across multiple days to avoid confounds of testing at late hours. For dark phase trials, testing started at 7pm and never past 1am. All experimental groups were tested simultaneously each hour in separate open field chambers (i.e. 4 mice run per hour).

Rearing and Climbing

Rearing and climbing testing was performed by placing mice under an overturned metal mesh pencil cup (Rolodex #82406) 4.375 inches in diameter and 5.5 inches in height for a 5 min trial period. Three mirror frames were placed behind the mesh pencil cup to capture full range of motion with a video recording camera. The number of rearing instances was recorded as instances in which both front paws left the ground and mouse fully supported on only the two hind legs. The number of climbing instances was recorded as instances in which all four paws left the ground and mouse was fully supported on the mesh cup. Scoring was performed by a blinded experimenter who did not know treatment group or genotypes of mice.

Rotarod

Rotarod testing was performed using an accelerating rotarod. Mice were trained using 3 × 5 min sessions with a fixed speed of 20 rotations per minute (RPM) and replaced on the rotarod after each fall. Mice were given 1 min of rest between training trials. Testing was performed on 3-5 consecutive days (beginning on day of training) with the rotarod accelerating from 5 RPM to 40 RPM over the course of 5 min. Day 1 of testing began 2 hours after completion of training. The time from the start of the trial until the mouse fell off the rod was measured as latency to fall. If a mouse completed two or more passive rotations, this was scored as a fall.

Burrowing assay

Mice were placed in individual large cages containing a clear, red tube filled with 140 g of normal food pellets. Percentage burrowed was calculated from weight of pellets remaining in the tube after 2 hours.

Statistical Analysis

Statistical analyses for behavior data, qPCR, and western blotting were performed using GraphPad Prism 9. Two-tailed, unpaired t test was used for comparison of two groups to assess significance (p-value < 0.05). Individual data points are shown representing either individual mice or human sample. Error bars represent standard error of the mean (SEM).

Supplemental Tables

Due to size, Supplemental Tables have been excluded from this thesis. For full Excel files please refer to [Garcia, Francisco J., et al. "Single-cell dissection of the human brain vasculature." Nature 603.7903 (2022): 893-899]. Supplementary Guide has been included for reference

Supplementary Table 1 (Excel File). Patient and sample information for *ex vivo, post mortem* ROSMAP, and *post mortem* Huntington's Disease and controls.

Supplementary Table 2 (Excel File). Differentially expressed genes in cerebrovasculature cell types, as reported by snRNA-seq from *ex vivo* and *post mortem* samples. Differential expression analysis is based on non-parameteric Wilcoxon rank sum test.

Supplementary Table 3 (Excel File). Differentially expressed genes from comparisons between cross-modal *ex vivo* vs. *post mortem* and cross-species human vs. mouse, as reported by snRNA-seq. Differential expression analysis is based on non-parameteric Wilcoxon rank sum test.

Supplementary Table 4 (Excel File). Differentially expressed genes in endothelial, mural, and fibroblasts, as reported by snRNA-seq from the caudate nucleus and putamen of HD patients (compared to controls), as well as WikiPathways, KEGG, and GOBP analysis. The differential gene expression analysis was performed at cell type-specific pseudo-bulk level using ACTIONet and limma with age, sex, PMI and disease group as design covariates and gene-wise single-cell-level variance as weights for the linear model.

Supplementary Table 5 (Excel File). Differentially expressed genes in vascular-related astrocyte and microglia subclusters, as reported by snRNA-seq from the caudate nucleus and putamen of HD patients (compared to controls). Differential expression analysis is based on non-parameteric Wilcoxon rank sum test.

Supplementary Table 6 (Excel File). List of antibody information.

References

Abbott, N. J., Rönnbäck, L., & Hansson, E. (2006). Astrocyte-endothelial interactions at the blood-brain barrier. *Nature Reviews. Neuroscience*, *7*(1), 41–53.

Aird, W. C. (2007a). Phenotypic heterogeneity of the endothelium: I. Structure, function, and mechanisms. *Circulation Research*, *100*(2), 158–173.

Aird, W. C. (2007b). Phenotypic heterogeneity of the endothelium: II. Representative vascular beds. *Circulation Research*, *100*(2), 174–190.

Al-Dalahmah, O., Sosunov, A. A., Shaik, A., Ofori, K., Liu, Y., Vonsattel, J. P., Adorjan, I., Menon, V., & Goldman, J. E. (2020). Single-nucleus RNA-seq identifies Huntington disease astrocyte states. *Acta Neuropathologica Communications*, *8*(1), 19.

Andreone, B. J., Chow, B. W., Tata, A., Lacoste, B., Ben-Zvi, A., Bullock, K., Deik, A. A., Ginty, D. D., Clish, C. B., & Gu, C. (2017). Blood-brain barrier permeability is regulated by lipid transport-dependent suppression of caveolae-mediated transcytosis. *Neuron*, *94*(3), 581-594.e5.

Andrew, S. E., Goldberg, Y. P., Kremer, B., Telenius, H., Theilmann, J., Adam, S., Starr, E., Squitieri, F., Lin, B., & Kalchman, M. A. (1993). The relationship between trinucleotide (CAG) repeat length and clinical features of Huntington's disease. *Nature Genetics*, *4*(4), 398–403.

Armulik, A., Genové, G., & Betsholtz, C. (2011). Pericytes: developmental, physiological, and pathological perspectives, problems, and promises. *Developmental Cell*, *21*(2), 193–215.

Armulik, A., Genové, G., Mäe, M., Nisancioglu, M. H., Wallgard, E., Niaudet, C., He, L., Norlin, J., Lindblom, P., Strittmatter, K., Johansson, B. R., & Betsholtz, C. (2010). Pericytes regulate the blood-brain barrier. *Nature*, *468*(7323), 557–561.

Ashburner, M., Ball, C. A., Blake, J. A., Botstein, D., Butler, H., Cherry, J. M., Davis, A. P., Dolinski, K., Dwight, S. S., Eppig, J. T., Harris, M. A., Hill, D. P., Issel-Tarver, L., Kasarskis, A., Lewis, S., Matese, J. C., Richardson, J. E., Ringwald, M., Rubin, G. M., & Sherlock, G. (2000). Gene ontology: tool for the unification of biology. The Gene Ontology Consortium. *Nature Genetics*, *25*(1), 25–29.

Attwell, D., Mishra, A., Hall, C. N., O'Farrell, F. M., & Dalkara, T. (2016). What is a pericyte? *Journal of Cerebral Blood Flow and Metabolism: Official Journal of the International Society of Cerebral Blood Flow and Metabolism*, *36*(2), 451–455.

Ayata, C. (2010). CADASIL. *Stroke; a Journal of Cerebral Circulation*, *41*(10_suppl_1). https://doi.org/10.1161/strokeaha.110.595207

Banks, W. A. (2016). From blood-brain barrier to blood-brain interface: new opportunities for CNS drug delivery. *Nature Reviews. Drug Discovery*, *15*(4), 275–292.

Barisano, G., Montagne, A., Kisler, K., Schneider, J. A., Wardlaw, J. M., & Zlokovic, B. V. (2022). Blood-brain barrier link to human cognitive impairment and Alzheimer's Disease. *Nature Cardiovascular Research*, *1*(2), 108–115.

Bayraktar, E. C., Baudrier, L., Özerdem, C., Lewis, C. A., Chan, S. H., Kunchok, T., Abu-Remaileh, M., Cangelosi, A. L., Sabatini, D. M., Birsoy, K., & Chen, W. W. (2019). MITO-Tag Mice enable rapid isolation and multimodal profiling of mitochondria from specific cell types in vivo. *Proceedings of the National Academy of Sciences of the United States of America*, *116*(1), 303–312.

Bennett, D. A., Buchman, A. S., Boyle, P. A., Barnes, L. L., Wilson, R. S., & Schneider, J. A. (2018). Religious Orders Study and Rush Memory and Aging Project. *Journal of Alzheimer's Disease: JAD*, *64*(s1), S161–S189.

Ben-Zvi, A., Lacoste, B., Kur, E., Andreone, B. J., Mayshar, Y., Yan, H., & Gu, C. (2014). Mfsd2a is critical for the formation and function of the blood-brain barrier. *Nature*, *509*(7501), 507–511.

Biffi, A., & Greenberg, S. M. (2011). Cerebral amyloid angiopathy: a systematic review. *Journal of Clinical Neurology (Seoul, Korea)*, *7*(1), 1–9.

Bir, S. C., Khan, M. W., Javalkar, V., Toledo, E. G., & Kelley, R. E. (2021). Emerging concepts in vascular dementia: A review. *Journal of Stroke and Cerebrovascular Diseases: The Official Journal of National Stroke Association*, *30*(8), 105864.

Bisht, K., Okojie, K. A., Sharma, K., Lentferink, D. H., Sun, Y.-Y., Chen, H.-R., Uweru, J. O., Amancherla, S., Calcuttawala, Z., Campos-Salazar, A. B., Corliss, B., Jabbour, L., Benderoth, J., Friestad, B., Mills, W. A., 3rd, Isakson, B. E., Tremblay, M.-È., Kuan, C.-Y., & Eyo, U. B. (2021). Capillary-associated microglia regulate vascular structure and function through PANX1-P2RY12 coupling in mice. *Nature Communications*, *12*(1), 5289.

Bonney, S. K., Sullivan, L. T., Cherry, T. J., Daneman, R., & Shih, A. Y. (2022). Distinct features of brain perivascular fibroblasts and mural cells revealed by in vivo two-photon imaging. *Journal of Cerebral Blood Flow and Metabolism: Official Journal of the International Society of Cerebral Blood Flow and Metabolism*, *42*(6), 966–978.

Butler, A., Hoffman, P., Smibert, P., Papalexi, E., & Satija, R. (2018). Integrating single-cell transcriptomic data across different conditions, technologies, and species. *Nature Biotechnology*, *36*(5), 411–420.

Cabrejo, L., Guyant-Maréchal, L., Laquerrière, A., Vercelletto, M., De la Fournière, F., Thomas-Antérion, C., Verny, C., Letournel, F., Pasquier, F., Vital, A., Checler, F., Frebourg, T.,

Campion, D., & Hannequin, D. (2006). Phenotype associated with APP duplication in five families. *Brain: A Journal of Neurology*, *129*(Pt 11), 2966–2976.

Cao, J., Spielmann, M., Qiu, X., Huang, X., Ibrahim, D. M., Hill, A. J., Zhang, F., Mundlos, S., Christiansen, L., Steemers, F. J., Trapnell, C., & Shendure, J. (2019). The single-cell transcriptional landscape of mammalian organogenesis. *Nature*, *566*(7745), 496–502.

Cao, X., Pfaff, S. L., & Gage, F. H. (2008). YAP regulates neural progenitor cell number via the TEA domain transcription factor. *Genes & Development*, *22*(23), 3320–3334.

Cepeda-Prado, E., Popp, S., Khan, U., Stefanov, D., Rodríguez, J., Menalled, L. B., Dow-Edwards, D., Small, S. A., & Moreno, H. (2012). R6/2 Huntington's disease mice develop early and progressive abnormal brain metabolism and seizures. *The Journal of Neuroscience: The Official Journal of the Society for Neuroscience*, *32*(19), 6456–6467.

Challis, R. C., Ravindra Kumar, S., Chan, K. Y., Challis, C., Beadle, K., Jang, M. J., Kim, H. M., Rajendran, P. S., Tompkins, J. D., Shivkumar, K., Deverman, B. E., & Gradinaru, V. (2019). Systemic AAV vectors for widespread and targeted gene delivery in rodents. *Nature Protocols*, *14*(2), 379–414.

Chan, K. Y., Jang, M. J., Yoo, B. B., Greenbaum, A., Ravi, N., Wu, W.-L., Sánchez-Guardado, L., Lois, C., Mazmanian, S. K., Deverman, B. E., & Gradinaru, V. (2017). Engineered AAVs for efficient noninvasive gene delivery to the central and peripheral nervous systems. *Nature Neuroscience*, *20*(8), 1172–1179.

Chen, E. Y., Tan, C. M., Kou, Y., Duan, Q., Wang, Z., Meirelles, G. V., Clark, N. R., & Ma'ayan, A. (2013). Enrichr: interactive and collaborative HTML5 gene list enrichment analysis tool. *BMC Bioinformatics*, *14*(1), 128.

Chen, J. J., Salat, D. H., & Rosas, H. D. (2012). Complex relationships between cerebral blood flow and brain atrophy in early Huntington's disease. *NeuroImage*, *59*(2), 1043–1051.

Chen, J., Van Gulden, S., McGuire, T. L., Fleming, A. C., Oka, C., Kessler, J. A., & Peng, C.-Y. (2018). BMP-responsive protease HtrA1 is differentially expressed in astrocytes and regulates astrocytic development and injury response. *The Journal of Neuroscience: The Official Journal of the Society for Neuroscience*, *38*(15), 3840–3857.

Chen, K. H., Boettiger, A. N., Moffitt, J. R., Wang, S., & Zhuang, X. (2015). RNA imaging. Spatially resolved, highly multiplexed RNA profiling in single cells. *Science (New York, N.Y.)*, *348*(6233), aaa6090.

Chen, X., Ravindra Kumar, S., Adams, C. D., Yang, D., Wang, T., Wolfe, D. A., Arokiaraj, C. M., Ngo, V., Campos, L. J., Griffiths, J. A., Ichiki, T., Mazmanian, S. K., Osborne, P. B., Keast, J. R., Miller, C. T., Fox, A. S., Chiu, I. M., & Gradinaru, V. (2022). Engineered AAVs for non-invasive gene delivery to rodent and non-human primate nervous systems. *Neuron*, *110*(14), 2242-2257.e6.

Chinnery, P. F., Crompton, D. E., Birchall, D., Jackson, M. J., Coulthard, A., Lombès, A., Quinn, N., Wills, A., Fletcher, N., Mottershead, J. P., Cooper, P., Kellett, M., Bates, D., & Burn, J. (2007). Clinical features and natural history of neuroferritinopathy caused by the FTL1 460InsA mutation. *Brain: A Journal of Neurology*, *130*(Pt 1), 110–119.

Chow, B. W., Nuñez, V., Kaplan, L., Granger, A. J., Bistrong, K., Zucker, H. L., Kumar, P., Sabatini, B. L., & Gu, C. (2020). Caveolae in CNS arterioles mediate neurovascular coupling. *Nature*, *579*(7797), 106–110.

Császár, E., Lénárt, N., Cserép, C., Környei, Z., Fekete, R., Pósfai, B., Balázsfi, D., Hangya, B., Schwarcz, A. D., Szabadits, E., Szöllősi, D., Szigeti, K., Máthé, D., West, B. L., Sviatkó,

K., Brás, A. R., Mariani, J.-C., Kliewer, A., Lenkei, Z., … Dénes, Á. (2022). Microglia modulate blood flow, neurovascular coupling, and hypoperfusion via purinergic actions. *The Journal of Experimental Medicine*, *219*(3). https://doi.org/10.1084/jem.20211071

Daneman, R., Agalliu, D., Zhou, L., Kuhnert, F., Kuo, C. J., & Barres, B. A. (2009). Wnt/beta-catenin signaling is required for CNS, but not non-CNS, angiogenesis. *Proceedings of the National Academy of Sciences of the United States of America*, *106*(2), 641–646.

Daniels, B. P., & Klein, R. S. (2015). Viral sensing at the blood-brain barrier: new roles for innate immunity at the CNS vasculature. *Clinical Pharmacology and Therapeutics*, *97*(4), 372–379.

de Leeuw, C. N., Dyka, F. M., Boye, S. L., Laprise, S., Zhou, M., Chou, A. Y., Borretta, L., McInerny, S. C., Banks, K. G., Portales-Casamar, E., Swanson, M. I., D'Souza, C. A., Boye, S. E., Jones, S. J. M., Holt, R. A., Goldowitz, D., Hauswirth, W. W., Wasserman, W. W., & Simpson, E. M. (2014). Targeted CNS delivery using human MiniPromoters and demonstrated compatibility with adeno-associated viral vectors. *Molecular Therapy. Methods & Clinical Development*, *1*(5), 5.

de Leeuw, C. N., Korecki, A. J., Berry, G. E., Hickmott, J. W., Lam, S. L., Lengyell, T. C., Bonaguro, R. J., Borretta, L. J., Chopra, V., Chou, A. Y., D'Souza, C. A., Kaspieva, O., Laprise, S., McInerny, S. C., Portales-Casamar, E., Swanson-Newman, M. I., Wong, K., Yang, G. S., Zhou, M., … Simpson, E. M. (2016). rAAV-compatible MiniPromoters for restricted expression in the brain and eye. *Molecular Brain*, *9*(1). https://doi.org/10.1186/s13041-016-0232-4

dela Paz, N. G., & D'Amore, P. A. (2009). Arterial versus venous endothelial cells. *Cell and Tissue Research*, *335*(1), 5–16.

Deo, A. K., Theil, F.-P., & Nicolas, J.-M. (2013). Confounding parameters in preclinical assessment of blood-brain barrier permeation: an overview with emphasis on species differences and effect of disease states. *Molecular Pharmaceutics*, *10*(5), 1581–1595.

DeSisto, J., O'Rourke, R., Jones, H. E., Pawlikowski, B., Malek, A. D., Bonney, S., Guimiot, F., Jones, K. L., & Siegenthaler, J. A. (2020). Single-cell transcriptomic analyses of the developing meninges reveal meningeal fibroblast diversity and function. *Developmental Cell*, *54*(1), 43-59.e4.

Di Pardo, A., Amico, E., Scalabrì, F., Pepe, G., Castaldo, S., Elifani, F., Capocci, L., De Sanctis, C., Comerci, L., Pompeo, F., D'Esposito, M., Filosa, S., Crispi, S., & Maglione, V. (2017). Impairment of blood-brain barrier is an early event in R6/2 mouse model of Huntington Disease. *Scientific Reports*, *7*, 41316.

Dorrier, C. E., Aran, D., Haenelt, E. A., Sheehy, R. N., Hoi, K. K., Pintarić, L., Chen, Y., Lizama, C. O., Cautivo, K. M., Weiner, G. A., Popko, B., Fancy, S. P. J., Arnold, T. D., & Daneman, R. (2021). CNS fibroblasts form a fibrotic scar in response to immune cell infiltration. *Nature Neuroscience*, *24*(2), 234–244.

Dorrier, C. E., Jones, H. E., Pintarić, L., Siegenthaler, J. A., & Daneman, R. (2022). Emerging roles for CNS fibroblasts in health, injury and disease. *Nature Reviews. Neuroscience*, *23*(1), 23–34.

Doyle, J. P., Dougherty, J. D., Heiman, M., Schmidt, E. F., Stevens, T. R., Ma, G., Bupp, S., Shrestha, P., Shah, R. D., Doughty, M. L., Gong, S., Greengard, P., & Heintz, N. (2009). Application of a translational profiling approach for the comparative analysis of CNS cell types. *Cell*, *139*(5), 1022.

Drouin-Ouellet, J., Sawiak, S. J., Cisbani, G., Lagacé, M., Kuan, W.-L., Saint-Pierre, M., Dury, R. J., Alata, W., St-Amour, I., Mason, S. L., Calon, F., Lacroix, S., Gowland, P. A., Francis, S. T., Barker, R. A., & Cicchetti, F. (2015). Cerebrovascular and blood-brain barrier impairments in Huntington's disease: Potential implications for its pathophysiology. *Annals of Neurology*, *78*(2), 160–177.

Engelhardt, B. (2003). Development of the blood-brain barrier. *Cell and Tissue Research*, *314*(1), 119–129.

Estevez-Fraga, C., Tabrizi, S. J., & Wild, E. J. (2022). Huntington's Disease Clinical Trials Corner: November 2022. *Journal of Huntington's Disease*, *11*(4), 351–367.

Farbehi, N., Patrick, R., Dorison, A., Xaymardan, M., Janbandhu, V., Wystub-Lis, K., Ho, J. W., Nordon, R. E., & Harvey, R. P. (2019). Single-cell expression profiling reveals dynamic flux of cardiac stromal, vascular and immune cells in health and injury. *ELife*, *8*. https://doi.org/10.7554/eLife.43882

Feekes, J. A., & Cassell, M. D. (2006). The vascular supply of the functional compartments of the human striatum. *Brain: A Journal of Neurology*, *129*(Pt 8), 2189–2201.

Fernández-Klett, F., Offenhauser, N., Dirnagl, U., Priller, J., & Lindauer, U. (2010). Pericytes in capillaries are contractile in vivo, but arterioles mediate functional hyperemia in the mouse brain. *Proceedings of the National Academy of Sciences of the United States of America*, *107*(51), 22290–22295.

Fernández-Klett, F., Potas, J. R., Hilpert, D., Blazej, K., Radke, J., Huck, J., Engel, O., Stenzel, W., Genové, G., & Priller, J. (2013). Early loss of pericytes and perivascular stromal cell-induced scar formation after stroke. *Journal of Cerebral Blood Flow and Metabolism:*

Official Journal of the International Society of Cerebral Blood Flow and Metabolism, *33*(3), 428–439.

Filosa, J. A., Bonev, A. D., Straub, S. V., Meredith, A. L., Wilkerson, M. K., Aldrich, R. W., & Nelson, M. T. (2006). Local potassium signaling couples neuronal activity to vasodilation in the brain. *Nature Neuroscience*, *9*(11), 1397–1403.

Finak, G., McDavid, A., Yajima, M., Deng, J., Gersuk, V., Shalek, A. K., Slichter, C. K., Miller, H. W., McElrath, M. J., Prlic, M., Linsley, P. S., & Gottardo, R. (2015). MAST: a flexible statistical framework for assessing transcriptional changes and characterizing heterogeneity in single-cell RNA sequencing data. *Genome Biology*, *16*(1), 278.

Franciosi, S., Ryu, J. K., Shim, Y., Hill, A., Connolly, C., Hayden, M. R., McLarnon, J. G., & Leavitt, B. R. (2012). Age-dependent neurovascular abnormalities and altered microglial morphology in the YAC128 mouse model of Huntington disease. *Neurobiology of Disease*, *45*(1), 438–449.

Fu, H., Hardy, J., & Duff, K. E. (2018). Selective vulnerability in neurodegenerative diseases. *Nature Neuroscience*, *21*(10), 1350–1358.

Fujioka, T., Kaneko, N., & Sawamoto, K. (2019). Blood vessels as a scaffold for neuronal migration. *Neurochemistry International*, *126*, 69–73.

Garcia, F. J., Sun, N., Lee, H., Godlewski, B., Mathys, H., Galani, K., Zhou, B., Jiang, X., Ng, A. P., Mantero, J., Tsai, L.-H., Bennett, D. A., Sahin, M., Kellis, M., & Heiman, M. (2022). Single-cell dissection of the human brain vasculature. *Nature*, *603*(7903), 893–899.

Garnett, E. S., Firnau, G., Nahmias, C., Carbotte, R., & Bartolucci, G. (1984). Reduced striatal glucose consumption and prolonged reaction time are early features in Huntington's disease. *Journal of the Neurological Sciences*, *65*(2), 231–237.

Genetic Modifiers of Huntington's Disease (GeM-HD) Consortium. Electronic address: gusella@helix.mgh.harvard.edu, & Genetic Modifiers of Huntington's Disease (GeM-HD) Consortium. (2019). CAG repeat not polyglutamine length determines timing of Huntington's disease onset. *Cell*, *178*(4), 887-900.e14.

Girouard, H., Bonev, A. D., Hannah, R. M., Meredith, A., Aldrich, R. W., & Nelson, M. T. (2010). Astrocytic endfoot Ca2+ and BK channels determine both arteriolar dilation and constriction. *Proceedings of the National Academy of Sciences of the United States of America*, *107*(8), 3811–3816.

Gonitel, R., Moffitt, H., Sathasivam, K., Woodman, B., Detloff, P. J., Faull, R. L. M., & Bates, G. P. (2008). DNA instability in postmitotic neurons. *Proceedings of the National Academy of Sciences of the United States of America*, *105*(9), 3467–3472.

Guemez-Gamboa, A., Nguyen, L. N., Yang, H., Zaki, M. S., Kara, M., Ben-Omran, T., Akizu, N., Rosti, R. O., Rosti, B., Scott, E., Schroth, J., Copeland, B., Vaux, K. K., Cazenave-Gassiot, A., Quek, D. Q. Y., Wong, B. H., Tan, B. C., Wenk, M. R., Gunel, M., … Gleeson, J. G. (2015). Inactivating mutations in MFSD2A, required for omega-3 fatty acid transport in brain, cause a lethal microcephaly syndrome. *Nature Genetics*, *47*(7), 809–813.

Guey, S., Lesnik Oberstein, S. A. J., Tournier-Lasserve, E., & Chabriat, H. (2021). Hereditary cerebral small vessel diseases and stroke: A guide for diagnosis and management. *Stroke; a Journal of Cerebral Circulation*, *52*(9), 3025–3032.

Habib, N., Avraham-Davidi, I., Basu, A., Burks, T., Shekhar, K., Hofree, M., Choudhury, S. R., Aguet, F., Gelfand, E., Ardlie, K., Weitz, D. A., Rozenblatt-Rosen, O., Zhang, F., & Regev, A. (2017). Massively parallel single-nucleus RNA-seq with DroNc-seq. *Nature Methods*, *14*(10), 955–958.

Halder, S. K., & Ueda, H. (2012). Regional distribution and cell type-specific subcellular localization of Prothymosin alpha in brain. *Cellular and Molecular Neurobiology*, *32*(1), 59–66.

Hara, K., Shiga, A., Fukutake, T., Nozaki, H., Miyashita, A., Yokoseki, A., Kawata, H., Koyama, A., Arima, K., Takahashi, T., Ikeda, M., Shiota, H., Tamura, M., Shimoe, Y., Hirayama, M., Arisato, T., Yanagawa, S., Tanaka, A., Nakano, I., … Onodera, O. (2009). Association of HTRA1 mutations and familial ischemic cerebral small-vessel disease. *The New England Journal of Medicine*, *360*(17), 1729–1739.

Harris, G. J., Codori, A. M., Lewis, R. F., Schmidt, E., Bedi, A., & Brandt, J. (1999). Reduced basal ganglia blood flow and volume in pre-symptomatic, gene-tested persons at-risk for Huntington's disease. *Brain: A Journal of Neurology*, *122*(9), 1667–1678.

Hartmann, D. A., Berthiaume, A.-A., Grant, R. I., Harrill, S. A., Koski, T., Tieu, T., McDowell, K. P., Faino, A. V., Kelly, A. L., & Shih, A. Y. (2021). Brain capillary pericytes exert a substantial but slow influence on blood flow. *Nature Neuroscience*, *24*(5), 633–645.

Heiman, M., Kulicke, R., Fenster, R. J., Greengard, P., & Heintz, N. (2014). Cell type-specific mRNA purification by translating ribosome affinity purification (TRAP). *Nature Protocols*, *9*(6), 1282–1291.

Heiman, M., Schaefer, A., Gong, S., Peterson, J. D., Day, M., Ramsey, K. E., Suárez-Fariñas, M., Schwarz, C., Stephan, D. A., Surmeier, D. J., Greengard, P., & Heintz, N. (2008). A

translational profiling approach for the molecular characterization of CNS cell types. *Cell*, *135*(4), 738–748.

Heithoff, B. P., George, K. K., Phares, A. N., Zuidhoek, I. A., Munoz-Ballester, C., & Robel, S. (2021). Astrocytes are necessary for blood-brain barrier maintenance in the adult mouse brain. *Glia*, *69*(2), 436–472.

Hellström, M., Kalén, M., Lindahl, P., Abramsson, A., & Betsholtz, C. (1999). Role of PDGF-B and PDGFR-beta in recruitment of vascular smooth muscle cells and pericytes during embryonic blood vessel formation in the mouse. *Development (Cambridge, England)*, *126*(14), 3047–3055.

Hill, R. A., Tong, L., Yuan, P., Murikinati, S., Gupta, S., & Grutzendler, J. (2015). Regional blood flow in the normal and ischemic brain is controlled by arteriolar smooth muscle cell contractility and not by capillary pericytes. *Neuron*, *87*(1), 95–110.

Hodge, R. D., Bakken, T. E., Miller, J. A., Smith, K. A., Barkan, E. R., Graybuck, L. T., Close, J. L., Long, B., Johansen, N., Penn, O., Yao, Z., Eggermont, J., Höllt, T., Levi, B. P., Shehata, S. I., Aevermann, B., Beller, A., Bertagnolli, D., Brouner, K., … Lein, E. S. (2019). Conserved cell types with divergent features in human versus mouse cortex. *Nature*, *573*(7772), 61–68.

Horng, S., Therattil, A., Moyon, S., Gordon, A., Kim, K., Argaw, A. T., Hara, Y., Mariani, J. N., Sawai, S., Flodby, P., Crandall, E. D., Borok, Z., Sofroniew, M. V., Chapouly, C., & John, G. R. (2017). Astrocytic tight junctions control inflammatory CNS lesion pathogenesis. *The Journal of Clinical Investigation*, *127*(8), 3136–3151.

Houlden, H., & Singleton, A. B. (2012). The genetics and neuropathology of Parkinson's disease. *Acta Neuropathologica*, *124*(3), 325–338.

Hua, J., Unschuld, P. G., Margolis, R. L., van Zijl, P. C. M., & Ross, C. A. (2014). Elevated arteriolar cerebral blood volume in prodromal Huntington's disease. *Movement Disorders: Official Journal of the Movement Disorder Society*, *29*(3), 396–401.

Huang, M. T., & Gorman, C. M. (1990). Intervening sequences increase efficiency of RNA 3' processing and accumulation of cytoplasmic RNA. *Nucleic Acids Research*, *18*(4), 937–947.

Hupe, M., Li, M. X., Kneitz, S., Davydova, D., Yokota, C., Kele, J., Hot, B., Stenman, J. M., & Gessler, M. (2017). Gene expression profiles of brain endothelial cells during embryonic development at bulk and single-cell levels. *Science Signaling*, *10*(487). https://doi.org/10.1126/scisignal.aag2476

Iadecola, C. (2013). The pathobiology of vascular dementia. *Neuron*, *80*(4), 844–866.

Iadecola, C. (2017). The neurovascular unit coming of age: A journey through neurovascular coupling in health and disease. *Neuron*, *96*(1), 17–42.

Iliff, J. J., Wang, M., Liao, Y., Plogg, B. A., Peng, W., Gundersen, G. A., Benveniste, H., Vates, G. E., Deane, R., Goldman, S. A., Nagelhus, E. A., & Nedergaard, M. (2012). A paravascular pathway facilitates CSF flow through the brain parenchyma and the clearance of interstitial solutes, including amyloid β. *Science Translational Medicine*, *4*(147), 147ra111.

Johnson, A. C. (2023). Hippocampal vascular supply and its role in vascular cognitive impairment. *Stroke; a Journal of Cerebral Circulation*, *54*(3), 673–685.

Joutel, A., Corpechot, C., Ducros, A., Vahedi, K., Chabriat, H., Mouton, P., Alamowitch, S., Domenga, V., Cécillion, M., Marechal, E., Maciazek, J., Vayssiere, C., Cruaud, C., Cabanis, E. A., Ruchoux, M. M., Weissenbach, J., Bach, J. F., Bousser, M. G., &

Tournier-Lasserve, E. (1996). Notch3 mutations in CADASIL, a hereditary adult-onset condition causing stroke and dementia. *Nature*, *383*(6602), 707–710.

Kamath, T., Abdulraouf, A., Burris, S. J., Langlieb, J., Gazestani, V., Nadaf, N. M., Balderrama, K., Vanderburg, C., & Macosko, E. Z. (2022). Single-cell genomic profiling of human dopamine neurons identifies a population that selectively degenerates in Parkinson's disease. *Nature Neuroscience*, *25*(5), 588–595.

Kaplan, L., Chow, B. W., & Gu, C. (2020). Neuronal regulation of the blood-brain barrier and neurovascular coupling. *Nature Reviews. Neuroscience*, *21*(8), 416–432.

Kay, C., Hayden, M. R., & Leavitt, B. R. (2017). Epidemiology of Huntington disease. *Handbook of Clinical Neurology*, *144*, 31–46.

Kelleher, J., Dickinson, A., Cain, S., Hu, Y., Bates, N., Harvey, A., Ren, J., Zhang, W., Moreton, F. C., Muir, K. W., Ward, C., Touyz, R. M., Sharma, P., Xu, Q., Kimber, S. J., & Wang, T. (2019). Patient-specific iPSC model of a genetic vascular dementia syndrome reveals failure of mural cells to stabilize capillary structures. *Stem Cell Reports*, *13*(5), 817–831.

Kessaris, N., Fogarty, M., Iannarelli, P., Grist, M., Wegner, M., & Richardson, W. D. (2006). Competing waves of oligodendrocytes in the forebrain and postnatal elimination of an embryonic lineage. *Nature Neuroscience*, *9*(2), 173–179.

Khuller, K., Yigit, G., Martínez Grijalva, C., Altmüller, J., Thiele, H., Nürnberg, P., Elcioglu, N. H., Yeter, B., Hehr, U., Stein, A., Della Marina, A., Köninger, A., Depienne, C., Kaiser, F. J., Wollnik, B., & Kuechler, A. (2021). MFSD2A-associated primary microcephaly - Expanding the clinical and mutational spectrum of this ultra-rare disease. *European Journal of Medical Genetics*, *64*(10), 104310.

Kingwell, K. (2021). Double setback for ASO trials in Huntington disease. *Nature Reviews. Drug Discovery*, *20*(6), 412–413.

Kirst, C., Skriabine, S., Vieites-Prado, A., Topilko, T., Bertin, P., Gerschenfeld, G., Verny, F., Topilko, P., Michalski, N., Tessier-Lavigne, M., & Renier, N. (2020). Mapping the fine-scale organization and plasticity of the brain vasculature. *Cell*, *180*(4), 780-795.e25.

Knopp, R. C., Banks, W. A., & Erickson, M. A. (2022). Physical associations of microglia and the vascular blood-brain barrier and their importance in development, health, and disease. *Current Opinion in Neurobiology*, *77*(102648), 102648.

Kuleshov, M. V., Jones, M. R., Rouillard, A. D., Fernandez, N. F., Duan, Q., Wang, Z., Koplev, S., Jenkins, S. L., Jagodnik, K. M., Lachmann, A., McDermott, M. G., Monteiro, C. D., Gundersen, G. W., & Ma'ayan, A. (2016). Enrichr: a comprehensive gene set enrichment analysis web server 2016 update. *Nucleic Acids Research*, *44*(W1), W90-7.

Langen, U. H., Ayloo, S., & Gu, C. (2019). Development and cell biology of the blood-brain barrier. *Annual Review of Cell and Developmental Biology*, *35*(1), 591–613.

Lee, H., Fenster, R. J., Pineda, S. S., Gibbs, W. S., Mohammadi, S., Davila-Velderrain, J., Garcia, F. J., Therrien, M., Novis, H. S., Gao, F., Wilkinson, H., Vogt, T., Kellis, M., LaVoie, M. J., & Heiman, M. (2020). Cell type-specific transcriptomics reveals that mutant huntingtin leads to mitochondrial RNA release and neuronal innate immune activation. *Neuron*, *107*(5), 891-908.e8.

Lee, Y.-K., Uchida, H., Smith, H., Ito, A., & Sanchez, T. (2019). The isolation and molecular characterization of cerebral microvessels. *Nature Protocols*, *14*(11), 3059–3081.

Lendahl, U., Nilsson, P., & Betsholtz, C. (2019). Emerging links between cerebrovascular and neurodegenerative diseases-a special role for pericytes. *EMBO Reports*, *20*(11), e48070.

Ley, K., Laudanna, C., Cybulsky, M. I., & Nourshargh, S. (2007). Getting to the site of inflammation: the leukocyte adhesion cascade updated. *Nature Reviews. Immunology*, *7*(9), 678–689.

Li, Q., & Barres, B. A. (2018). Microglia and macrophages in brain homeostasis and disease. *Nature Reviews. Immunology*, *18*(4), 225–242.

Lim, R. G., Quan, C., Reyes-Ortiz, A. M., Lutz, S. E., Kedaigle, A. J., Gipson, T. A., Wu, J., Vatine, G. D., Stocksdale, J., Casale, M. S., Svendsen, C. N., Fraenkel, E., Housman, D. E., Agalliu, D., & Thompson, L. M. (2017). Huntington's disease iPSC-derived brain microvascular endothelial cells reveal WNT-mediated angiogenic and blood-brain barrier deficits. *Cell Reports*, *19*(7), 1365–1377.

Lim, Y.-H., Kwon, D.-H., Kim, J., Park, W. J., Kook, H., & Kim, Y.-K. (2018). Identification of long noncoding RNAs involved in muscle differentiation. *PloS One*, *13*(3), e0193898.

Lin, C.-Y., Hsu, Y.-H., Lin, M.-H., Yang, T.-H., Chen, H.-M., Chen, Y.-C., Hsiao, H.-Y., Chen, C.-C., Chern, Y., & Chang, C. (2013). Neurovascular abnormalities in humans and mice with Huntington's disease. *Experimental Neurology*, *250*, 20–30.

Liu, H., Zhang, C., Xu, J., Jin, J., Cheng, L., Miao, X., Wu, Q., Wei, Z., Liu, P., Lu, H., van Zijl, P. C. M., Ross, C. A., Hua, J., & Duan, W. (2021). Huntingtin silencing delays onset and slows progression of Huntington's disease: a biomarker study. *Brain: A Journal of Neurology*, *144*(10), 3101–3113.

Lubeck, E., Coskun, A. F., Zhiyentayev, T., Ahmad, M., & Cai, L. (2014). Single-cell in situ RNA profiling by sequential hybridization [Review of *Single-cell in situ RNA profiling by sequential hybridization*]. *Nature Methods*, *11*(4), 360–361. Springer Science and Business Media LLC.

Macdonald, M. (1993). A novel gene containing a trinucleotide repeat that is expanded and unstable on Huntington's disease chromosomes. *Cell*, *72*(6), 971–983.

Macosko, E. Z., Basu, A., Satija, R., Nemesh, J., Shekhar, K., Goldman, M., Tirosh, I., Bialas, A. R., Kamitaki, N., Martersteck, E. M., Trombetta, J. J., Weitz, D. A., Sanes, J. R., Shalek, A. K., Regev, A., & McCarroll, S. A. (2015). Highly parallel genome-wide expression profiling of individual cells using nanoliter droplets. *Cell*, *161*(5), 1202–1214.

Månberg, A., Skene, N., Sanders, F., Trusohamn, M., Remnestål, J., Szczepińska, A., Aksoylu, I. S., Lönnerberg, P., Ebarasi, L., Wouters, S., Lehmann, M., Olofsson, J., von Gohren Antequera, I., Domaniku, A., De Schaepdryver, M., De Vocht, J., Poesen, K., Uhlén, M., Anink, J., … Lewandowski, S. A. (2021). Altered perivascular fibroblast activity precedes ALS disease onset. *Nature Medicine*, *27*(4), 640–646.

Mastorakos, P., & McGavern, D. (2019). The anatomy and immunology of vasculature in the central nervous system. *Science Immunology*, *4*(37), eaav0492.

Mathys, H., Davila-Velderrain, J., Peng, Z., Gao, F., Mohammadi, S., Young, J. Z., Menon, M., He, L., Abdurrob, F., Jiang, X., Martorell, A. J., Ransohoff, R. M., Hafler, B. P., Bennett, D. A., Kellis, M., & Tsai, L.-H. (2019). Single-cell transcriptomic analysis of Alzheimer's disease. *Nature*, *570*(7761), 332–337.

McGinnis, C. S., Murrow, L. M., & Gartner, Z. J. (2019). DoubletFinder: Doublet detection in single-cell RNA sequencing data using artificial nearest neighbors. *Cell Systems*, *8*(4), 329-337.e4.

Menalled, L. B., Kudwa, A. E., Miller, S., Fitzpatrick, J., Watson-Johnson, J., Keating, N., Ruiz, M., Mushlin, R., Alosio, W., McConnell, K., Connor, D., Murphy, C., Oakeshott, S., Kwan, M., Beltran, J., Ghavami, A., Brunner, D., Park, L. C., Ramboz, S., & Howland,

D. (2012). Comprehensive behavioral and molecular characterization of a new knock-in mouse model of Huntington's disease: zQ175. *PloS One, 7*(12), e49838.

Miniarikova, J., Evers, M. M., & Konstantinova, P. (2018). Translation of MicroRNA-based huntingtin-lowering therapies from preclinical studies to the clinic. *Molecular Therapy: The Journal of the American Society of Gene Therapy*, *26*(4), 947–962.

Miniarikova, J., Zanella, I., Huseinovic, A., van der Zon, T., Hanemaaijer, E., Martier, R., Koornneef, A., Southwell, A. L., Hayden, M. R., van Deventer, S. J., Petry, H., & Konstantinova, P. (2016). Design, characterization, and lead selection of therapeutic miRNAs targeting huntingtin for development of gene therapy for Huntington's disease. *Molecular Therapy. Nucleic Acids*, *5*(e297), e297.

Mohammadi, S., Davila-Velderrain, J., & Kellis, M. (2020). A multiresolution framework to characterize single-cell state landscapes. *Nature Communications, 11*(1), 5399.

Mondo, E., Becker, S. C., Kautzman, A. G., Schifferer, M., Baer, C. E., Chen, J., Huang, E. J., Simons, M., & Schafer, D. P. (2020). A developmental analysis of juxtavascular microglia dynamics and interactions with the vasculature. *The Journal of Neuroscience: The Official Journal of the Society for Neuroscience*, *40*(34), 6503–6521.

Montagne, A., Barnes, S. R., Sweeney, M. D., Halliday, M. R., Sagare, A. P., Zhao, Z., Toga, A. W., Jacobs, R. E., Liu, C. Y., Amezcua, L., Harrington, M. G., Chui, H. C., Law, M., & Zlokovic, B. V. (2015). Blood-brain barrier breakdown in the aging human hippocampus. *Neuron*, *85*(2), 296–302.

Morrone, C. D., Bishay, J., & McLaurin, J. (2020). Potential role of venular amyloid in Alzheimer's disease pathogenesis. *International Journal of Molecular Sciences*, *21*(6), 1985.

Muhl, L., Genové, G., Leptidis, S., Liu, J., He, L., Mocci, G., Sun, Y., Gustafsson, S., Buyandelger, B., Chivukula, I. V., Segerstolpe, Å., Raschperger, E., Hansson, E. M., Björkegren, J. L. M., Peng, X.-R., Vanlandewijck, M., Lendahl, U., & Betsholtz, C. (2020). Single-cell analysis uncovers fibroblast heterogeneity and criteria for fibroblast and mural cell identification and discrimination. *Nature Communications*, *11*(1), 3953.

Nation, D. A., Sweeney, M. D., Montagne, A., Sagare, A. P., D'Orazio, L. M., Pachicano, M., Sepehrband, F., Nelson, A. R., Buennagel, D. P., Harrington, M. G., Benzinger, T. L. S., Fagan, A. M., Ringman, J. M., Schneider, L. S., Morris, J. C., Chui, H. C., Law, M., Toga, A. W., & Zlokovic, B. V. (2019). Blood-brain barrier breakdown is an early biomarker of human cognitive dysfunction. *Nature Medicine*, *25*(2), 270–276.

O'Brien, J. T., & Thomas, A. (2015). Vascular dementia. *Lancet*, *386*(10004), 1698–1706.

Padel, T., Roth, M., Gaceb, A., Li, J.-Y., Björkqvist, M., & Paul, G. (2018). Brain pericyte activation occurs early in Huntington's disease. *Experimental Neurology*, *305*, 139–150.

Pardridge, W. M. (2019). Blood-brain barrier and delivery of protein and gene therapeutics to brain. *Frontiers in Aging Neuroscience*, *11*, 373.

Park, C., Kim, T. M., & Malik, A. B. (2013). Transcriptional regulation of endothelial cell and vascular development. *Circulation Research*, *112*(10), 1380–1400.

Pérez-Martínez, L., & Jaworski, D. M. (2005). Tissue inhibitor of metalloproteinase-2 promotes neuronal differentiation by acting as an anti-mitogenic signal. *The Journal of Neuroscience: The Official Journal of the Society for Neuroscience*, *25*(20), 4917–4929.

Pollak, T. A., Drndarski, S., Stone, J. M., David, A. S., McGuire, P., & Abbott, N. J. (2018). The blood-brain barrier in psychosis. *The Lancet. Psychiatry*, *5*(1), 79–92.

Portales-Casamar, E., Swanson, D. J., Liu, L., de Leeuw, C. N., Banks, K. G., Ho Sui, S. J., Fulton, D. L., Ali, J., Amirabbasi, M., Arenillas, D. J., Babyak, N., Black, S. F., Bonaguro, R. J., Brauer, E., Candido, T. R., Castellarin, M., Chen, J., Chen, Y., Cheng, J. C. Y., … Simpson, E. M. (2010). A regulatory toolbox of MiniPromoters to drive selective expression in the brain. *Proceedings of the National Academy of Sciences of the United States of America*, *107*(38), 16589–16594.

Pulido, R. S., Munji, R. N., Chan, T. C., Quirk, C. R., Weiner, G. A., Weger, B. D., Rossi, M. J., Elmsaouri, S., Malfavon, M., Deng, A., Profaci, C. P., Blanchette, M., Qian, T., Foreman, K. L., Shusta, E. V., Gorman, M. R., Gachon, F., Leutgeb, S., & Daneman, R. (2020). Neuronal activity regulates blood-brain barrier efflux transport through endothelial circadian genes. *Neuron*, *108*(5), 937-952.e7.

Rajan, A. M., Ma, R. C., Kocha, K. M., Zhang, D. J., & Huang, P. (2020). Dual function of perivascular fibroblasts in vascular stabilization in zebrafish. *PLoS Genetics*, *16*(10), e1008800.

Ramilowski, J. A., Goldberg, T., Harshbarger, J., Kloppmann, E., Lizio, M., Satagopam, V. P., Itoh, M., Kawaji, H., Carninci, P., Rost, B., & Forrest, A. R. R. (2016). Corrigendum: A draft network of ligand-receptor-mediated multicellular signalling in human. *Nature Communications*, *7*(1), 10706.

Rasmussen, M. K., Mestre, H., & Nedergaard, M. (2022). Fluid transport in the brain. *Physiological Reviews*, *102*(2), 1025–1151.

Ravindra Kumar, S., Miles, T. F., Chen, X., Brown, D., Dobreva, T., Huang, Q., Ding, X., Luo, Y., Einarsson, P. H., Greenbaum, A., Jang, M. J., Deverman, B. E., & Gradinaru, V.

(2020). Multiplexed Cre-dependent selection yields systemic AAVs for targeting distinct brain cell types. *Nature Methods*, *17*(5), 541–550.

Reiner, A., Albin, R. L., Anderson, K. D., D'Amato, C. J., Penney, J. B., & Young, A. B. (1988). Differential loss of striatal projection neurons in Huntington disease. *Proceedings of the National Academy of Sciences of the United States of America*, *85*(15), 5733–5737.

Restrepo, A., Trevisiol, A., Restrepo-Arango, C., Depp, C., Sasmita, A. O., Keller, A., Tzvetanova, I. D., Hirrlinger, J., & Nave, K.-A. (2022). Axo-vascular coupling mediated by oligodendrocytes. In *bioRxiv*. https://doi.org/10.1101/2022.06.16.495900

Reyahi, A., Nik, A. M., Ghiami, M., Gritli-Linde, A., Pontén, F., Johansson, B. R., & Carlsson, P. (2015). Foxf2 is required for brain pericyte differentiation and development and maintenance of the blood-brain barrier. *Developmental Cell*, *34*(1), 19–32.

Ritchie, M. E., Phipson, B., Wu, D., Hu, Y., Law, C. W., Shi, W., & Smyth, G. K. (2015). limma powers differential expression analyses for RNA-sequencing and microarray studies. *Nucleic Acids Research*, *43*(7), e47.

Romanitan, M. O., Popescu, B. O., Spulber, S., Băjenaru, O., Popescu, L. M., Winblad, B., & Bogdanovic, N. (2010). Altered expression of claudin family proteins in Alzheimer's disease and vascular dementia brains. *Journal of Cellular and Molecular Medicine*, *14*(5), 1088–1100.

Sabbagh, M. F., Heng, J. S., Luo, C., Castanon, R. G., Nery, J. R., Rattner, A., Goff, L. A., Ecker, J. R., & Nathans, J. (2018). Transcriptional and epigenomic landscapes of CNS and non-CNS vascular endothelial cells. *ELife*, *7*. https://doi.org/10.7554/eLife.36187

Salter, M. W., & Stevens, B. (2017). Microglia emerge as central players in brain disease. *Nature Medicine*, *23*(9), 1018–1027.

Sanz, E., Yang, L., Su, T., Morris, D. R., McKnight, G. S., & Amieux, P. S. (2009). Cell-type-specific isolation of ribosome-associated mRNA from complex tissues. *Proceedings of the National Academy of Sciences of the United States of America*, *106*(33), 13939–13944.

Saunders, A., Macosko, E. Z., Wysoker, A., Goldman, M., Krienen, F. M., de Rivera, H., Bien, E., Baum, M., Bortolin, L., Wang, S., Goeva, A., Nemesh, J., Kamitaki, N., Brumbaugh, S., Kulp, D., & McCarroll, S. A. (2018). Molecular diversity and specializations among the cells of the adult mouse brain. *Cell*, *174*(4), 1015-1030.e16.

Schizophrenia Working Group of the Psychiatric Genomics Consortium. (2014). Biological insights from 108 schizophrenia-associated genetic loci. *Nature*, *511*(7510), 421–427.

Sellal, F., Wallon, D., Martinez-Almoyna, L., Marelli, C., Dhar, A., Oesterlé, H., Rovelet-Lecrux, A., Rousseau, S., Kourkoulis, C. E., Rosand, J., DiPucchio, Z. Y., Frosch, M., Gombert, C., Audoin, B., Miné, M., Riant, F., Frebourg, T., Hannequin, D., Campion, D., … Nicolas, G. (2017). APP mutations in cerebral amyloid angiopathy with or without cortical calcifications: Report of three families and a literature review. *Journal of Alzheimer's Disease: JAD*, *56*(1), 37–46.

Shelbourne, P. F., Keller-McGandy, C., Bi, W. L., Yoon, S.-R., Dubeau, L., Veitch, N. J., Vonsattel, J. P., Wexler, N. S., US-Venezuela Collaborative Research Group, Arnheim, N., & Augood, S. J. (2007). Triplet repeat mutation length gains correlate with cell-type specific vulnerability in Huntington disease brain. *Human Molecular Genetics*, *16*(10), 1133–1142.

Slatko, B. E., Gardner, A. F., & Ausubel, F. M. (2018). Overview of next-generation sequencing technologies. *Et al [Current Protocols in Molecular Biology]*, *122*(1), e59.

Smyth, L. C. D., Rustenhoven, J., Scotter, E. L., Schweder, P., Faull, R. L. M., Park, T. I. H., & Dragunow, M. (2018). Markers for human brain pericytes and smooth muscle cells. *Journal of Chemical Neuroanatomy*, *92*, 48–60.

Snapyan, M., Lemasson, M., Brill, M. S., Blais, M., Massouh, M., Ninkovic, J., Gravel, C., Berthod, F., Götz, M., Barker, P. A., Parent, A., & Saghatelyan, A. (2009). Vasculature guides migrating neuronal precursors in the adult mammalian forebrain via brain-derived neurotrophic factor signaling. *The Journal of Neuroscience: The Official Journal of the Society for Neuroscience*, *29*(13), 4172–4188.

Song, H. W., Foreman, K. L., Gastfriend, B. D., Kuo, J. S., Palecek, S. P., & Shusta, E. V. (2020). Transcriptomic comparison of human and mouse brain microvessels. *Scientific Reports*, *10*(1), 12358.

Ståhl, P. L., Salmén, F., Vickovic, S., Lundmark, A., Navarro, J. F., Magnusson, J., Giacomello, S., Asp, M., Westholm, J. O., Huss, M., Mollbrink, A., Linnarsson, S., Codeluppi, S., Borg, Å., Pontén, F., Costea, P. I., Sahlén, P., Mulder, J., Bergmann, O., … Frisén, J. (2016). Visualization and analysis of gene expression in tissue sections by spatial transcriptomics. *Science (New York, N.Y.)*, *353*(6294), 78–82.

Stark, R., Grzelak, M., & Hadfield, J. (2019). RNA sequencing: the teenage years. *Nature Reviews. Genetics*, *20*(11), 631–656.

Stevens, B., & Schafer, D. P. (2018). Roles of microglia in nervous system development, plasticity, and disease. *Developmental Neurobiology*, *78*(6), 559–560.

Su, Y., Wang, X., Yang, Y., Chen, L., Xia, W., Hoi, K. K., Li, H., Wang, Q., Yu, G., Chen, X., Wang, S., Wang, Y., Xiao, L., Verkhratsky, A., Fancy, S. P. J., Yi, C., & Niu, J. (2023).

Astrocyte endfoot formation controls the termination of oligodendrocyte precursor cell perivascular migration during development. *Neuron*, *111*(2), 190-201.e8.

Sweeney, M. D., Kisler, K., Montagne, A., Toga, A. W., & Zlokovic, B. V. (2018). The role of brain vasculature in neurodegenerative disorders. *Nature Neuroscience*, *21*(10), 1318–1331.

Sweeney, M. D., Sagare, A. P., & Zlokovic, B. V. (2018). Blood–brain barrier breakdown in Alzheimer disease and other neurodegenerative disorders. *Nature Reviews. Neurology*, *14*(3), 133–150.

Sweeney, M. D., Zhao, Z., Montagne, A., Nelson, A. R., & Zlokovic, B. V. (2019). Blood-brain barrier: From physiology to disease and back. *Physiological Reviews*, *99*(1), 21–78.

Syvänen, S., Lindhe, O., Palner, M., Kornum, B. R., Rahman, O., Långström, B., Knudsen, G. M., & Hammarlund-Udenaes, M. (2009). Species differences in blood-brain barrier transport of three positron emission tomography radioligands with emphasis on P-glycoprotein transport. *Drug Metabolism and Disposition: The Biological Fate of Chemicals*, *37*(3), 635–643.

Tadic, V., Westenberger, A., Domingo, A., Alvarez-Fischer, D., Klein, C., & Kasten, M. (2015). Primary familial brain calcification with known gene mutations: a systematic review and challenges of phenotypic characterization. *JAMA Neurology*, *72*(4), 460–467.

The Gene Ontology Consortium. (2019). The Gene Ontology Resource: 20 years and still GOing strong. *Nucleic Acids Research*, *47*(D1), D330–D338.

Tong, X., Yang, Q., Ritchey, M. D., George, M. G., Jackson, S. L., Gillespie, C., & Merritt, R. K. (2019). The burden of cerebrovascular disease in the United States. *Preventing Chronic Disease*, *16*(180411), E52.

Toth, P., Tarantini, S., Davila, A., Valcarcel-Ares, M. N., Tucsek, Z., Varamini, B., Ballabh, P., Sonntag, W. E., Baur, J. A., Csiszar, A., & Ungvari, Z. (2015). Purinergic glio-endothelial coupling during neuronal activity: role of P2Y1 receptors and eNOS in functional hyperemia in the mouse somatosensory cortex. *American Journal of Physiology. Heart and Circulatory Physiology*, *309*(11), H1837-45.

Tsai, H.-H., Niu, J., Munji, R., Davalos, D., Chang, J., Zhang, H., Tien, A.-C., Kuo, C. J., Chan, J. R., Daneman, R., & Fancy, S. P. J. (2016). Oligodendrocyte precursors migrate along vasculature in the developing nervous system. *Science (New York, N.Y.)*, *351*(6271), 379–384.

Ueda, H., Sasaki, K., Halder, S. K., Deguchi, Y., Takao, K., Miyakawa, T., & Tajima, A. (2017). Prothymosin alpha-deficiency enhances anxiety-like behaviors and impairs learning/memory functions and neurogenesis. *Journal of Neurochemistry*, *141*(1), 124–136.

Vandebroek, A., & Yasui, M. (2020). Regulation of AQP4 in the central nervous system. *International Journal of Molecular Sciences*, *21*(5), 1603.

Vanlandewijck, M., He, L., Mäe, M. A., Andrae, J., Ando, K., Del Gaudio, F., Nahar, K., Lebouvier, T., Laviña, B., Gouveia, L., Sun, Y., Raschperger, E., Räsänen, M., Zarb, Y., Mochizuki, N., Keller, A., Lendahl, U., & Betsholtz, C. (2018). A molecular atlas of cell types and zonation in the brain vasculature. *Nature*, *554*(7693), 475–480.

Verghese, P. B., Castellano, J. M., & Holtzman, D. M. (2011). Apolipoprotein E in Alzheimer's disease and other neurological disorders. *Lancet Neurology*, *10*(3), 241–252.

Vis, J. C., Nicholson, L. F., Faull, R. L., Evans, W. H., Severs, N. J., & Green, C. R. (1998). Connexin expression in Huntington's diseased human brain. *Cell Biology International*, *22*(11–12), 837–847.

Vonsattel, J.-P., Myers, R. H., Stevens, T. J., Ferrante, R. J., Bird, E. D., & Richardson, E. P., Jr. (1985). Neuropathological Classification of Huntington's Disease. *Journal of Neuropathology and Experimental Neurology*, *44*(6), 559–577.

Wälchli, T., Bisschop, J., Carmeliet, P., Zadeh, G., Monnier, P. P., De Bock, K., & Radovanovic, I. (2023). Shaping the brain vasculature in development and disease in the single-cell era. *Nature Reviews. Neuroscience*. https://doi.org/10.1038/s41583-023-00684-y

Wang, D., Liu, S., Warrell, J., Won, H., Shi, X., Navarro, F. C. P., Clarke, D., Gu, M., Emani, P., Yang, Y. T., Xu, M., Gandal, M. J., Lou, S., Zhang, J., Park, J. J., Yan, C., Rhie, S. K., Manakongtreecheep, K., Zhou, H., … Gerstein, M. B. (2018). Comprehensive functional genomic resource and integrative model for the human brain. *Science (New York, N.Y.)*, *362*(6420), eaat8464.

Weber, B. (2002). White matter glucose metabolism during intracortical electrostimulation: A quantitative [18F]fluorodeoxyglucose autoradiography study in the rat. *NeuroImage*, *16*(4), 993–998.

Wertz, M. H., Mitchem, M. R., Pineda, S. S., Hachigian, L. J., Lee, H., Lau, V., Powers, A., Kulicke, R., Madan, G. K., Colic, M., Therrien, M., Vernon, A., Beja-Glasser, V. F., Hegde, M., Gao, F., Kellis, M., Hart, T., Doench, J. G., & Heiman, M. (2020). Genome-wide in vivo CNS screening identifies genes that modify CNS neuronal survival and mHTT toxicity. *Neuron*, *106*(1), 76-89.e8.

Whitman, M. C., Fan, W., Rela, L., Rodriguez-Gil, D. J., & Greer, C. A. (2009). Blood vessels form a migratory scaffold in the rostral migratory stream. *The Journal of Comparative Neurology*, *516*(2), 94–104.

Wingo, A. P., Fan, W., Duong, D. M., Gerasimov, E. S., Dammer, E. B., Liu, Y., Harerimana, N. V., White, B., Thambisetty, M., Troncoso, J. C., Kim, N., Schneider, J. A., Hajjar, I. M., Lah, J. J., Bennett, D. A., Seyfried, N. T., Levey, A. I., & Wingo, T. S. (2020). Shared proteomic effects of cerebral atherosclerosis and Alzheimer's disease on the human brain. *Nature Neuroscience*, *23*(6), 696–700.

Winkler, E. A., Kim, C. N., Ross, J. M., Garcia, J. H., Gil, E., Oh, I., Chen, L. Q., Wu, D., Catapano, J. S., Raygor, K., Narsinh, K., Kim, H., Weinsheimer, S., Cooke, D. L., Walcott, B. P., Lawton, M. T., Gupta, N., Zlokovic, B. V., Chang, E. F., … Nowakowski, T. J. (2022). A single-cell atlas of the normal and malformed human brain vasculature. *Science (New York, N.Y.)*, *375*(6584), eabi7377.

Wolf, R. C., Grön, G., Sambataro, F., Vasic, N., Wolf, N. D., Thomann, P. A., Saft, C., Landwehrmeyer, G. B., & Orth, M. (2011). Magnetic resonance perfusion imaging of resting-state cerebral blood flow in preclinical Huntington's disease. *Journal of Cerebral Blood Flow and Metabolism: Official Journal of the International Society of Cerebral Blood Flow and Metabolism*, *31*(9), 1908–1918.

Wood, C. A. P., Zhang, J., Aydin, D., Xu, Y., Andreone, B. J., Langen, U. H., Dror, R. O., Gu, C., & Feng, L. (2021). Structure and mechanism of blood-brain-barrier lipid transporter MFSD2A. *Nature*, *596*(7872), 444–448.

Xie, Z., Bailey, A., Kuleshov, M. V., Clarke, D. J. B., Evangelista, J. E., Jenkins, S. L., Lachmann, A., Wojciechowicz, M. L., Kropiwnicki, E., Jagodnik, K. M., Jeon, M., &

Ma'ayan, A. (2021). Gene set knowledge discovery with Enrichr. *Current Protocols*, *1*(3), e90.

Yang, A. C., Stevens, M. Y., Chen, M. B., Lee, D. P., Stähli, D., Gate, D., Contrepois, K., Chen, W., Iram, T., Zhang, L., Vest, R. T., Chaney, A., Lehallier, B., Olsson, N., du Bois, H., Hsieh, R., Cropper, H. C., Berdnik, D., Li, L., … Wyss-Coray, T. (2020). Physiological blood-brain transport is impaired with age by a shift in transcytosis. *Nature*, *583*(7816), 425–430.

Yang, A. C., Vest, R. T., Kern, F., Lee, D. P., Agam, M., Maat, C. A., Losada, P. M., Chen, M. B., Schaum, N., Khoury, N., Toland, A., Calcuttawala, K., Shin, H., Pálovics, R., Shin, A., Wang, E. Y., Luo, J., Gate, D., Schulz-Schaeffer, W. J., … Wyss-Coray, T. (2022). A human brain vascular atlas reveals diverse mediators of Alzheimer's risk. *Nature*, *603*(7903), 885–892.

Zeisel, A., Hochgerner, H., Lönnerberg, P., Johnsson, A., Memic, F., van der Zwan, J., Häring, M., Braun, E., Borm, L. E., La Manno, G., Codeluppi, S., Furlan, A., Lee, K., Skene, N., Harris, K. D., Hjerling-Leffler, J., Arenas, E., Ernfors, P., Marklund, U., & Linnarsson, S. (2018). Molecular architecture of the mouse nervous system. *Cell*, *174*(4), 999-1014.e22.

Zhang, C., Zheng, H., Li, X., Li, S., Li, W., Wang, Z., Niu, S., Wang, X., & Zhang, Z. (2022). Novel mutations in HTRA1-related cerebral small vessel disease and comparison with CADASIL. *Annals of Clinical and Translational Neurology*, *9*(10), 1586–1595.

Zhao, Z., Sagare, A. P., Ma, Q., Halliday, M. R., Kong, P., Kisler, K., Winkler, E. A., Ramanathan, A., Kanekiyo, T., Bu, G., Owens, N. C., Rege, S. V., Si, G., Ahuja, A., Zhu, D., Miller, C. A., Schneider, J. A., Maeda, M., Maeda, T., … Zlokovic, B. V. (2015).

Central role for PICALM in amyloid-β blood-brain barrier transcytosis and clearance. *Nature Neuroscience*, *18*(7), 978–987.